(12) INTERNATIONAL APPLICATION PUBLISHED UNDER THE PATENT COOPERATION TREATY (PCT)

(19) World Intellectual Property Organization
International Bureau

(43) International Publication Date
04 October 2018 (04.10.2018)

WIPO | PCT

(10) International Publication Number
WO 2018/182532 A1

(51) International Patent Classification:
G01L 1/22 (2006.01) *A61B 5/11* (2006.01)
G01B 7/16 (2006.01)

(21) International Application Number:
PCT/SG2018/050161

(22) International Filing Date:
29 March 2018 (29.03.2018)

(25) Filing Language: English

(26) Publication Language: English

(30) Priority Data:
10201702581S 30 March 2017 (30.03.2017) SG

(71) Applicant: **NANYANG TECHNOLOGICAL UNIVERSITY** [SG/SG]; 50 Nanyang Avenue, Singapore 639798 (SG).

(72) Inventors: **LIU, Zhiyuan**; c/o Nanyang Technological University, 50 Nanyang Avenue, Singapore 639798 (SG). **CHEN, Xiaodong**; c/o Nanyang Technological University, 50 Nanyang Avenue, Singapore 639798 (SG).

(74) Agent: **VIERING, JENTSCHURA & PARTNER LLP**; P.O. Box 1088, Rochor Post Office, Rochor Road, Singapore 911833 (SG).

(81) Designated States *(unless otherwise indicated, for every kind of national protection available)*: AE, AG, AL, AM, AO, AT, AU, AZ, BA, BB, BG, BH, BN, BR, BW, BY, BZ, CA, CH, CL, CN, CO, CR, CU, CZ, DE, DJ, DK, DM, DO, DZ, EC, EE, EG, ES, FI, GB, GD, GE, GH, GM, GT, HN, HR, HU, ID, IL, IN, IR, IS, JO, JP, KE, KG, KH, KN, KP, KR, KW, KZ, LA, LC, LK, LR, LS, LU, LY, MA, MD, ME, MG, MK, MN, MW, MX, MY, MZ, NA, NG, NI, NO, NZ, OM, PA, PE, PG, PH, PL, PT, QA, RO, RS, RU, RW, SA, SC, SD, SE, SG, SK, SL, SM, ST, SV, SY, TH, TJ, TM, TN, TR, TT, TZ, UA, UG, US, UZ, VC, VN, ZA, ZM, ZW.

(84) Designated States *(unless otherwise indicated, for every kind of regional protection available)*: ARIPO (BW, GH, GM, KE, LR, LS, MW, MZ, NA, RW, SD, SL, ST, SZ, TZ, UG, ZM, ZW), Eurasian (AM, AZ, BY, KG, KZ, RU, TJ, TM), European (AL, AT, BE, BG, CH, CY, CZ, DE, DK, EE, ES, FI, FR, GB, GR, HR, HU, IE, IS, IT, LT, LU, LV, MC, MK, MT, NL, NO, PL, PT, RO, RS, SE, SI, SK, SM,

(54) Title: STRAIN SENSOR, METHOD OF FORMING AND OPERATING THE SAME

FIG. 1

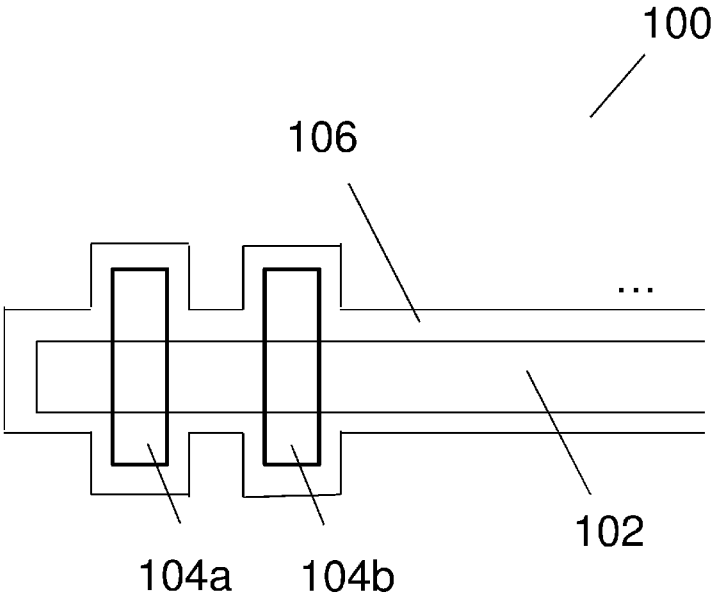

(57) Abstract: Various embodiments may relate to a strain sensor. The strain sensor may include a fiber. The strain sensor may further include a plurality of microstructures along the fiber. The strain sensor may also include an electrically conductive layer in contact with the fiber and the plurality of microstructures.

WO 2018/182532 A1

[Continued on next page]

TR), OAPI (BF, BJ, CF, CG, CI, CM, GA, GN, GQ, GW, KM, ML, MR, NE, SN, TD, TG).

Published:

— *with international search report (Art. 21(3))*
— *in black and white; the international application as filed contained color or greyscale and is available for download from PATENTSCOPE*

STRAIN SENSOR, METHOD OF FORMING AND OPERATING THE SAME

CROSS-REFERENCE TO RELATED APPLICATION

[0001] This application claims the benefit of priority of Singapore application No. 10201702581S filed March 30, 2017, the contents of it being hereby incorporated by reference in its entirety for all purposes.

TECHNICAL FIELD

[0002] Various aspects of this disclosure relate to a strain sensor. Various aspects of this disclosure relate to a method of forming a strain sensor. Various aspects of this disclosure relate to a method of operating a strain sensor.

BACKGROUND

[0003] Stretchable strain sensors, as one of the critical components for wearable electronics, are developed to obtain the real-time mechanical feedback for purposes of healthcare, rehabilitation, soft exoskeleton suits, and so forth. Reported stretchable strain sensors are commonly based on flat films, while fiber-shaped stretchable strain sensors with small testing areas that could be directly woven into textiles have also been increasingly reported. The fiber-shaped stretchable strain sensors have improved wearability and integrability, thus allowing for wearable electronics.

[0004] Recently, non-fiber-shaped stretchable strain sensors based on graphene, carbon/carbon nanotubes, liquid metal, metal-semiconductor hybrid, hydrogel, self-healing materials, conductive polymer and micro fluidics have been reported. It is easier to fabricate two dimensional (2D) flat active layers or three dimensional (3D) channels on a flat substrate.

[0005] In contrast, it would be quite difficult to fabricate high-sensitivity fiber-shaped sensors due to the following two reasons. Firstly, there is a lack of a method for large-scale production of stretchable micro fibers of thermosetting polymers (also referred to as thermoset polymers), e.g., polydimethylsiloxane (PDMS), with controllable diameters. Secondly, compared with well-developed substrate-structure-design technology (e.g. photolithography) for flat films, it is quite hard to carve micro structures on a micro fiber. Although there are several fiber-shaped sensors

reported, the sensitivity of these sensors is still far away from satisfactory.

SUMMARY

[0006] Various embodiments may relate to a strain sensor. The strain sensor may include a fiber. The strain sensor may further include a plurality of microstructures along the fiber. The strain sensor may also include an electrically conductive layer in contact with the fiber and the plurality of microstructures.

[0007] Various embodiments may relate to a method of forming a strain sensor. The method may include forming a plurality of microstructures along a fiber. The method may also include forming an electrically conductive layer in contact with the fiber and the plurality of microstructures.

[0008] Various embodiments may relate to a method of operating a strain sensor. The method may include attaching a strain sensor onto an object. The method may also include determining a change in electrical resistance of the strain sensor due to a strain of the object.

BRIEF DESCRIPTION OF THE DRAWINGS

[0009] The invention will be better understood with reference to the detailed description when considered in conjunction with the non-limiting examples and the accompanying drawings, in which:

FIG. 1 is a general illustration of a strain sensor according to various embodiments.

FIG. 2 is a general illustration showing a method of forming a strain sensor according to various embodiments.

FIG. 3 is a general illustration showing a method of operating a strain sensor according to various embodiments.

FIG. 4A is a schematic showing the surface strain distribution of a fiber with a plurality of microstructures according to various embodiments and a conventional fiber.

FIG. 4B is a plot of normalized strain as a function of length (in millimeters or mm) showing the strain distribution along the fiber with microstructures and along the conventional fiber.

FIG. 5 is a schematic of a fiber and a plurality of microstructures according to various embodiments.

FIG. 6 is a table comparing strain sensors according to various embodiments with conventional flat-film strain sensors.

FIG. 7 shows (left) an image of oil flowing along a wire, (middle) a schematic of a fiber with beads according to various embodiments, and (right) a strain sensor with the fiber, and beads according to various embodiments.

FIG. 8A shows a method of forming fibers according to various embodiments.

FIG. 8B shows an optical image of a cross-section of an as-prepared fiber according to various embodiments.

FIG. 8C shows another optical image of a cross-section of an as-prepared fiber according to various embodiments.

FIG. 9 shows a method of forming fibers according to various embodiments.

FIG. 10A shows a method of forming beads on a fiber according to various embodiments.

FIG. 10B shows an optical image of a fiber with beads according to various embodiments, with the inset showing a magnified image of a section contain a bead.

FIG. 11A is a plot of dynamic viscosity (in Pascals seconds or Pa s) as a function of time (in minutes or min) showing the change in viscosity of the mixture according to various embodiments with precuring time.

FIG. 11B is a plot of fiber diameter (in micrometre or μm) as a function of viscosity (in Pascals seconds or Pa s) showing the relationship between dynamic viscosity and diameter of the fiber according to various embodiments.

FIG. 12A is a schematic showing evolution of the profile of a fiber according to various embodiments with time under gravity (within 3 seconds).

FIG. 12B is a schematic showing the profile of the fiber according to various embodiments at 3.4 seconds, with the inset showing a magnified view of a portion of the fiber.

FIG. 13A is a schematic of a fiber according to various embodiments with indications showing the positions at which the fiber is cut.

FIG. 13B is a plot of normalized fiber diameter as a function of traction time (in seconds or s) showing variation of fiber uniformity with different traction time applied to fibers of different initial viscosity according to various embodiments.

FIG. 14A is a schematic showing the profile changing trajectory of a fiber according to various embodiments under gravity at different time periods. The fiber may be kept as a parabola.

FIG. 14B shows (above) a plot of normalized fiber diameter as a function of position along the fiber according to various embodiments, and (below) the measurement points along the fiber according to various embodiments.

FIG. 15A is an image of a fiber according to various embodiments with a diameter of about 90 μm under low magnification.

FIG. 15B is an image of the fiber shown in FIG. 15A according to various embodiments under high magnification.

FIG. 15C is an image of another fiber according to various embodiments with a diameter of about 10 μm under low magnification.

FIG. 15D is an image of the fiber shown in FIG. 15C according to various embodiments under high magnification.

FIG. 15E is an image of an as-prepared fiber according to various embodiments with meters of length.

FIG. 16A shows an optical image of a fiber with beads according to various embodiments.

FIG. 16B shows a scanning electron microscopy (SEM) image of another fiber with beads according to various embodiments.

FIG. 16C is a plot of bead diameter (in micrometre or μm) as a function of viscosity (in Pascals seconds or Pa s) showing the relationship between dynamic viscosity and diameter of the bead according to various embodiments.

FIG. 16D shows a sketch of a fiber with a bead according to various embodiments illustrating the protrusion thickness H.

FIG. 16E is a plot of bead protrusion height (in micrometer or μm) as a function of viscosity (in Pascals seconds or Pa s) showing the relationship between dynamic viscosity and bead protrusion height of the bead according to various embodiments.

FIG. 17A shows (left) a fiber with beads according to various embodiments, and (right) the fiber with beads coated with a stretchable gold film according to various embodiments.

FIG. 17B is a plot of normalized resistance change (i.e. ratio of resistance change over initial resistance, i.e. R/R_0) as a function of applied tensile strain (in percent or %) of a strain sensor according to various embodiments.

FIG. 17C is a plot of normalized resistance change (i.e. ratio of resistance change under strain over initial resistance, i.e. R/R_0) as a function of the number of cycles showing long term stability of the strain sensor according to various embodiments upon exposure to 5000 tensile strain cycles at an applied strain of 30%, with the inset showing a magnified view of the a portion of the response.

FIG. 18A is a plot of resistance (in ohms or Ω) as a function of number of cycles showing the initial resistance change of the sensor according to various embodiments during the first few tensile strain cycles.

FIG. 18B is a plot of normalized resistance change (i.e. ratio of resistance change under strain over initial resistance, i.e. R/R_0) as a function of number of cycles showing performance of the strain sensor according to various embodiments under cyclic tensile strain of 50%.

FIG. 18C is a plot of normalized resistance change (i.e. ratio of resistance change under strain over initial resistance, i.e. R/R_0) as a function of number of cycles showing performance of the strain sensor according to various embodiments under cyclic tensile strain of 100%.

FIG. 18D is a plot of normalized resistance change (i.e. ratio of resistance change under strain over initial resistance, i.e. R/R_0) as a function of number of cycles showing performance of the strain sensor according to various embodiments under cyclic tensile strain of 120%.

FIG. 19A shows (above) a schematic of a strain sensor according to various embodiments, and (below) scanning electron microscopy (SEM) images corresponding to various areas of the strain sensor as indicated.

FIG. 19B is a plot of crack length (in micrometers or μm) as a function of number showing statistical analysis of the crack lengths of the sensor shown in FIG. 19A as well as a conventional fiber according to various embodiments.

FIG. 20A is a plot of normalized resistance change (i.e. ratio of resistance change under strain over initial resistance, i.e. R/R_0) as a function of strain (in percent or %) showing the resistance of the gold coating on a conventional polydimethysiloxane (PDMS) fiber.

FIG. 20B is a plot of gauge factor as a function of bead diameter (in micrometers or μm) showing the effect of the bead diameter on the strain sensitivity of a strain sensor according to various embodiments.

FIG. 20C is a plot of gauge factor as a function of protrusion height (in micrometers or μm) showing the quantitative analysis of the effect of the bead diameter on the sensitivity of a strain sensor according to various embodiments.

FIG. 20D is a plot of normalized resistance change (i.e. ratio of resistance change under strain over initial resistance, i.e. R/R_0) as a function of time (in seconds or s) showing resistance changes with different strain cycles for strain sensors with stretchable carbon nanotube films according to various embodiments when tensile strain of 10% is applied to the strain sensors.

FIG. 20E is a chart comparing the gauge factor of nanotube-coated fibers without beads and nanotube-coated fibers with beads according to various embodiments showing sensitivity enhancement of the nanotube-coated fibers with beads.

FIG. 21 is a table comparing strain sensor according to various embodiments (denoted with **) with several conventional sensors reported recently.

FIG. 22 is a plot of gauge factor as a function of bead spacing (in millimeters or mm) showing experimental data of the effect of bead spacing on the sensitivity of strain sensors according to various embodiments, with insets showing strain sensors having different bead spacings according to various embodiments.

FIG. 23A is a plot of force (in newtons or N) as a function of tensile strain (in percent or %) showing results of an adhesion test between a polydimethylsiloxane (PDMS) film and the kinesiology tape, with the insets showing images of the setup and result of the test.

FIG. 23B shows images of (top right) a monitoring device including a stretchable strain sensor attached to a kinesiology tape according to various embodiments, (top left) the monitoring device according to various embodiments adhered onto a joint of the lower limb for monitoring, (bottom right) the monitoring device according to various embodiments during operation when the person is squatting, and (bottom left) the monitoring device according to various embodiments during operation when the person is standing.

FIG. 23C shows images of the monitoring device according to various embodiments being used during leg lifting exercises (left) when the legs are at rest, and (right) when the legs are lifted.

FIG. 23D shows an image of a customized circuit included in the monitoring device according to various embodiments.

FIG. 23E is a plot of normalized resistance change (i.e. ratio of resistance change under strain over initial resistance, i.e. R/R_0) as a function of time (in seconds or s) showing data obtained by the strain sensor according to various embodiments during slow squatting and fast squatting.

FIG. 23F is a plot of normalized resistance change (i.e. ratio of resistance change under strain over initial resistance, i.e. R/R_0) as a function of time (in seconds or s) showing data obtained by the strain sensor according to various embodiments during slow leg lifting and fast leg lifting.

FIG. 24A is a schematic illustrating the leg bending angle θ.

FIG. 24B is a plot of normalized resistance change (i.e. ratio of resistance change under strain over initial resistance, i.e. R/R_0) as a function of bending cycle illustrating the resistance change of the strain sensor according to various embodiments in relation to the bending cycle.

FIG. 25 shows an optical image of a fiber-shaped strain sensor according to various embodiments that is weaved into clothes.

FIG. 26A shows an image of an opened software, *ImageJ*.

FIG. 26B shows an SEM image being opened in the software.

FIG. 26C shows an image of the software with "Measure" being clicked to measure the length of the curve that has been drawn.

FIG. 27A is a schematic showing a gold film according to various embodiments with randomly distributed initial defects.

FIG. 27B is a schematic showing the gold film in FIG. 27A according to various embodiments with randomly-distributed micro cracks after strain is applied.

FIG. 27C is a schematic showing the gold film in FIG. 27B according to various embodiments with the further crack propagation pattern after further strain is applied.

FIG. 28A is a scanning electron microscopy (SEM) image of the gold film according to various embodiments with randomly distributed initial defects without any strain applied.

FIG. 28B is another scanning electron microscopy (SEM) image of a portion of the gold film over a neck portion of the bead according to various embodiments under strain of 80%.

FIG. 28C is yet another scanning electron microscopy (SEM) image of a strain concentrated area of the gold film according to various embodiments.

FIG. 29A is a chart comparing the width of the gold micro-islands in a strain concentrated area and the width of the gold micro-islands in a normal area of a gold film according to various embodiments.

FIG. 29B shows a simulation image of a crack-induced strain concentration of a gold film according to various embodiments.

DETAILED DESCRIPTION

[0010] The following detailed description refers to the accompanying drawings that show, by way of illustration, specific details and embodiments in which the invention may be practiced. These embodiments are described in sufficient detail to enable those skilled in the art to practice the invention. Other embodiments may be utilized and structural, and logical changes may be made without departing from the scope of the invention. The various embodiments are not necessarily mutually exclusive, as some embodiments can be combined with one or more other embodiments to form new embodiments.

[0011] Embodiments described in the context of one of the methods or strain sensors are analogously valid for the other methods or strain sensors. Similarly, embodiments described in the context of a method are analogously valid for a strain sensor, and vice versa.

[0012] Features that are described in the context of an embodiment may correspondingly be applicable to the same or similar features in the other embodiments. Features that are described in the context of an embodiment may correspondingly be applicable to the other embodiments, even if not explicitly described in these other embodiments. Furthermore, additions and/or combinations and/or alternatives as described for a feature in the context of an embodiment may correspondingly be applicable to the same or similar feature in the other embodiments.

[0013] The word "over" used with regards to a deposited material formed “over” a side or surface, may be used herein to mean that the deposited material may be formed "directly on", e.g. in direct contact with, the implied side or surface. The word "over" used with regards to a deposited material formed “over” a side or surface, may also be used herein to mean that the deposited material may be formed "indirectly on" the implied side or surface with one or more additional layers being arranged between the implied side or surface and the deposited material. In other words, a first layer “over” a second layer may refer to the first layer directly on the second

layer, or that the first layer and the second layer are separated by one or more intervening layers. Further, in the current context, a layer "over" or "on" a side or surface may not necessarily mean that the layer is above a side or surface. A layer "on" a side or surface may mean that the layer is formed in direct contact with the side or surface, and a layer "over" a side or surface may mean that the layer is formed in direct contact with the side or surface or may be separated from the side or surface by one or more intervening layers.

[0014] The strain sensor as described herein may be operable in various orientations, and thus it should be understood that the terms "top", "bottom", etc., when used in the following description are used for convenience and to aid understanding of relative positions or directions, and not intended to limit the orientation of the strain sensor.

[0015] In the context of various embodiments, the articles "a", "an" and "the" as used with regard to a feature or element include a reference to one or more of the features or elements.

[0016] In the context of various embodiments, the term "about" or "approximately" as applied to a numeric value encompasses the exact value and a reasonable variance.

[0017] As used herein, the term "and/or" includes any and all combinations of one or more of the associated listed items.

[0018] FIG. 1 is a general illustration of a strain sensor 100 according to various embodiments. The strain sensor 100 may include a fiber 102. The strain sensor may further include a plurality of microstructures 104a, 104b along the fiber 102. The strain sensor 100 may also include an electrically conductive layer 106 in contact with the fiber 102 and the plurality of microstructures 104a, 104b.

[0019] In other words, the strain sensor 100 may be a fiber 102 with a plurality of microstructures 104a, 104b along a length of the fiber 102. The strain sensor 100 may further include an electrically conductive layer 106 on surfaces of the fiber 102 and the plurality of microstructures 104a, 104b.

[0020] For avoidance of doubt, while FIG. 1 shows two microstructures 104a 104b, various embodiments may have more than two microstructures.

[0021] Various embodiments may seek to address the issues faced by conventional strain sensors. Various embodiments may be a fiber-shaped strain sensor. Various embodiments may provide high sensitivity, while providing the ease of being weaved into materials such as textiles.

[0022] The fiber 102 may be a microfiber. The diameter of the fiber 102 may be any one value selected from a range of about 10 μm to about 1000 μm, e.g. of about 10 μm to about 500 μm. The length of the fiber 102 may be any one value selected from a range of about 100 μm to about 1 m, e.g. of about 100 μm to about 10 cm.

[0023] The plurality of microstructures 104a-b may be microbeads. A microbead may be a microstructure with a curved outer surface. The microbead may have a substantially spherical shape, a substantially hemispherical shape, or a substantially droplet shape. Each microstructure may have a dimension, e.g. a diameter or a width, of any one value in the range of about 10 μm to about 1200 μm, any one value in the range of 200 μm to 900 μm, any one value in the range of about 250 μm to about 550 μm.

[0024] The plurality of microstructures 104a, 104b may be spaced apart from one another. A microstructure of the plurality of microstructures may be spaced apart from a neighbouring microstructure of the plurality of microstructures. In various embodiments, a distance between neighboring microstructures may be substantially equal. In other words, the plurality of microstructures 104a, 104b may have a periodic arrangement. In various other embodiments, the plurality of microstructures 104a, 104b may have an aperiodic arrangement.

[0025] In various embodiments, a distance or spacing between neighboring microstructures may be less than 5 mm, e.g. less than 2 mm, e.g. less than 1.2 mm, e.g. less than 0.8 mm. A smaller distance or spacing between neighboring microstructures may lead to a sensor with higher sensitivity.

[0026] Neighbouring microstructures may refer to a pair of a first microstructure and a second microstructure, such that a distance between the second microstructure and the first microstructure is smaller than a distance between any other microstructure and the first microstructure.

[0027] In various embodiments, the fiber 102 may include or consist of a polymer, such as an elastomer. The polymer included in the fiber 102 may be a thermoset polymer such as polydimethylsiloxane (PDMS). In various embodiments, the fiber may be a natural fiber such as cellulose, cotton, jute, keratin, wool, or silk.

[0028] In various embodiments, the plurality of microstructures 104a-b may include or consist of a polymer, such as an elastomer. The polymer included in the plurality of microstructures 104a-b may be a thermoset polymer such as polydimethylsiloxane (PDMS).

[0029] A material included in the fiber 102 and a material included in the plurality of microstructures 104a-b may be the same. For instance, both the fiber 102 and the plurality of microstructures 104a-b may include or consist of PDMS. The fiber 102 and the plurality of microstructures 104a-b may form a continuous structure.

[0030] In various embodiments, a modulus of the plurality of microstructures 104a-b may be higher than a modulus of the fiber 102. The modulus of the plurality of microstructures 104a-b may be more than 5 times, e.g. more than 7 times, e.g. about 10 times, larger than the modulus of the fiber 102.

[0031] In various embodiments, the electrically conductive layer 106 may include a metal such as gold, carbon nanotubes, silver, or platinum.

[0032] In various embodiments, the electrically conductive layer 106 may include cracks, such as microcracks and/or nanocracks. A nanocrack may be defined as a crack having a length of any value from 1 nm to 100 nm. A microcrack may be defined as a crack having a length of any value from 1 μm to 100 μm.

[0033] In various embodiments, a gauge factor of the strain sensor 100 may be greater than 25, may be greater than 40, may be greater than 80, e.g. may be about 100.

[0034] FIG. 2 is a general illustration showing a method of forming a strain sensor according to various embodiments. The method may include, in 202, forming a plurality of microstructures along a fiber. The method may also include, in 204, forming an electrically conductive layer in contact with the fiber and the plurality of microstructures.

[0035] In other words, forming the strain sensor may include forming microstructures along a length of a fiber, and coating the fiber and the microstructures with an electrically conductive material.

[0036] The plurality of microstructures may be spaced apart from one another.

[0037] Forming the plurality of microstructures along the fiber may include immersing, putting or providing the fiber in a mixture (which may be referred to as a beads precursor mixture) including a polymer precursor, such as an oligomer like linear di-vinyl-terminated poly(dimethylsiloxanes). The mixture may further include a crosslinker, such as a platinum-based catalyst, or 2,2,6,6-tetramethylpiperidinyloxyl (TEMPO) and dicumyl peroxide (DCP). The cross linker may catalyse or facilitate the cross-linking to form the polymer. In various embodiments,

the mixture may be or may include PDMS 184 (Sigma-Aldrich), which may include polymer precursors di-vinyl-terminated poly(dimethylsiloxane), dimethylvinylated and trimethylated silica, tetra (trimethoxysiloxy) silane, and ethyl benzene, as well as cross-linkers or curing agents dimethyl methylhydrogen siloxane, dimethylvinyl terminated dimethyl siloxane, dimethylvinylated and trimethylated silica, tetramethyl tetravinyl cyclotetra siloxane, and ethyl benzene. The method may also include removing the fiber from the mixture (including the polymer precursor) with droplets of the polymer precursor in contact with the fiber. The fibers with the droplets may be suspended vertically. The method may additionally include introducing the fiber into heated oil, e.g. heated silicone oil (also referred to as silicon oil), so that the droplets form the plurality of microstructures. The plurality of microstructures may include a polymer formed from the polymer precursor. When the polymer precursor and the crosslinker are heated, cross-linking of the polymer precursor oligomers, monomers, molecules or chains may occur to form the polymer.

[0038] The method may also include forming the fiber. Forming the fiber may include mixing a predetermined ratio of a further polymer precursor and a cross linker to form a mixture (which may be referred to as a fiber precursor mixture) including the further polymer precursor and the cross linker. In various embodiments, the further polymer precursor and the polymer precursor may be the same. The further polymer precursor may include an oligomer like linear di-vinyl-terminated poly(dimethylsiloxanes). The mixture may further include a crosslinker, such as a platinum-based catalyst, or 2,2,6,6-tetramethylpiperidinyloxyl (TEMPO) and dicumyl peroxide (DCP). The cross linker may catalyse or facilitate the cross-linking to form the polymer.

[0039] In various alternate embodiments, the further polymer precursor may be different from the polymer precursor.

[0040] The mixture may be of high viscosity, i.e. the mixture may be a thick mixture. The mixture may have a viscosity index of any value within a range of 25 Pa s to 100 Pa s, e.g. 40 Pa s to 80 Pa s, at room temperature. If the viscosity is too small or too large, the fiber may not be formed. The viscosity of polymer precursor may be dependent on the type of polymer precursor. The method may also include stretching an amount of the mixture (including the further polymer precursor and the cross linker. The method may further include introducing the amount of stretched mixture into heated oil, e.g. silicone oil, to form the fiber. When the further polymer precursor and

the crosslinker are heated, cross-linking of the further polymer precursor oligomers, monomers, molecules or chains may occur to form the further polymer. In various embodiments, the polymer and the further polymer may be the same. In various alternate embodiments, the further polymer may be different from the polymer.

[0041] In various embodiments, forming the electrically conductive layer may include evaporating or sputtering electrically conductive material onto the fiber and the plurality of microstructures. The electrically conductive material may be a metal such as gold. The fiber with the plurality of microstructures may be provided within a chamber. A metal source, e.g. a gold source, may be introduced into the chamber. Metal from the metal source may be sputtered or evaporated onto the fiber and the plurality of microstructures.

[0042] In various embodiments, forming the electrically conductive layer may include introducing the fiber with the plurality of microstructures to a mixture including an electrically conductive material, such as carbon nanotubes, so that the fiber with the plurality of microstructures is coated with the electrically conductive material. The method may further include heating the coated fiber with the plurality of microstructures to form the electrically conductive layer. Forming the electrically conductive layer may further include exposing the fiber with the plurality of microstructures to oxygen plasma before introducing the fiber with the plurality of microstructures to the mixture including the electrically conductive material, e.g. carbon nanotubes. Oxygen plasma modification to the fiber with the plurality of microstructures may improve the adhesion of the electrically conductive material, e.g. carbon nanotubes, to the modified fiber with the plurality of microstructures.

[0043] The carbon nanotubes may be modified with an acid, such as carboxylic acid. The acid modification of the carbon nanotubes may be carried out before introducing the fiber with the plurality of microstructures to the mixture including the electrically conductive material. The acid may improve the adhesion of the carbon nanotubes to the fiber with the plurality of microstructures. Acid-treated carbon nanotubes may readily dissolve in water. Further, oxygen plasma modification may be carried out to make the fiber with plurality of microstructures more hydrophilic so as to improve the adhesion between the acid-treated carbon nanotubes and fibers with plurality of microstructures. In various embodiments, oxygen plasma treatment may be used on one or more selected regions of the fiber with microstructures. The one or more selected regions

exposed to the oxygen plasma may become hydrophilic while one or more remaining regions of the fiber with microstructures not exposed to the oxygen plasma may remain hydrophobic or less hydrophilic. The acid-treated nanotubes may then adhere to only the one or more selected regions, thereby forming a patterned electrically conductive layer.

[0044] Various embodiments may provide a strain sensor formed by a method as described herein.

[0045] FIG. 3 is a general illustration showing a method of operating a strain sensor according to various embodiments. The method may include, in 302, attaching a strain sensor as described herein to an object. The method may also include, in 304, determining a change in electrical resistance of the strain sensor due to a strain of the object.

[0046] In other words, determining a strain of an object may include attaching a strain sensor as described herein onto the object, and determining a change in electrical resistance of the strain sensor upon the object undergoing a strain.

[0047] The strain may be determined based on the change in the electrical resistance of the strain sensor.

[0048] In various embodiments, the strain sensor may be weaved onto an object such as textile. When the object such as textile is stretched or strained, the strain sensor may also undergo a strain corresponding to the strain of the object, thus causing a change in electrical resistance of the strain sensor.

[0049] Various embodiments may relate to a monitoring device including the strain sensor. The monitoring device may include a textile, such as a kinesiology tape. The strain sensor may be adhered, attached or woven onto the textile.

[0050] The monitoring device may further include a circuit arrangement, such as a customized circuit. The circuit arrangement may be coupled to the strain sensor, e.g. via wired or wireless means.

[0051] A "circuit" may be understood as any kind of a logic implementing entity, which may be special purpose circuitry or a processor executing software stored in a memory, firmware, or any combination thereof. Thus, in various embodiments, a "circuit" may be a hard-wired logic circuit or a programmable logic circuit such as a programmable processor, e.g. a microprocessor (e.g. a Complex Instruction Set Computer (CISC) processor or a Reduced Instruction Set

Computer (RISC) processor). A "circuit" may also be a processor executing software, e.g. any kind of computer program, e.g. a computer program using a virtual machine code such as e.g. Java. Any other kind of implementation of the respective functions which will be described in more detail may also be understood as a "circuit" in accordance with various alternative embodiments.

[0052] Various embodiments may relate to a fiber-shaped stretchable strain sensor. A strategy of strain redistribution in an elastic substrate employing the principle of Plateau-Rayleigh instability to fabricate structures or beads on a fiber may significantly enhance the sensitivity of the strain sensor.

[0053] Various embodiments may relate to a method of using transient thermal curing to fabricate fibers including a thermosetting polymer such as PDMS in a large scale, with each fiber having a diameter of micrometers. The fiber diameter can be controlled from about 10 μm to about 1000 μm. The dynamic fabrication process may be used to fabricate fibers with good uniformity.

[0054] The principle of Plateau-Rayleigh instability may be used to modify fibers with uniformly distributed self-assembled beads. These beads may be used to tune the strain distribution along the fiber, rearranging the strain distribution from the portions of the fibers in contact with the beads to the fiber segments in between the beads, thus inducing the strain concentration. The local strain may be magnified by this process, resulting in longer cracks in the stretchable electrically conductive layer (e.g. a gold film or a carbon nanotube (CNT) film) on the surface of the fiber, which may significantly improve the sensitivity. The sensitivity of the strain sensor with beads may be significantly improved compared to the sensitivity of the strain sensor without beads.

[0055] The beads-on-fiber stretchable strain sensor may be weaved into the textile to monitor the joint motion and muscle expansion. Similarly, fibers with beads based on other thermosetting polymers may be fabricated to enhance sensitivity.

[0056] The strategy of strain redistribution may also be applied to non-fiber-shaped stretchable strain sensors. Even for flat films, methods to enhance sensitivity have been mainly focused on optimizing the conductive materials itself, e.g. by tuning the cracks, constructing the film thickness, designing new nanostructures, and so on. There are few literature relating to mechanical design of the elastic substrate of flat strain sensors.

[0057] According to structural mechanical analysis, when a certain work, W, is applied to a system, the energy may be absorbed/stored as the strain in the materials. The work, W, is provided by Equation (1) as follows:

$$W = \int E\varepsilon^2 \, dV \quad (1)$$

wherein E is the modulus, ϵ is the strain, and V is the volume of the materials.

[0058] For the same work applied, a more significant change in the electrical conductivity of electrically conductive layers or active materials may be equivalent to higher sensitivity of the sensor. For a smooth fiber, the energy efficiency may be quite low, because V remains constant for each differential length of this fiber and the strain is dispersed uniformly in the fiber.

[0059] In contrary, if the strain could be accumulated at certain positions, it may induce more significant change in the electrical conductivity of active materials, i.e., the higher sensitivity. Therefore, the redistribution the surface strain of the fiber to achieve the strain accumulation may be the critical issue.

[0060] According to the energy conservation principle, although the average strain is constant for a given volume under the same applied work, the local strain distribution may be enlarged by relatively decreasing the local volume. Therefore, for the resistive stretchable strain sensors, the sensitivity may be significantly improved if the stretchable conductive materials are deposited in the region(s) where the local strain is magnified.

[0061] By employing finite element modeling (FEM), it is found that the strain may indeed be redistributed by proper design. For example, the maximum achievable local strain may almost be doubled by introducing microstructures along the fiber (shown in FIGS. 4A-B). FIG. 4A is a schematic showing the surface strain distribution of a fiber 402 with a plurality of microstructures 404a-d according to various embodiments and a conventional fiber 450. FIG. 4B is a plot of normalized strain as a function of length (in millimeters or mm) showing the strain distribution along the fiber with microstructures and along the conventional fiber.

[0062] In addition, if high-modulus materials were employed in the low-strain (i.e. large volume) regions, the maximum strain may be further enhanced. FIG. 5 is a schematic of a fiber 502 and a plurality of microstructures 504a-b according to various embodiments. The modulus of the larger square regions 504a-b may be set to be about 10 times that of the fiber 502.

[0063] Following this way of reasoning, surface strain redistribution may be used to significantly enhance the sensitivity of fiber-shaped stretchable strain sensors. In order to demonstrate this strategy, a method of transient thermal curing to achieve large-scale fabrication of microfibers with uniform predefined diameters may be provided. The microfibers may be polydimethylsiloxane (PDMS).

[0064] Compared to the well-established technologies of flat-film fabrication, it may still be challenging to introduce microstructures to one single fiber. One way may be to make use of the principle of Plateau–Rayleigh instability to modify microfibers with uniformly distributed microbeads.

[0065] These microbeads may tune the strain distribution along the fiber by rearranging the strain from the areas in contact with the beads to the areas in-between the beads—a strategy that may effectively result in strain concentration. The local strain may be magnified by this process, resulting in longer microcracks in electrically conductive layers, such as stretchable gold films/CNT films deposited on the surface of the fiber, leading to significantly improved sensitivity compared to fibers without microbeads.

[0066] It is demonstrated that the beads-on-fiber stretchable strain sensor according to various embodiments may be employed to reliably monitor sports activity.

[0067] In addition, it is found that the sensitivity enhancement methods for flat-film stretchable strain sensors may currently be limited to the active materials design. FIG. 6 is a table comparing strain sensors according to various embodiments (denoted as **) with conventional flat-film strain sensors.

[0068] As discussed previously, the sensitivity of the fiber-shaped stretchable strain sensor may be enhanced with microstructures, which may introduce uneven distribution of strain.

[0069] It is well known that when oil flows along one fiber, the oil may automatically be split into droplets because of Plateau–Rayleigh instability. Inspired by this natural phenomenon, PDMS fibers with microstructures that could take advantage of the strain redistribution effect may be produced. FIG. 7 shows (left) an image of oil flowing along a wire, (middle) a schematic of a fiber 702 with beads 704 according to various embodiments, and (right) a strain sensor with the fiber 702, and beads 704 according to various embodiments.

[0070] For thermoplastic polymers, it may be relatively easier to fabricate fibers by using micro-jetting method after the thermoplastic polymers have been melted. Thermoset polymers such as PDMS may not be melted and jetted. Molding may be used on thermoset polymers but it may be difficult to fabricate microfibers with millimetre length at low cost.

[0071] A feasible, cost effective method for large-scale fabrication of thermoset polymer or PDMS microfibers may be as described herein. A method of transient thermal curing may be used to achieve the efficient fabrication of the micro fibers. The basic principle is that after proper control of the viscosity of the thermoset polymer or the PDMS precursor, the microfibers may be fabricated by applying traction strain and then be immersed into hot oil bath immediately to be fully cured (using transient curing).

[0072] FIG. 8A shows a method of forming fibers 802 according to various embodiments. The method may include, as shown in (I), providing a mixture 808 including a polymer precursor, such as PDMS precursor. The mixture may also include a crosslinker. The method may further include, as shown in (II), using a stick 810a to dip into the mixture 808, and as shown in (III), pulling the stick 810a away from the mixture 808 to form a fiber including the polymer precursor. The fiber 802 may also include the crosslinker. The method may also include, as shown in (IV), using the stick 810a and a further stick 810b, each adhered to an opposite end of the fiber 802, to stretch the fiber 802. FIG. 8B shows an optical image of a cross-section of an as-prepared fiber according to various embodiments. FIG. 8C shows another optical image of a cross-section of an as-prepared fiber according to various embodiments.

[0073] FIG. 9 shows a method of forming fibers 902 according to various embodiments. In (I), a fiber 902 including a polymer precursor, such as PDMS precursor, may be formed by dynamic traction. The viscosity of the polymer or PDMS precursor may control the physical properties of the fiber 902, such as the length and the diameter. Traction time and traction length during subsequent fabrication processes may also control the physical properties of the fiber 902. Pre-curing may be carried out to form a polymer precursor fiber 902 with the desired viscosity. In (II), transient curing may be carried out on the polymer precursor fiber 902 to cure the polymer precursor. In other words, transient curing may be used to form a fiber 902 including a polymer, e.g. PDMS, from the polymer precursor fiber 902. The polymer precursor fiber 902 may be cured in silicone oil 912 at a temperature of any value in the range from 170 °C to 180 °C. Boiling water

may not be used for curing PDMS as the boiling water would upset the fiber structure. Further, PDMS is intrinsically hydrophobic and may not be fully immersed in hot water. Accordingly, silicone oil may be used for transient curing. Silicone oil may have a lower density than PDMS, but may have a higher boiling point than water. Importantly, silicone oil is compatible with PDMS and may be removed by normal detergents. (III) shows an image of a cured PDMS fiber. The inset shows a magnified portion of the fiber 902.

[0074] FIG. 10A shows a method of forming beads on a fiber 1002 according to various embodiments. The as-prepared fibers 1002 may be washed and dried as shown in (I). (II) shows polymer precursor beads form automatically on the fibers 1002 due to Plateau-Rayleigh instability after the fibers 1002 are dipped or immersed into a mixture including polymer precursor, e.g. PDMS precursor. The mixture may also include a cross-linker. In (III), the fibers with beads may be put into the silicone oil 1012 to undergo transient curing. The silicone oil 1012 may be at a temperature of any value in the range from 170 °C to 180 °C. FIG. 10B shows an optical image of a fiber with beads according to various embodiments, with the inset showing a magnified image of a section contain a bead. The bead may have a diameter D, while the fiber may have a diameter R.

[0075] PDMS fibers with good uniformity along the length direction and with predefined diameters may be formed by adjusting the viscosity of PDMS and the traction time. The dynamic viscosity of the mixture of PDMS and crosslinker may be tuned by a precuring process. FIG. 11A is a plot of dynamic viscosity (in Pascals seconds or Pa s) as a function of time (in minutes or min) showing the change in viscosity of the mixture according to various embodiments with precuring time. As shown in FIG. 11A, with an increase in precuring time, there may be more polymerization and/or greater cross-linking between the PDMS and the crosslinker, thus resulting in a higher viscosity.

[0076] The viscosity of the mixture may influence the fiber diameter. FIG. 11B is a plot of fiber diameter (in micrometre or μm) as a function of viscosity (in Pascals seconds or Pa s) showing the relationship between dynamic viscosity and diameter of the fiber according to various embodiments. By keeping other fabrication parameters constant, the fiber diameter may be tuned by adjusting the dynamic viscosity of the mixture. The line shows the fitting curve.

[0077] In order to achieve uniform fibers for a mixture of a predetermined viscosity, the period over which the traction strain is applied may need to be strictly controlled. The fiber morphology may be simulated by considering the traction process as a viscous catenary flow under gravity.

[0078] FIG. 12A is a schematic showing evolution of the profile of a fiber 1202 according to various embodiments with time under gravity (within 3 seconds). The diameter of the fiber 1202 may remain uniformly distributed during the first 3 s.

[0079] The fiber 1202 may then gradually turned thicker in the middle and thinner near the traction point. In various embodiments, the PDMS precursor may be stretched in a short time of less than 4 seconds for uniformity. FIG. 12B is a schematic showing the profile of the fiber 1202 according to various embodiments at 3.4 seconds, with the inset showing a magnified view of a portion of the fiber 1202. The inset illustrates the nonuniformity of the diameter of the fiber 1202.

[0080] The reason behind may be that the viscous PDMS precursor may not be fully cured during the traction and may still flow from the ends to the middle under gravity. The fiber may then become thicker in the middle and thinner near the traction points, i.e. the ends of the fiber at which the fiber is held. The lower the viscosity is, the better the mobility. The fibers may therefore be immersed into the hot silicone oil bath in the first few seconds after traction in order to obtain the fibers with relatively uniform diameter.

[0081] The fibers may be cut at different positions along the length direction, and the diameter may be measured to ensure reproducible uniformity. FIG. 13A is a schematic of a fiber 1302 according to various embodiments with indications showing the positions at which the fiber 1302 is cut. The diameter of the fiber 1302 may be indicated as R_1 at a quarter of the fiber length, and may be indicated as R_2 at half of the fiber length. FIG. 13B is a plot of normalized fiber diameter as a function of traction time (in seconds or s) showing variation of fiber uniformity with different traction time applied to fibers of different initial viscosity according to various embodiments. The normalized fiber diameter may be defined as R_1/R_2. FIG. 13B shows that the fibers may remain fairly uniform within the first few seconds, and may become non-uniform as the traction time increases. Further, FIG. 13B shows that an initial more viscous precursor may result in a more uniform fiber, while an initial less viscous precursor may result in a more non-uniform fiber.

[0082] FIG. 14A is a schematic showing the profile changing trajectory of a fiber 1402 according to various embodiments under gravity at different time periods. The fiber 1402 may be

kept as a parabola. FIG. 14B shows (above) a plot of normalized fiber diameter as a function of position along the fiber 1402 according to various embodiments, and (below) the measurement points along the fiber 1402 according to various embodiments. The fiber 1402 may have fairly uniform diameter.

[0083] The diameter of the fiber, R, may be controlled by the amount of added PDMS, its viscosity, and the traction length. A fiber with a minimum diameter of about 10 μm and 4 cm in length may be obtained by rapidly increasing the traction range. The length-to-diameter ratio achieved may be around 4000. A fiber with a maximum fiber diameter of around 1 mm and a length of 8 cm in length may be obtained by decreasing the traction range.

[0084] FIG. 15A is an image of a fiber according to various embodiments with a diameter of about 90 μm under low magnification. FIG. 15B is an image of the fiber shown in FIG. 15A according to various embodiments under high magnification.

[0085] FIG. 15C is an image of another fiber according to various embodiments with a diameter of about 10 μm under low magnification. FIG. 15D is an image of the fiber shown in FIG. 15C according to various embodiments under high magnification. FIG. 15E is an image of an as-prepared fiber according to various embodiments with meters of length.

[0086] By repeating the fabrication process, meters of the fiber may be fabricated in a short time.

[0087] After the fiber fabrication process, beads may be formed or modified on the fiber to enhance the sensitivity as discussed above. Beads-on-fiber phenomena has been reported for nanosized fibers formed by electro-spinning processes, but only a few reports have been published for micron-size fibers.

[0088] Beads may automatically form when a viscous liquid flows along a vertically aligned fiber. The formation mechanism has been studied in detail. Competition and balance between the surface tension and gravity (also referred to as Plateau–Rayleigh instability) may explain this behaviour.

[0089] FIG. 16A shows an optical image of a fiber with beads according to various embodiments. FIG. 16B shows a scanning electron microscopy (SEM) image of another fiber with beads according to various embodiments.

[0090] The Bond number, G, may be used to predict the occurrence of bead formation. The dimensionless Bond number, G, may be provided by

$$G = \rho g R^3 / 8\gamma h_0 \quad (2)$$

where ρ is the density of the liquid, g is the gravitational acceleration constant, R is the diameter of the fiber, γ is the surface tension, and h_0 is the undisturbed film thickness of the polymer precursor (e.g. PDMS precursor).

[0091] According to this principle, the fiber diameter may significantly affect the attachment and distribution of the beads.

[0092] A bond number (G) of 0.7 may normally be regarded as a critical value for bead formation. When G is larger than 0.7, the viscous liquid may be in steady flow and beads may not form, but for when G is equal or smaller than 0.7, beads may form.

[0093] In order to tune the diameter of the bead, D, as discussed above, the viscosity, traction time, and distance may be controlled. By applying the same traction time and distance, the effect of the viscosity on the bead diameter may be investigated. In various embodiments, the diameter of the beads may be any one value from about 200 μm to about 900 μm.

[0094] FIG. 16C is a plot of bead diameter (in micrometre or μm) as a function of viscosity (in Pascals seconds or Pa s) showing the relationship between dynamic viscosity and diameter of the bead according to various embodiments. The fiber diameter used may be around 250 μm.

[0095] FIG. 16D shows a sketch of a fiber 1602 with a bead 1604 according to various embodiments illustrating the protrusion thickness H. H may be defined as the protrusion thickness of the polymer film on the fiber, and H_{max} may be defined as the maximum value of H. H_{max} may be provided by:

$$H_{max} = \frac{D-R}{2} \quad (3)$$

[0096] As shown in the inset of FIG. 10B, D may be defined as the diameter of a bead, while R may be defined as the diameter of the fiber.

[0097] The maximum protrusion diameter H_{max} may be provided as follows:

$$H_{max} = 1.2860c^{2/3} - 1.413 - 0.2904c^{-1/3} + O(c^{-2/3}) \quad (4)$$

where c is the migration speed of the bead. O represents higher order term in mathematics which may be ignored in calculations.

[0098] The relationship between the Bond number, G, and c may be provided by:

$$G = 0.5960 + 0.33c^{-2/3} + 0.19c^{-1} + O(c^{-4/3}) \quad (5)$$

[0099] As such, for a given Bond number, the bead diameter may be predicted. The obtained values may be in agreement with those found experimentally.

[00100] FIG. 16E is a plot of bead protrusion height (in micrometer or μm) as a function of viscosity (in Pascals seconds or Pa s) showing the relationship between dynamic viscosity and bead protrusion height of the bead according to various embodiments.

[00101] FIG. 17A shows (left) a fiber with beads according to various embodiments, and (right) the fiber with beads coated with a stretchable gold film according to various embodiments. Various active layers, i.e. electrically conductive layers, may be deposited on a platform of the fiber with beads, including stretchable carbon nanotubes layers or films, or stretchable gold layers or films.

[00102] FIG. 17B is a plot of normalized resistance change (i.e. ratio of resistance change over initial resistance, i.e. R/R_0) as a function of applied tensile strain (in percent or %) of a strain sensor according to various embodiments. The stretchability of the fiber-shaped stretchable strain sensor may reach about 125% or about 120%.

[00103] The strain sensor may also possess good linear response with applied strain. FIG. 17C is a plot of normalized resistance change (i.e. ratio of resistance change under strain over initial resistance, i.e. R/R_0) as a function of the number of cycles showing long term stability of the strain sensor according to various embodiments upon exposure to 5000 tensile strain cycles at an applied strain of 30%, with the inset showing a magnified view of the a portion of the response. The initial resistance may refer to the resistance of the sensor when the sensor is unstrained. The sensor may remain stable after more than 5000 strain cycles at 30% strain.

[00104] The initial resistance of the fiber may be monitored. FIG. 18A is a plot of resistance (in ohms or Ω) as a function of number of cycles showing the initial resistance change of the sensor according to various embodiments during the first few tensile strain cycles. The initial resistance may increase in the initial cycles, and may remain relatively constant after that.

[00105] The cyclic performance of the strain sensor under 50%, 100%, and 200% strain may also be investigated. FIG. 18B is a plot of normalized resistance change (i.e. ratio of resistance

change under strain over initial resistance, i.e. R/R_0) as a function of number of cycles showing performance of the strain sensor according to various embodiments under cyclic tensile strain of 50%. FIG. 18C is a plot of normalized resistance change (i.e. ratio of resistance change over initial resistance, i.e. R/R_0) as a function of number of cycles showing performance of the strain sensor according to various embodiments under cyclic tensile strain of 100%. FIG. 18D is a plot of normalized resistance change (i.e. ratio of resistance change over initial resistance, i.e. R/R_0) as a function of number of cycles showing performance of the strain sensor according to various embodiments under cyclic tensile strain of 120%. The sensor may show good stability for the different strain ranges.

[00106] Scanning electron microscopy (SEM) may also be employed to investigate the strain redistribution effect induced by the beads. FIG. 19A shows (above) a schematic of a strain sensor according to various embodiments, and (below) scanning electron microscopy (SEM) images corresponding to various areas of the strain sensor as indicated.

[00107] The beads may tune the strain distribution and may induce the strain concentration, which may further determine the crack distribution of the deposited gold film. The stretchable gold film may still be electrically conductive under large mechanical deformation. The underlying mechanism may relate to numerous randomly distributed initial nanocracks that develop into microcracks to release the applied tensile strain. These microcracks may be taken as the tracking signal for the surface strain distribution.

[00108] It may be observed from FIG. 19A that cracks indeed became longer and wider at the strain concentration areas compared to those found in areas exposed to a smaller strain. FIG. 19B is a plot of crack length (in micrometers or μm) as a function of number showing statistical analysis of the crack lengths of the sensor shown in FIG. 19A as well as a conventional fiber according to various embodiments. The dots indicate the crack lengths analyzed. The statistical analysis also confirmed that cracks in fibers with beads may become longer than those observed in fibers without beads. It may also be worth mentioning that the resistance change may be determined by the longest cracks that were more abundant in the fibers with beads. The resistance of the fiber may be modeled as a series circuit, and the resistance change of the fiber with beads may be much greater than the resistance change of the fiber without beads.

[00109] As a result, the fiber with beads may possess larger resistance change, i.e., higher gauge factor, than that without beads. FIG. 20A is a plot of normalized resistance change (i.e. ratio of resistance change under strain over initial resistance, i.e. R/R_0) as a function of strain (in percent or %) showing the resistance change of the gold coating on a conventional polydimethysiloxane (PDMS) fiber. FIG. 20B is a plot of gauge factor as a function of bead diameter (in micrometers or μm) showing the effect of the bead diameter on the strain sensitivity of a strain sensor according to various embodiments. The line may be the fitting line. FIG. 20C is a plot of gauge factor as a function of protrusion height (in micrometers or μm) showing the quantitative analysis of the effect of the bead diameter on the sensitivity of a strain sensor according to various embodiments. The inset formula may represent the fitting curve. Adj. R-Square represents the goodness of the fitting. A value near 1 may indicate good fitting.

[00110] Other stretchable conductive materials may also be applied for this sensitivity-enhanced platform to fabricate fiber-shaped sensors. For example, carbon nanotubes may be employed as the electrically conductive layer. FIG. 20D is a plot of normalized resistance change (i.e. ratio of resistance change under strain over initial resistance, i.e. R/R_0) as a function of time (in seconds or s) showing resistance changes with different strain cycles for strain sensors with stretchable carbon nanotube films according to various embodiments when tensile strain of 10% is applied to the strain sensors. FIG. 20E is a chart comparing the gauge factor of nanotube-coated fibers without beads and nanotube-coated fibers with beads according to various embodiments showing sensitivity enhancement of the nanotube-coated fibers with beads. As shown in FIG. 20E, the gauge factor for nanotube-coated fibers with beads may be increased to a value around 100.

[00111] The performance comparison of sensors according to various embodiments with other sensors recently reported is shown in FIG. 21. FIG. 21 is a table comparing strain sensor according to various embodiments (denoted with **) with several conventional sensors reported recently. The effect of bead spacing on the sensitivity may also be investigated. The sensitivity may significantly be enhanced with the decrease of the beads spacing. FIG. 22 is a plot of gauge factor as a function of bead spacing (in millimeters or mm) showing experimental data of the effect of bead spacing on the sensitivity of strain sensors according to various embodiments, with insets showing strain sensors having different bead spacings according to various embodiments.

[00112] With a decrease in the spacing between, the number of the beads on the fiber may increase, leading to an enhancement in the strain redistribution effect. The sensitivity of the strain sensor may be tuned by the elastic substrate or fiber. Moreover, since the strain may be tuned, any active material may be utilized to enhance the sensitivity. Various embodiments may provide an opportunity to tune the sensitivity by employing a hybrid approach where the supporting elastic substrate, i.e. the fiber and/or the beads, is different from the active material itself (i.e. the electrically conductive layer).

[00113] Various embodiments may provide a fiber-shaped stretchable strain sensor that can be used to monitor strain-induced during sports activity. A practical issue in wearable stretchable strain sensing may relate to proper strain transfer from the object (muscle/joint) to the sensor. The default hypothesis assumes that the object properly interfaces with stretchable strain sensor, and that the only issue worthwhile considering may be the sensitivity of the sensor.

[00114] However, the adaptability of the wearable sensor to the object upon deformation may also need to be considered to ensure that the strain is accurately transferred to the sensor to avoid the signal distortion. It may be difficult to obtain an accurate measurement when the strain transfer is poor. The interlocking effect between PDMS and textile (e.g., kinesiology tape) may provide a reliable adhesion mechanism that guarantees proper strain transfer. FIG. 23A is a plot of force (in newtons or N) as a function of tensile strain (in percent or %) showing results of an adhesion test between a polydimethylsiloxane (PDMS) film and the kinesiology tape, with the insets showing images of the setup and result of the test.

[00115] The PDMS precursor may be half-cured and then poured onto the porous fibrous textile. The mechanical test shows that the strength of the junction area of PDMS and textile may be greater than that of PDMS itself.

[00116] Moreover, the kinesiology tape may be a good candidate to support the stretchable strain sensor. It may adhere tightly and conformably to skin and may be insensitive to sweat. Data may be recorded wirelessly using the sensor integrated with a customized circuit or chip. FIG. 23B shows images of (top right) a monitoring device including a stretchable strain sensor attached to a kinesiology tape according to various embodiments, (top left) the monitoring device according to various embodiments adhered onto a joint of the lower limb for monitoring, (bottom right) the monitoring device according to various embodiments during operation when the person is

squatting, and (bottom left) the monitoring device according to various embodiments during operation when the person is standing. The kinesiology tape may be used to support the strain sensor, and may adhere to the skin quite tightly and comfortably, and may be insensitive to sweat. FIG. 23D shows an image of a customized circuit included in the monitoring device according to various embodiments to monitor leg lifting exercises (FIG. 23C left) when the legs are at rest, and (FIG. 23C right) when the legs are lifted. The customized circuit may be electrically connected to the strain sensor. The customized circuit may include a main controller, a sensor interface, a program interface, a Bluetooth module, a working indicator, a regulator, and a power supply. FIG. 23E is a plot of normalized resistance change (i.e. ratio of resistance change under strain over initial resistance, i.e. R/R_0) as a function of time (in seconds or s) showing data obtained by the strain sensor according to various embodiments during slow squatting and fast squatting. The circuit may alternatively be referred to as a power management module.

[00117] FIG. 23F is a plot of normalized resistance change (i.e. ratio of resistance change under strain over initial resistance, i.e. R/R_0) as a function of time (in seconds or s) showing data obtained by the strain sensor according to various embodiments during slow leg lifting and fast leg lifting.

[00118] The strain change of the monitoring device may correspond to the leg bending angle. FIG. 24A is a schematic illustrating the leg bending angle θ. The leg bending angle may switch between a first value θ_1 and a second value θ_2. FIG. 24B is a plot of normalized resistance change (i.e. ratio of resistance change under strain over initial resistance, i.e. R/R_0) as a function of bending cycle illustrating the resistance change of the strain sensor according to various embodiments in relation to the bending cycle.

[00119] An advantage of fiber-shaped stretchable strain sensor over the flat-film strain sensor is that the fiber-shaped stretchable strain sensor may be more conveniently weaved into the clothes.

[00120] FIG. 25 shows an optical image of a fiber-shaped strain sensor according to various embodiments that is weaved into clothes. The stretchable strain sensor shown in FIG. 25 may be weaved into a piece of elastic clothing by hand, and may function as a wearable sensor. Bending actions may then be monitored by wearing the clothing,

[00121] Fiber-shaped sensors may be of importance to the development of wearable electronics as the sensors may be weaved into clothes directly based on well-developed textile machinery, which may facilitate low-cost and large-scale manufacturing processes of wearable electronics. In

addition, the strain sensor may cooperate with other sensors, like acceleration sensors and temperature sensors, to realize full monitoring of sports activities. The fiber-shaped sensors may be further integrated with other fiber-shaped batteries/supercapacitors to achieve the smart textile in the near future for potential healthcare, rehabilitation and sports monitoring, and so forth.

[00122] Various embodiments may relate to surface strain redistribution through delicate structure designs to enhance the sensitivity of the fiber-shaped stretchable strain sensor. Various embodiments may relate to a beads-on-fiber stretchable strain sensor based on the principle of Plateau–Rayleigh instability. Various embodiments may relate to a method including thermal transient curing to achieve large-scale PDMS fiber fabrication. The fiber diameter and the diameter uniformity along the length direction may be well controlled.

[00123] Various embodiments may relate to a fiber-shaped stretchable strain sensor can be reliably used to monitor the sports activities. The sensitivity of the fiber-shaped stretchable strain sensor may be further enhanced, and other thermosetting polymer based fiber sensors may be be fabricated. Moreover, surface strain redistribution may be independent of the active materials utilized and may open up a new perspective of the sensitivity enhancement. Surface strain redistribution may also be applied to non fiber-shaped stretchable strain sensors.

[00124] Definition Of Gauge Factor

Gauge factor (GF) may be defined as:

$$GF = \frac{\Delta R/R_0}{\Delta \varepsilon} \quad (6)$$

where ΔR is the resistance change induced by the strain $\Delta \varepsilon$ applied, and R_0 is the initial resistance.

[00125] PDMS Microfibers Fabrication

[00126] Generally speaking, for thermoplastic polymers, it may be convenient to employ the micro-jetting method to produce fibers from the polymer melt. However, PDMS cannot be melted and jetted. Molding is an alternative method, but it may be difficult to fabricate microfibers with millimeter length at reasonable cost. Inspired by Ramen, a traditional noodle processing methodology may be employed to fabricate micro fibers in large quantities.

[00127] There are three typical procedures to prepare Ramen noodles: dough preparation, traction by hand/machine, and cooking in boiling water. The physical concepts behind each of them are: proper viscosity adjustment, dynamic application of traction strain, and transient curing

(see FIGS. 8A, 9). Herein, a pre-curing method may be used to obtain the proper viscosity, followed by applying traction strain and then transient curing.

[00128] In detail, the initial PDMS precursor may not have any special shape before the dynamic traction process to fabricate micro fibers. The method may be a mold-free method.

[00129] A mixture may be formed from PDMS 184 (Sigma Aldrich) elastomer kit having a ratio of monomer : cross-linker of 1: 10. The mixture may be deformed in vacuum, and may be pre-cured in an oven at a temperature of about 60° for around 25 minutes, and may be kept in room temperature for different periods of time to obtain mixtures of different viscosities.

[00130] In various embodiments, 15 g of the mixture may be poured into a small chamber first. An identical chamber may be used for fabrication each time, as the boundary of the viscous mixture may affect the fiber formation during the traction. After adjusting or controlling the viscosity of the mixture, a stick with the diameter of 2 mm may be inserted about 5 mm deep into the liquid mixture, followed by lifting out to around 10 mm above the liquid surface. Another stick may be used to catch the lower part and the traction was applied between these two sticks. The viscosity range for the mixture may be around 40 to 80 Pa·s. If the viscosity is too low or too high, it may be difficult to form the fiber.

[00131] The PDMS precursor may be stretched in a short time of less than 4 seconds for uniformity. Then, the PDMS precursor fiber formed from the mixture may be put or introduced into a hot silicone oil bath. The cross-section of the fiber may automatically become a quasi-circular shape (FIGS. 8B-C). The more uniform the temperature field of the silicone oil, the better the quality of the fiber. The micro fibers may be cured within 5 seconds in the hot oil, and difference in the temperature field may induce different thermal expansion within the fiber, thus leading to abnormal deformation.

[00132] The fiber may be removed from the hot oil after a few seconds, followed by washing using daily-used cleaning fluid and deionized (DI) water. The fibers may be immersed in DI water overnight and may then be dried in a 60° oven.

[00133] A difference between the Ramen approach and the method of forming a fiber according to various embodiments is that boiling water cannot be used for curing of PDMS as boiling water

may affect the fiber structure. In addition, PDMS or PDMS precursor may be intrinsically hydrophobic, making it difficult to fully immerse the PDMS or PDMS precursor in hot water.

[00134] Instead, silicone oil (170 - 180 °C) may be used for transient curing. Silicone oil has slightly lower density than PDMS, but the boiling point of silicone oil may be much higher than water. Silicone oil may be compatible with PDMS or PDMS precursor, and may be removed easily using normal detergents.

[00135] Fabrication Of Beads Onto Fibers

[00136] The viscosity tuning process of the mixture including the PDMS precursor may be the same with that described in the fabrication of the fiber. The fibers may be immersed into the mixture for a few seconds and may then be suspended vertically along the length direction. After tens of seconds, beads may appear. The fiber with beads may be put into the hot oil following the same process described before. The beads diameter may be further regulated by using the PDMS precursor with different viscosities.

[00137] Fabrication of Stretchable Gold Film Or Carbon Nanotube Film Over Fiber

[00138] One example of an active layer which may be provided over the fiber with beads is a stretchable gold film or layer. The fiber with beads may be placed in a chamber for evaporation of gold over the fiber with beads. There may be no advanced treatment or pre-treatment to the fiber before placing of the fiber in the chamber. The thermal evaporation speed may be around 0.9 Å/s, and the film thickness may be about 80 nm. The film may include initial nano cracks without strain applied. These nano cracks may grow into micro cracks releasing the strain in the first strain cycle. Then subsequently, micro cracks may open and close during subsequent strain cycles, inducing the resistance changes, while achieving the stretchability of the gold film.

[00139] Another example of an active layer may be a stretchable carbon nanotube film. The single-walled carbon nanotubes (SWCNTs) modified with carboxylic acid may be purchased from Carbon Solution, Inc. The SWCNTs may easily dissolve in the deionized water under ultrasound. The concentration of the SWCNTs used here may be 2 g L^{-1}. After oxygen plasma modification, the fiber may be ready to be dropped with the CNT solution. Then, after drying at the room temperature, the fiber with beads coated with the SWCNTs may be put into oven overnight. The CNT film may follow similar principles as the gold firm to achieve the stretchability. MTS model

42 may be employed to apply the tensile strain. A liquid metal alloy (gallium-indium eutectic, Aldrich) may be used as the wire bonding adhesive to bond copper wires with the CNT film. The copper wires may electrically connect the CNT film with a measuring instrument. Keithley 4200-SCS may be used to do the measurement by using the sampling rate of 125 samples per second.

[00140] Demonstration of the fiber sensor in textile

The textile was purchased in a sports shop and may be initially used for the elbow protection. Some textile fibers may be replaced by our beads-on-fiber (i.e. fiber with beads) stretchable strain sensors. The replacement process may require the careful operation and the integrated customized chip may be coupled or connected with the sensor to wirelessly collect the data.

[00141] Simulation Of Viscous Catenary

[00142] The simulation was conducted by using software *COMSOL* following the solution reported (see FIGS. 5, 19A). The fiber may be taken as a standard cylinder with 0.6 mm in diameter and 15 mm in length. The PDMS precursor may be taken as a Newtonian fluid with uniform density of 965 kg m^{-3}. The viscosity may be set to 60 Pa·s and the surface tension coefficient may be set to 20 mN/m.

[00143] Fixed boundary conditions may be applied to two ends of the cylinder and the applied force may be gravitational force. In order to show the uniformity quantitatively by experiment, the normalized fiber diameter may set as

$$N = R_1/R_2 \quad (7)$$

where R_1, R_2 are the fiber diameters of the different positions along the same fiber. The first position corresponding to R_1 may be located at a point with distance of 1/4 length of the whole fiber from the left, and the second position corresponding to R_2 may be located at a point with distance of 1/2 length of the whole fiber from the left (see FIG. 13A). Therefore, if N differs significantly from 1, the fiber may not be uniform. FIG. 13B shows that in the first several seconds after the traction, the uniformity of the fiber may be quite good, but may worsen dramatically after that, which may be due to the low viscosity of the PDMS precursor.

[00144] Fitting models and Theoretical Prediction

The formula fitted to predict the fiber diameter (R) based in dynamic viscosity (see FIG. 11B) may be provided by:

$$R = 505.8 - 19.34v + 0.3v^2 \quad (8)$$

where R is the diameter of the fiber, and v is the viscosity of the PDMS precursor.

[00145] The formula fitted to predict the value of gauge factor (GF) by bead diameter (see FIG. 20B) may be provided by:

$$GF = 10.43 + 0.025(D - 250) \quad (9)$$

where D is the diameter of the bead, and GF is the gauge factor.

[00146] In relation to the theoretical prediction of the bead diameter, the surface tension γ as given in Equation (2), may be provided by:

$$\gamma = Aexp(-\frac{B}{\eta}) \quad (10)$$

where A and B are constants, and η is the viscosity.

[00147] Equation (10) may be used in the computation of G in Equation (2), and further H_{max} in Equations (4) and (5). Constants A and B for PDMS precursor may be easily determined by using tested two sets of values of (η_1, γ_1), (η_2, γ_2). Herein, the viscosity of PDMS precursor may be measured by using Brookfield DV3T and the surface tension by Dataphysics OCA 15Pro.

[00148] Method To Do Statistic Analysis Of The Crack Length

[00149] The crack length may be obtained from SEM images by using the open-code image analyzing software, *ImageJ* (download link: https://imagej.net/Downloads). There are different versions for different platforms. ImageJ 1.50b may be used for Windows. The method to obtain crack length statistics may be as follows:

1. Open the software. FIG. 26A shows an image of the opened software.
2. Open an SEM image and then draw a straight line according to the scale bar of the SEM image to set the scale for the software. FIG. 26B shows an SEM image being opened in the software.
3. Draw one curve along one crack and then click "Measure". The software would calculate the crack length automatically. FIG. 26C shows an image of the software with "Measure" being clicked to measure the length of the curve that has been drawn.

[00150] Mechanism Of Microcracks

[00151] The mechanism of stretchability may be explained by randomly-distributed microcracks. For a gold film with initial randomly distributed nano defects, randomly-distributed

micro cracks may be developed or grown based on the initial defects when the film is under tensile strain. The gold film may develop into inter-connected gold micro-islands. If further tensile strain is applied, these microcracks may further propagate, but the conductive network may remain. The film may achieve stretchability while remaining electrically conductive, until a crack develops through the film (throughout crack) and completely divides or breaks the film.

[00152] FIG. 27A is a schematic showing a gold film according to various embodiments with randomly distributed initial defects. FIG. 27B is a schematic showing the gold film in FIG. 27A according to various embodiments with randomly-distributed micro cracks after strain is applied. FIG. 27C is a schematic showing the gold film in FIG. 27B according to various embodiments with the further crack propagation pattern after further strain is applied.

[00153] FIG. 28A is a scanning electron microscopy (SEM) image of the gold film according to various embodiments with randomly distributed initial defects without any strain applied. FIG. 28B is another scanning electron microscopy (SEM) image of a portion of the gold film over a neck portion of the bead according to various embodiments under strain of 80%. FIG. 28C is yet another scanning electron microscopy (SEM) image of a strain concentrated area of the gold film according to various embodiments.

[00154] In a previous study, an electrochemical method may be used to seal the initial nano defects by platinum. The crack density may decrease significantly under the same strain, and many throughout cracks may form, causing the film lose stretchability.

[00155] Therefore, the crack density may be determined by the initial nano defects, not by the strain.

[00156] Statistic analysis on the width of the gold micro-islands at the strain concentration area and the normal fiber area may also be carried out. FIG. 29A is a chart comparing the width of the gold micro-islands in a strain concentrated area and the width of the gold micro-islands in a normal area of a gold film according to various embodiments. The analysis shows little difference in the width of the micro-islands in the strain concentration area and the normal fiber area.

[00157] The analysis may appear to indicate that there is little change in the crack density, because if the crack density increases significantly, the width of the micro-islands should decrease a lot. The further strain applied in the metal film may mainly increase the length of the cracks.

[00158] The further strain applied may increase a length of the cracks but may not generate new micro cracks.

[00159] A simulation of the strain distribution in a gold film with a crack on PDMS may be carried out using finite element modeling. An elastic model may be employed in order to simplify the system. The tensile strain may be applied at two ends of the PDMS substrate. FIG. 29B shows a simulation image of a crack-induced strain concentration of a gold film according to various embodiments. From the strain distribution in the gold film shown in FIG. 29B, the strain concentration at the crack tip may be almost two orders of magnitude higher than the strain at other locations. Also, the strain concentration area may be nearby the crack tip, indicating that for a further strain applied, the crack tip may be affected much more significantly and the crack may further propagate. Therefore, microcracks in a strain concentration area may tend to combine into longer cracks at this area (see FIG. 28C and FIG. 19A).

[00160] While the invention has been particularly shown and described with reference to specific embodiments, it should be understood by those skilled in the art that various changes in form and detail may be made therein without departing from the spirit and scope of the invention as defined by the appended claims. The scope of the invention is thus indicated by the appended claims and all changes which come within the meaning and range of equivalency of the claims are therefore intended to be embraced.

CLAIMS

1. A strain sensor comprising:

   a fiber;

   a plurality of microstructures along the fiber; and

   an electrically conductive layer in contact with the fiber and the plurality of microstructures.

2. The strain sensor according to claim 1,

   wherein the plurality of microstructures are microbeads.

3. The strain sensor according to claim 1 or claim 2,

   wherein the fiber comprises a polymer.

4. The strain sensor according to claim 3,

   wherein the polymer comprised in the fiber is polydimethylsiloxane (PDMS).

5. The strain sensor according to any one of claims 1 to 4,

   wherein the plurality of microstructures comprises a polymer.

6. The strain sensor according to claim 5,

   wherein the polymer comprised in the plurality of microstructures is polydimethylsiloxane (PDMS).

7. The strain sensor according to any one of claims 1 to 6,

   wherein the electrically conductive layer comprises gold, carbon nanotubes, silver, or platinum.

8. The strain sensor according to any one of claims 1 to 7,

   wherein a gauge factor of the strain sensor is greater than 25.

9. The strain sensor according to claim 8,
wherein the gauge factor of the strain sensor is greater than 80.

10. A method of forming a strain sensor, the method comprising:
forming a plurality of microstructures along a fiber; and
forming an electrically conductive layer in contact with the fiber and the plurality of microstructures.

11. The method according to claim 10,
wherein forming the plurality of microstructures along the fiber comprises:
immersing the fiber in a mixture comprising a polymer precursor;
removing the fiber from the mixture comprising the polymer precursor with droplets of the polymer precursor in contact with the fiber; and
introducing the fiber into heated oil so that the droplets form the plurality of microstructures.

12. The method according to claim 10 or claim 11, further comprising:
forming the fiber.

13. The method according to claim 12,
wherein forming the fiber comprises:
mixing a predetermined ratio of a further precursor and a cross linker to form a mixture comprising the further polymer precursor and the cross linker;
stretching an amount of the mixture; and
introducing the amount of stretched mixture into heated oil to form the fiber.

14. The method according to any one of claims 10 to 13,

wherein forming the electrically conductive layer comprises evaporating electrically conductive material onto the fiber and the plurality of microstructures.

15. The method according to claim 14,

wherein the electrically conductive material is gold.

16. The method according to any one of claims 10 to 13,

wherein forming the electrically conductive layer comprises:

introducing the fiber with the plurality of microstructures to a mixture comprising an electrically conductive material so that the fiber with the plurality of microstructures is coated with the electrically conductive material; and

heating the coated fiber with the plurality of microstructures to form the electrically conductive layer.

17. The method according to claim 16,

wherein forming the electrically conductive layer further comprises:

exposing the fiber with the plurality of microstructures to oxygen plasma before introducing the fiber with the plurality of microstructures to the mixture comprising the electrically conductive material.

18. The method according to claim 16 or claim 17,

wherein the electrically conductive material is carbon nanotubes.

19. The method according to claim 18,

wherein the carbon nanotubes are modified with an acid.

20. A method of operating a strain sensor, the method comprising:

attaching a strain sensor according to any one of claims 1 to 9 to an object; and

determining a change in electrical resistance of the strain sensor due to a strain of the object.

21. The method according to claim 20,

wherein the strain is determined based on the change in the electrical resistance of the strain sensor.

FIG. 1

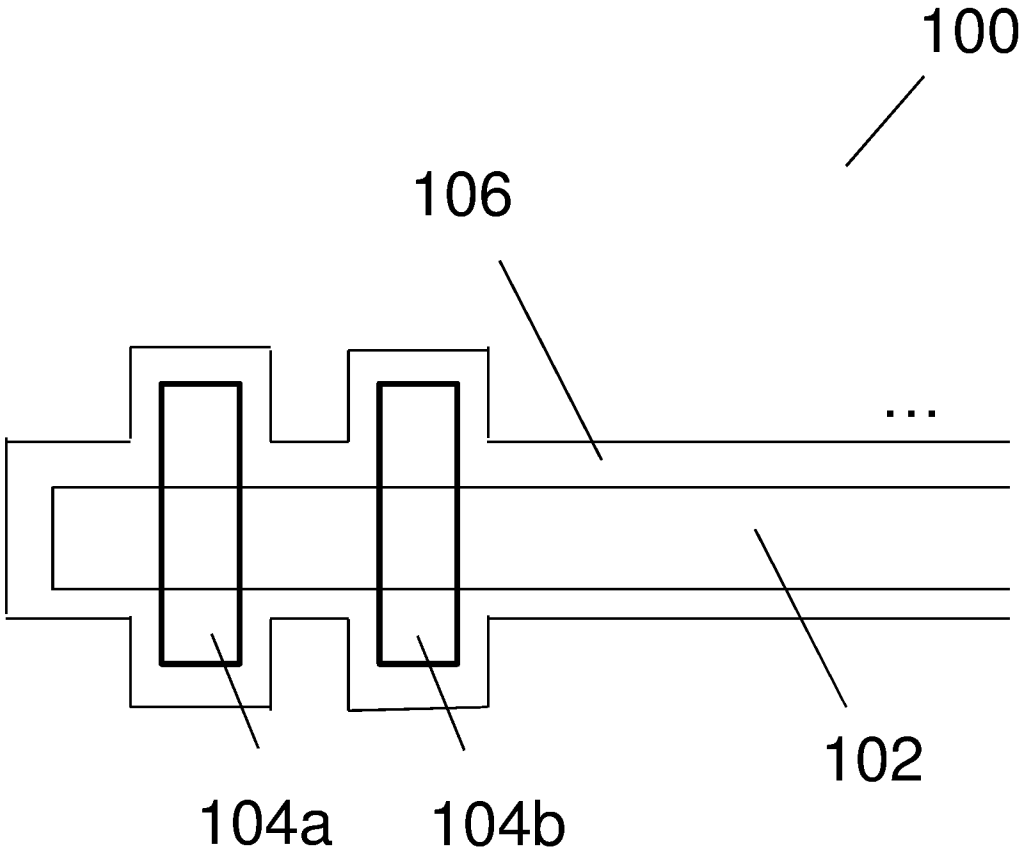

FIG. 2

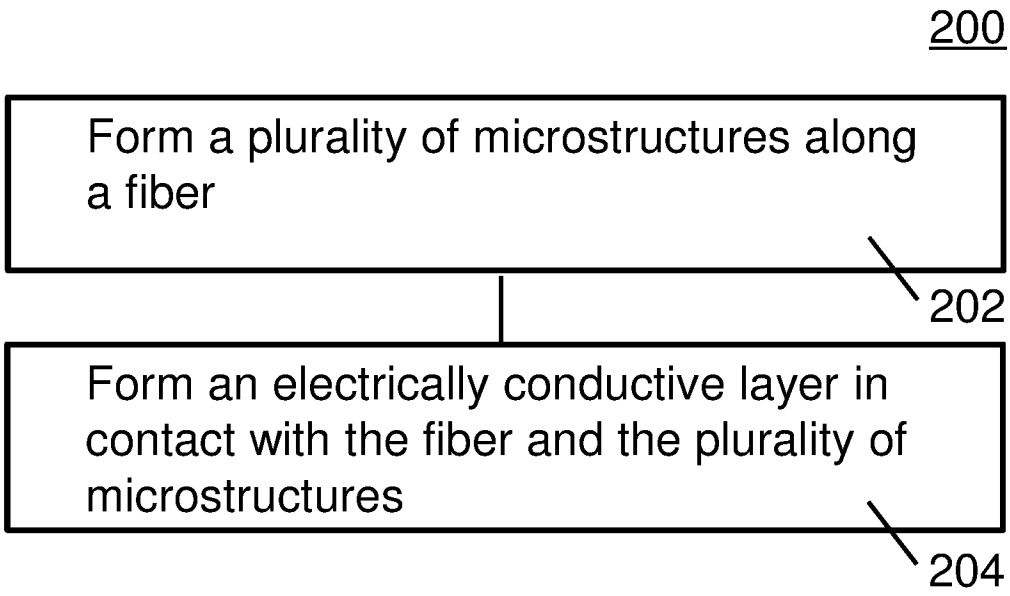
200
Form a plurality of microstructures along a fiber
202
Form an electrically conductive layer in contact with the fiber and the plurality of microstructures
204

FIG. 3

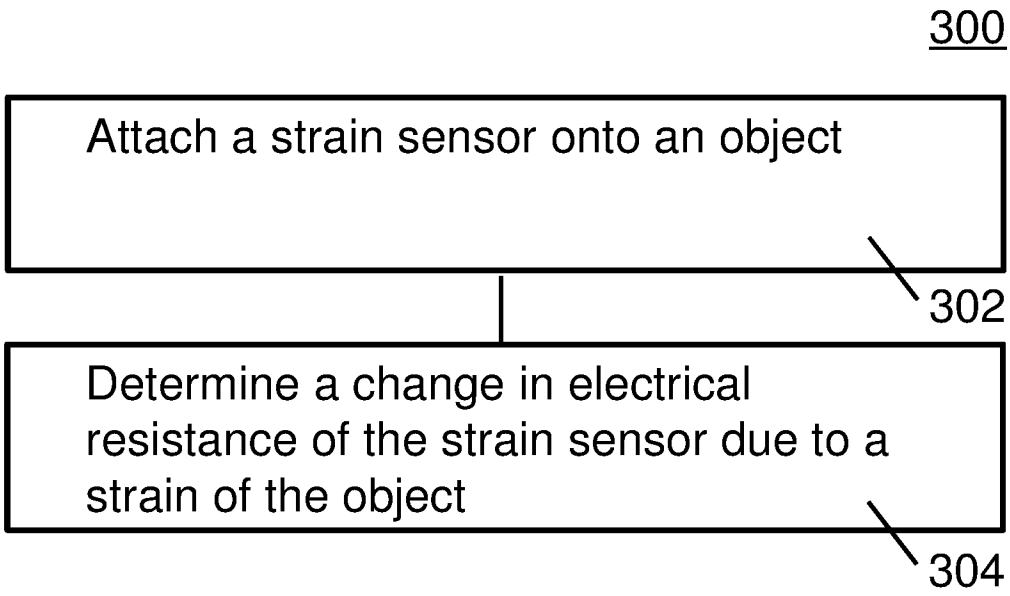
300
Attach a strain sensor onto an object
302
Determine a change in electrical resistance of the strain sensor due to a strain of the object
304

FIG. 4A

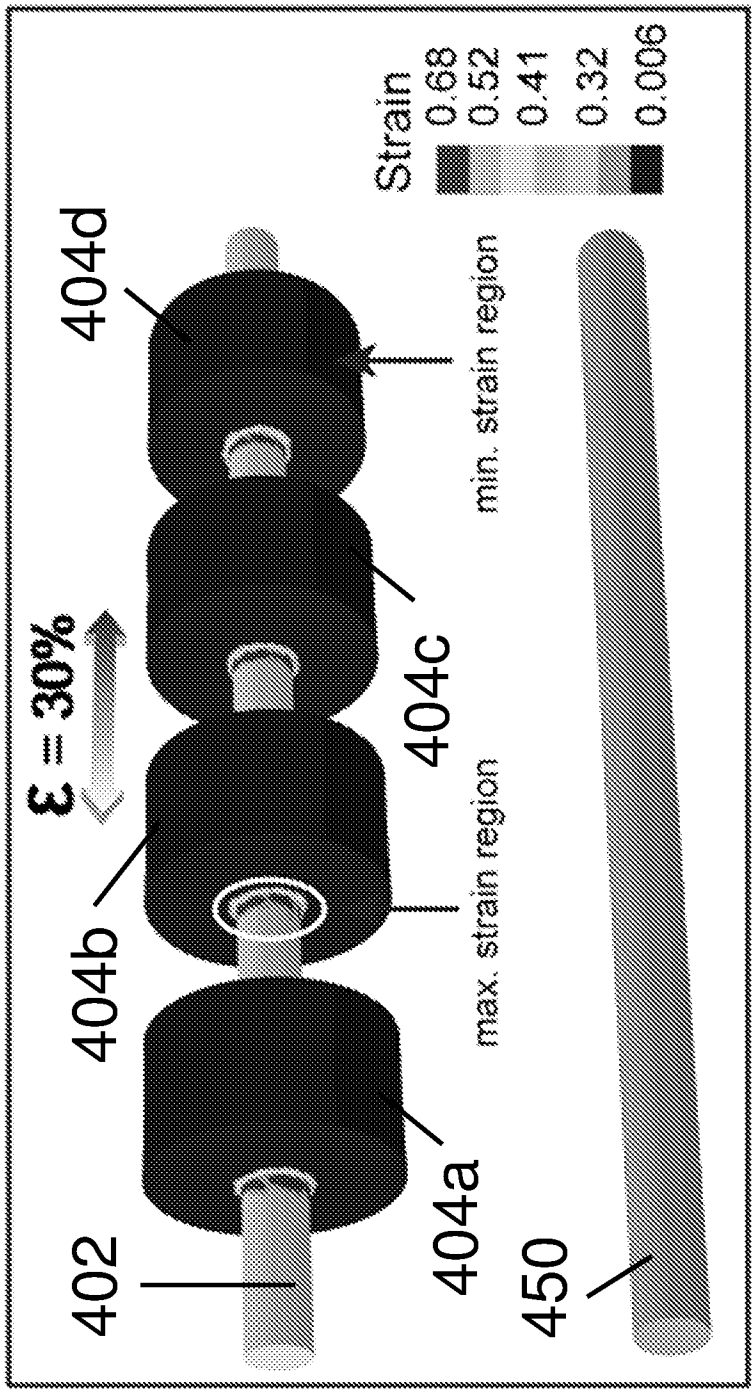
Strain
0.68
0.52
0.41
0.32
0.006
404d
min. strain region
ε = 30%
404c
404b
max. strain region
402
404a
450

FIG. 4B

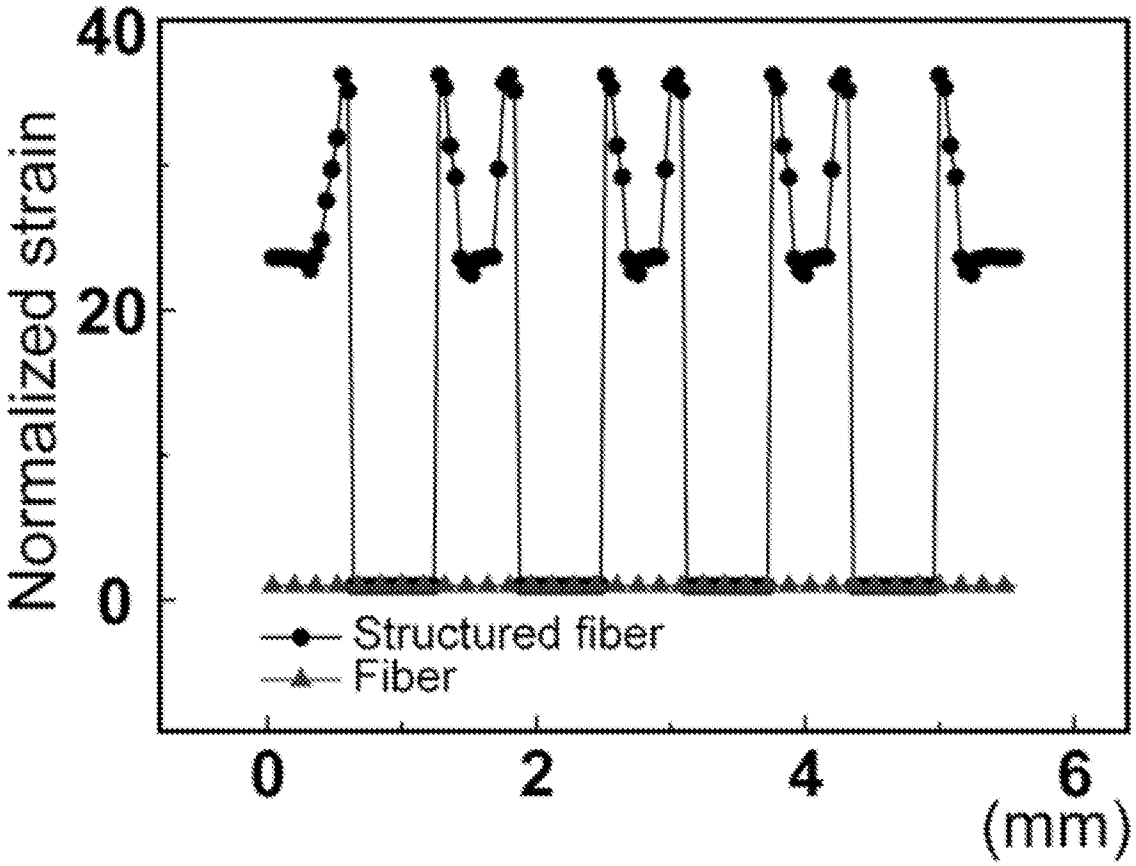

FIG. 5

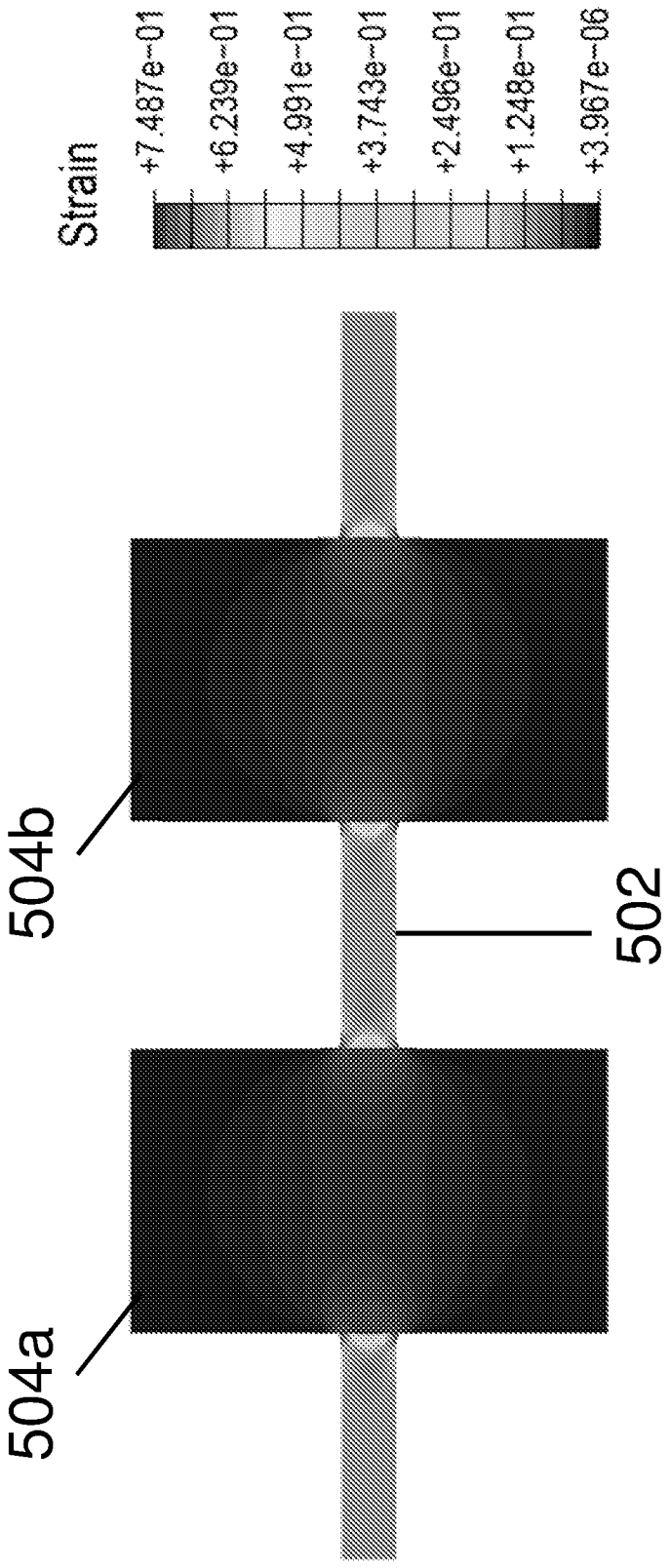
Strain
+7.487e-01
+6.239e-01
+4.991e-01
+3.743e-01
+2.496e-01
+1.248e-01
+3.967e-06
504b
502
504a

FIG. 6

Active Materials	Substrate	Methods to enhance sensitivity
Gold**	PDMS	Surface strain redistribution
CNTs**	PDMS	Surface strain redistribution
CNT	PDMS	Not shown
AgNPs	PDMS	Not shown
AgNWs	PDMS	Not shown
CNT &PEDOT	PU	Active materials design
AgNWs	PDMS	Active materials design
CNT	PDMS	Active materials design
Carbon grease	Ecoflex	Not shown
AgNPs/graphene	TPU	Active materials design
Carbon	PDMS	Active materials design
Graphene	PDMS	Active materials design
Silver	3M elastomer	Not shown
ZnO NWs	PDMS	Active materials design
CNT fiber	Ecoflex	Active materials design
Pt-coated nanofibers	PDMS	Active materials design

** This work

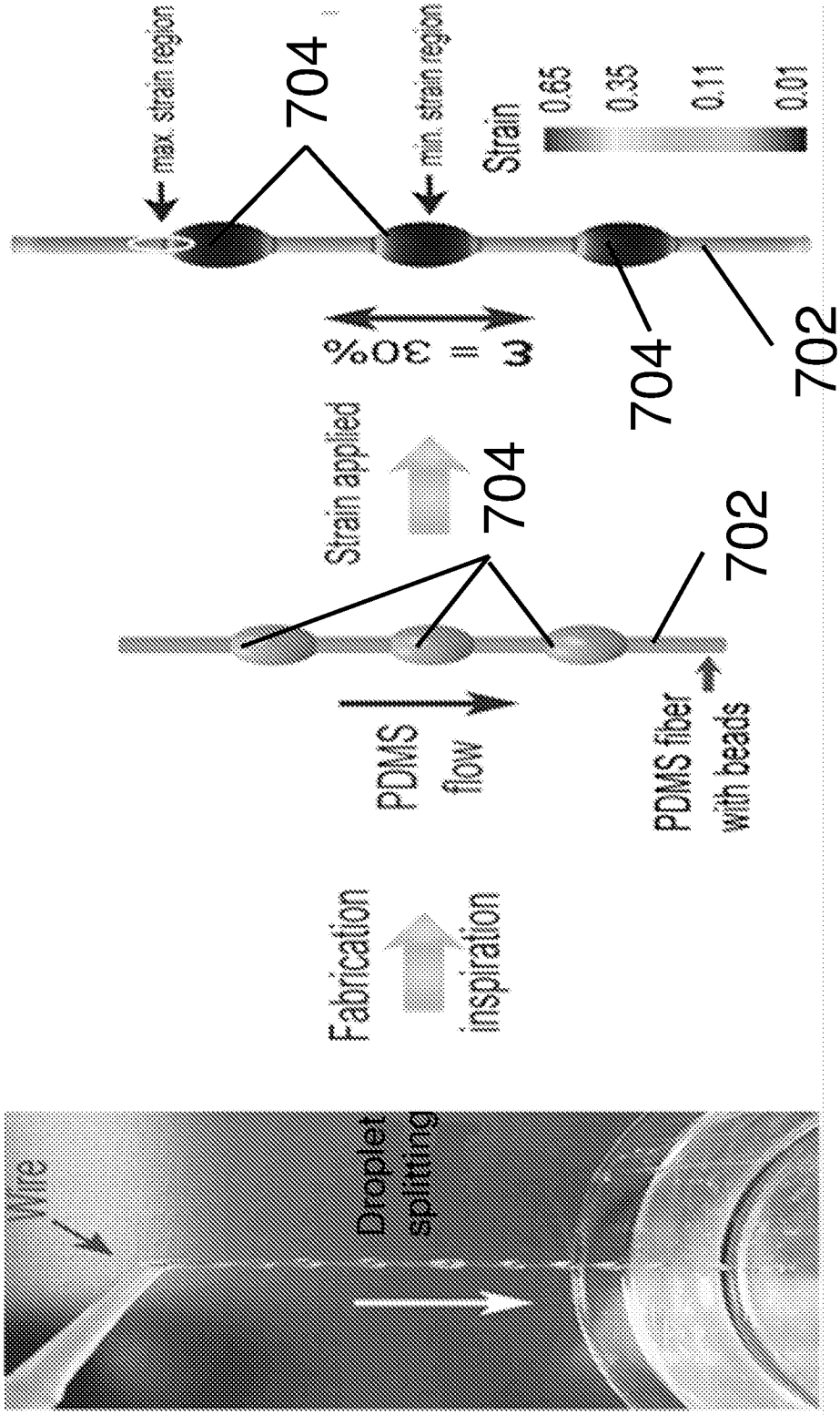
Wire
Droplet splitting
Fabrication
inspiration
PDMS flow
PDMS fiber with beads
702
704
Strain applied
%0ε = ω
704
702
max. strain region
min. strain region
704
Strain
0.65
0.35
0.11
0.01

FIG. 7

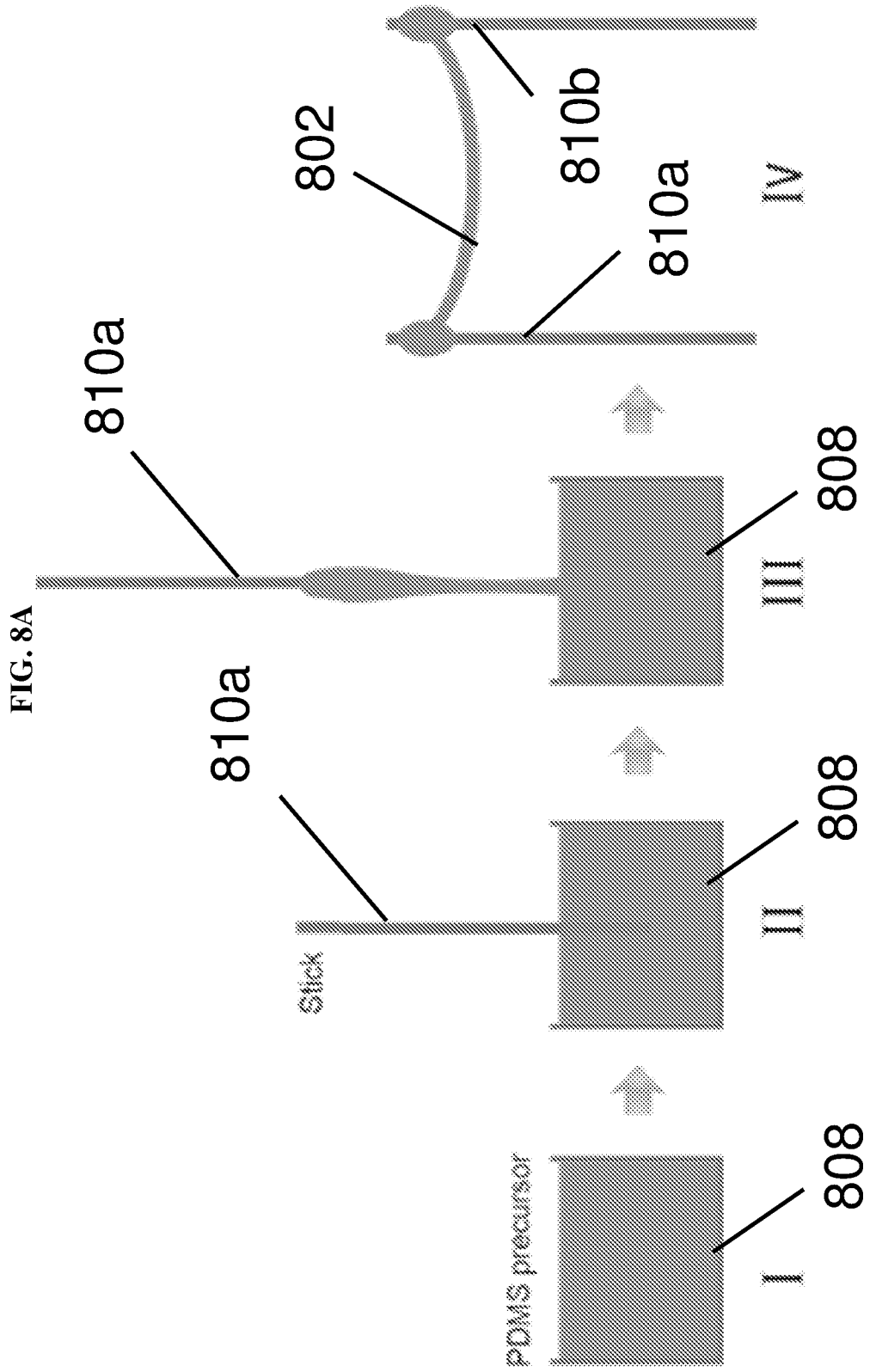
PDMS precursor
808
I
Stick
810a
808
II
810a
808
III
810a
802
810b
810a
IV

FIG. 8A

FIG. 8B

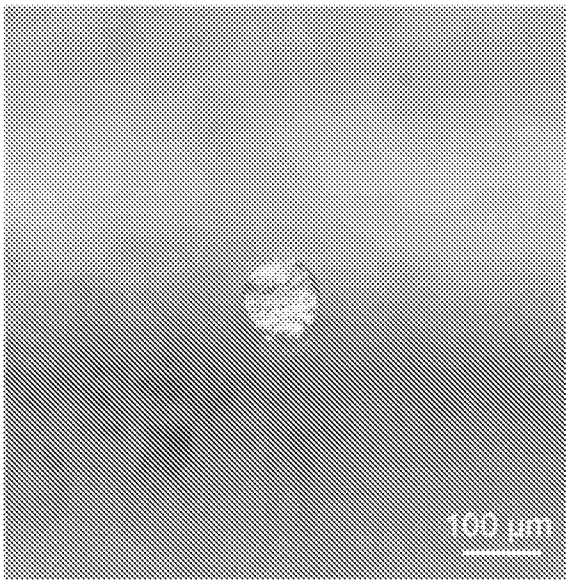

FIG. 8C

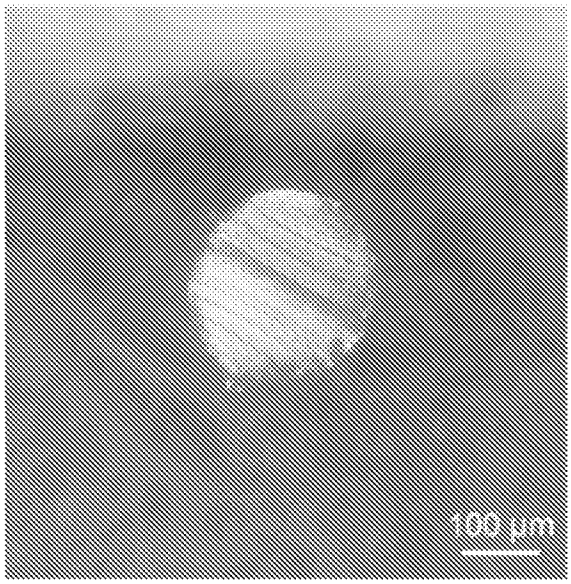

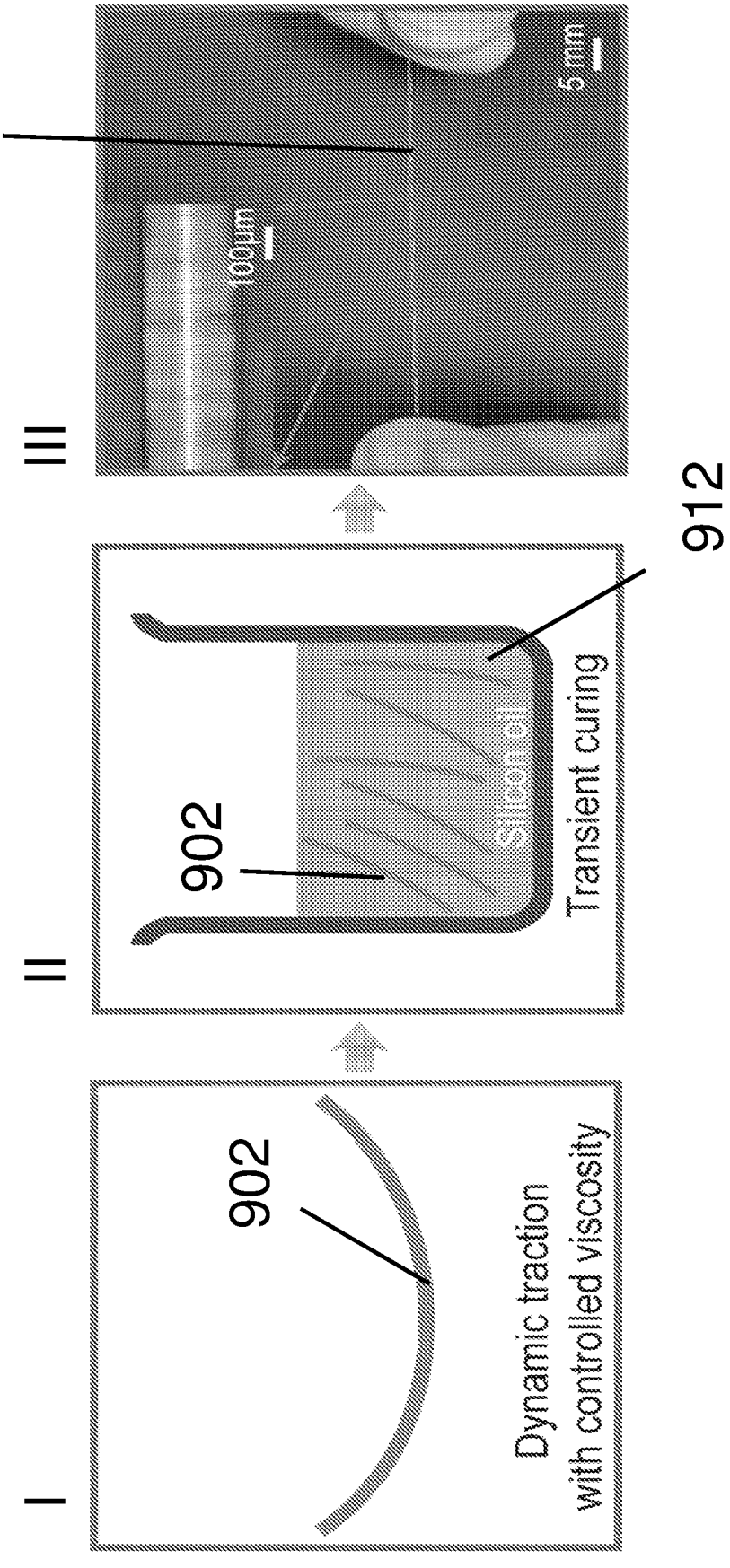
I
902
Dynamic traction
with controlled viscosity
II
902
Silicon oil
Transient curing
912
III
902
100μm
5 mm

FIG. 9

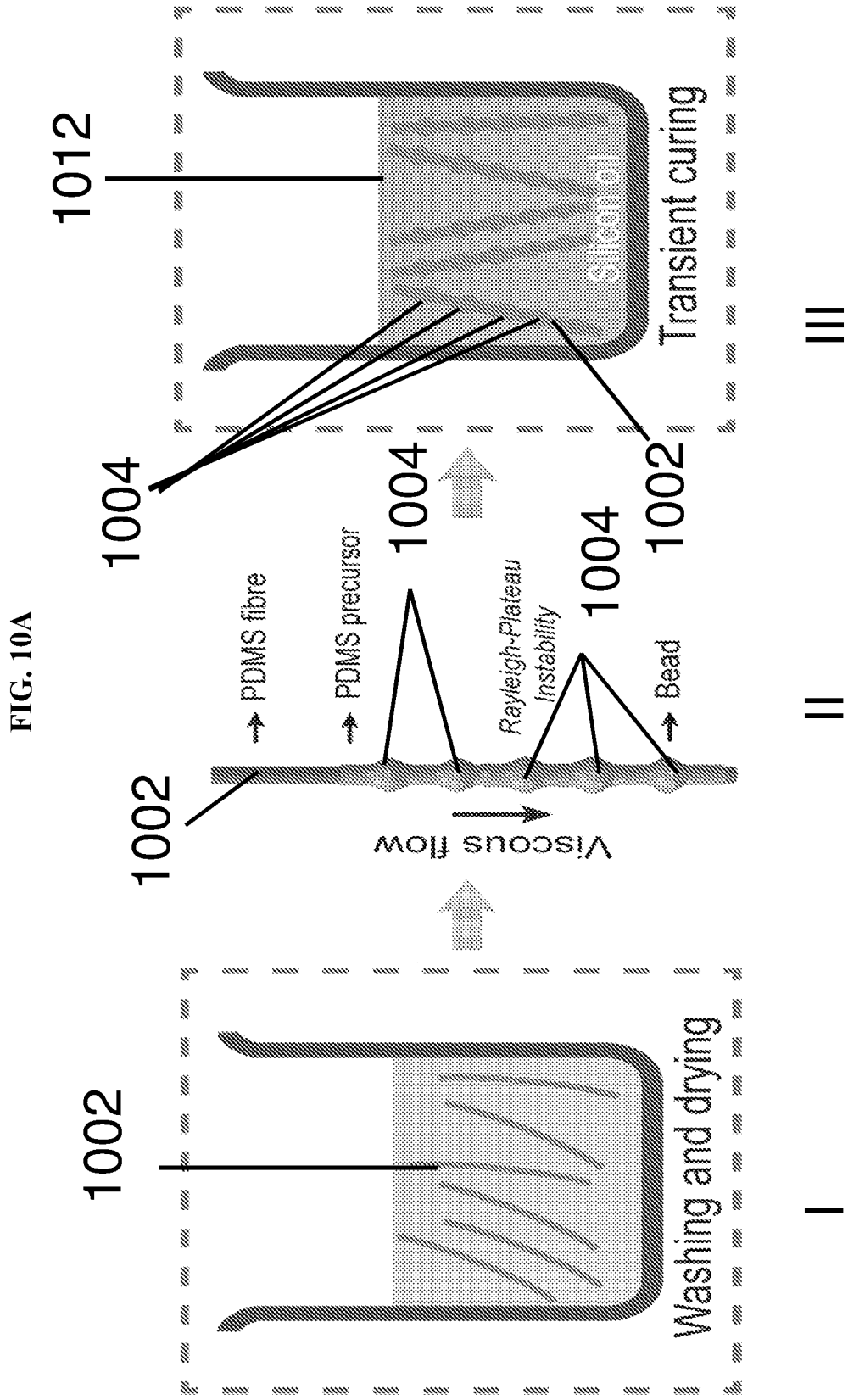
1012
Transient curing
Silicon oil
1004
1002
PDMS fibre
PDMS precursor
1004
Rayleigh-Plateau Instability
1004
1002
Bead
Viscous flow
1002
Washing and drying
I
II
III

FIG. 10A

FIG. 10B

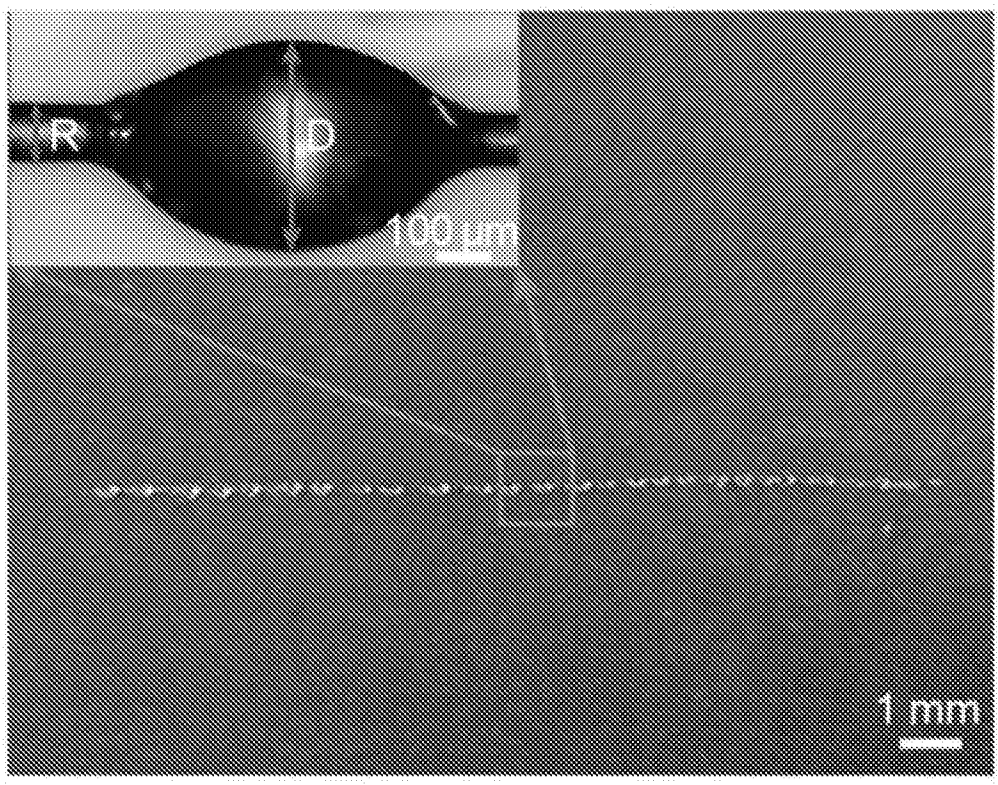

FIG. 11A

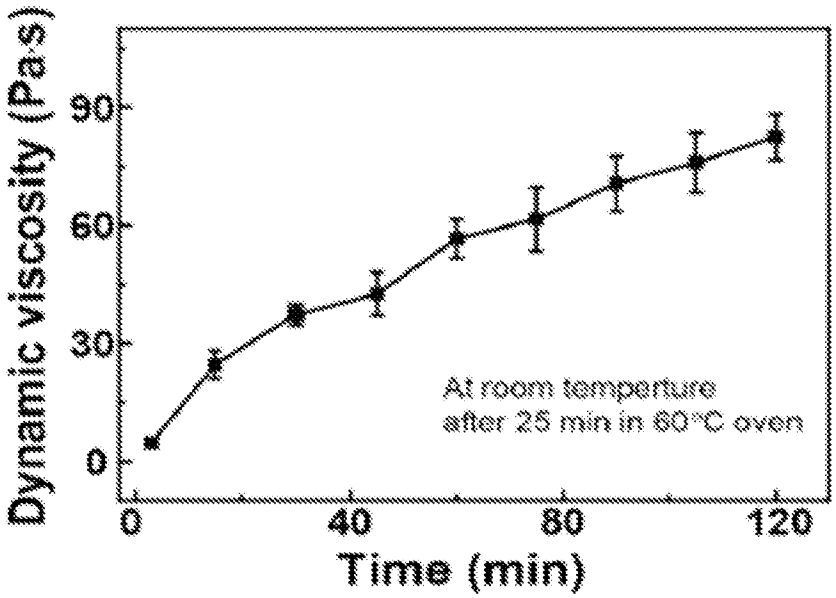

FIG. 11B

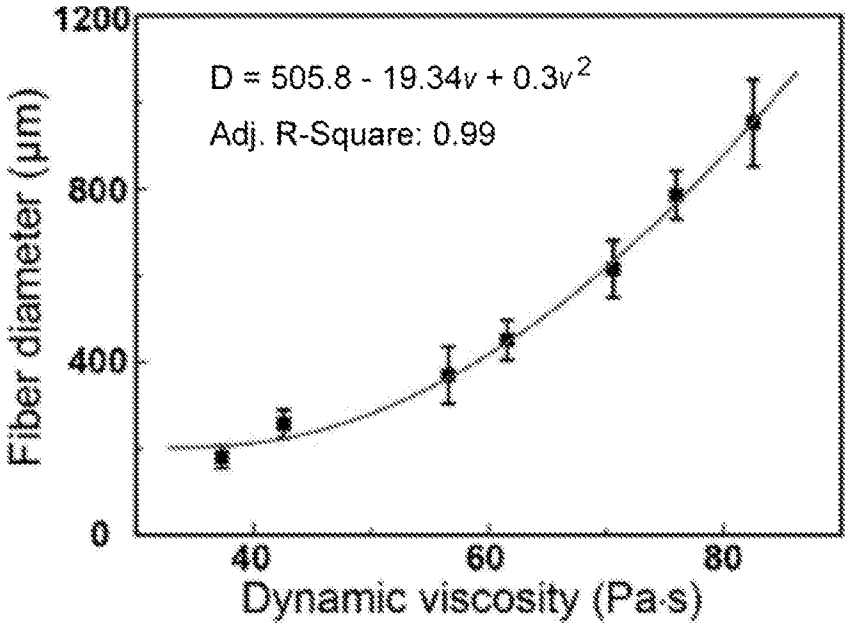

FIG. 12A

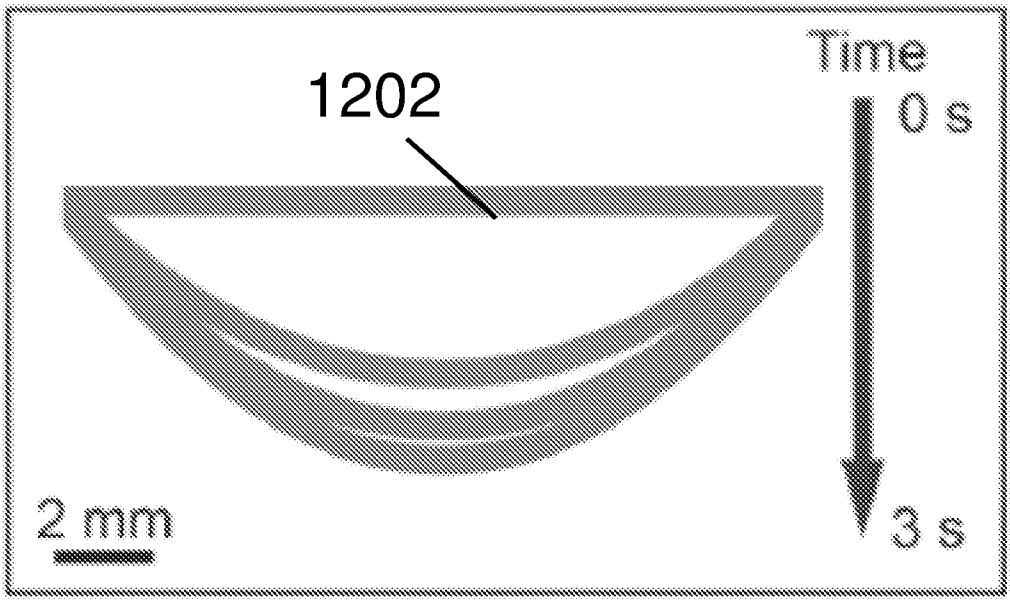

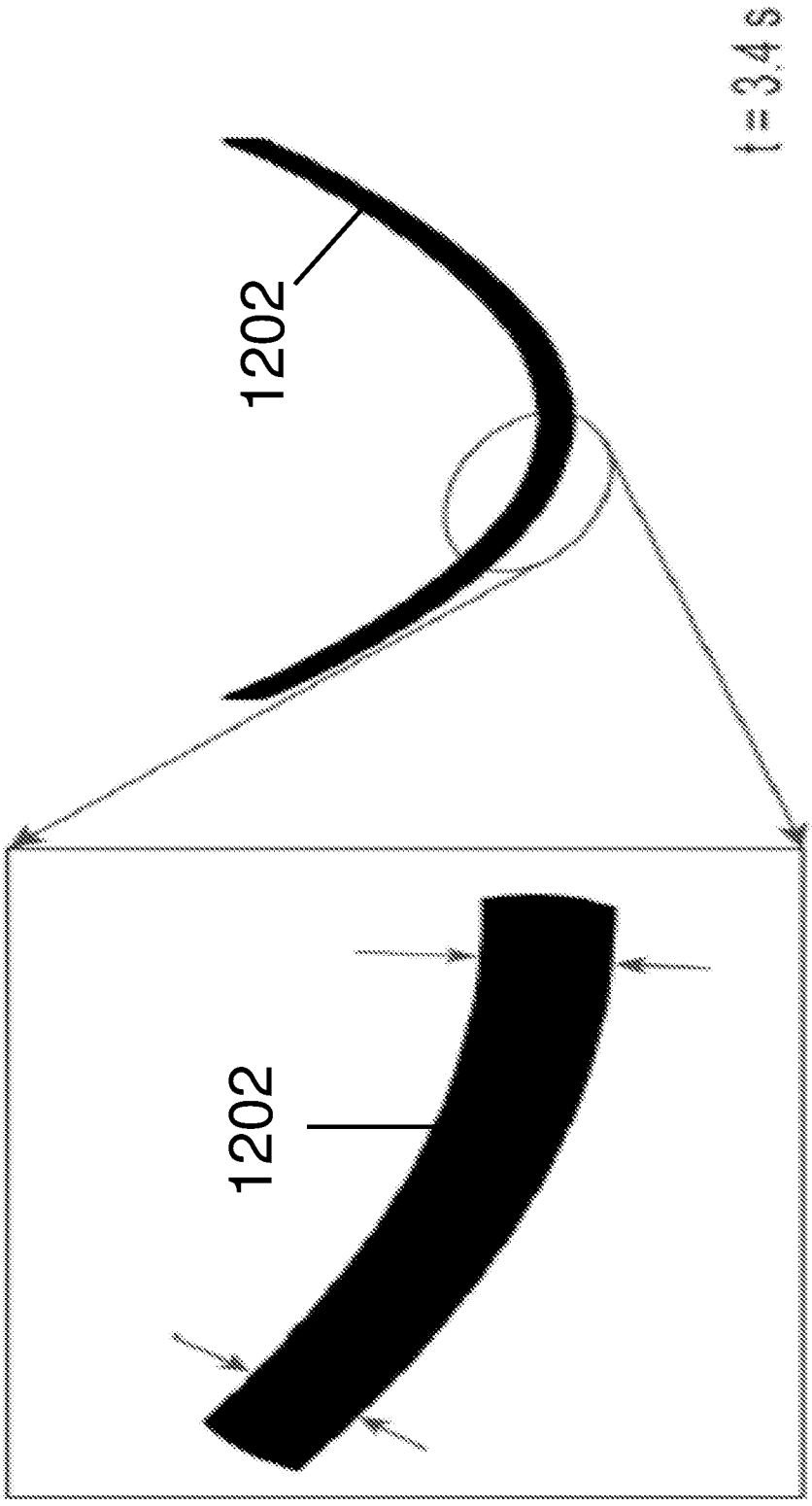

FIG. 12B

FIG. 13A

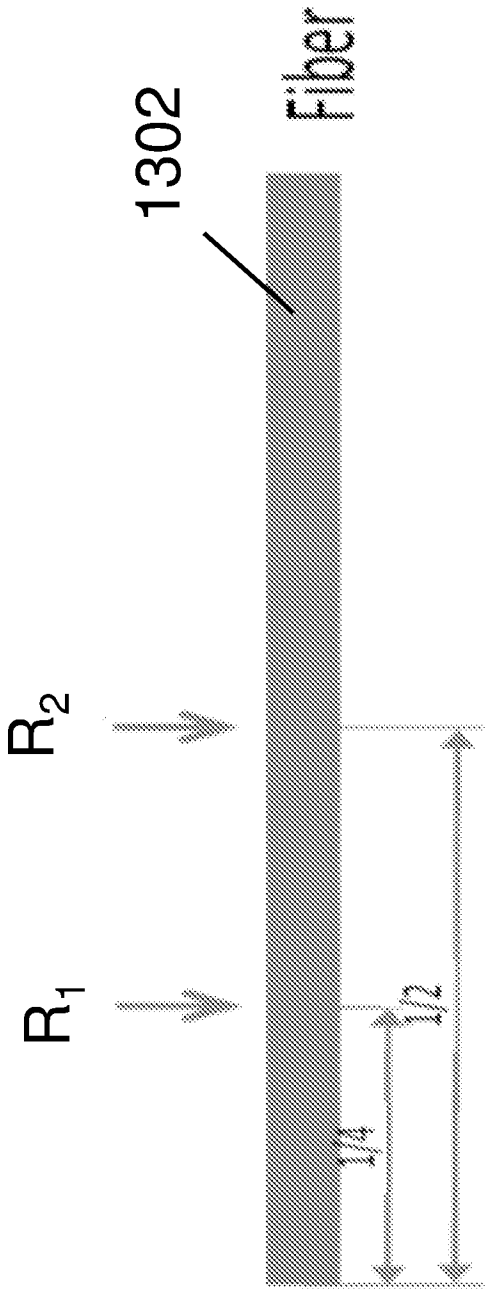

FIG. 13B

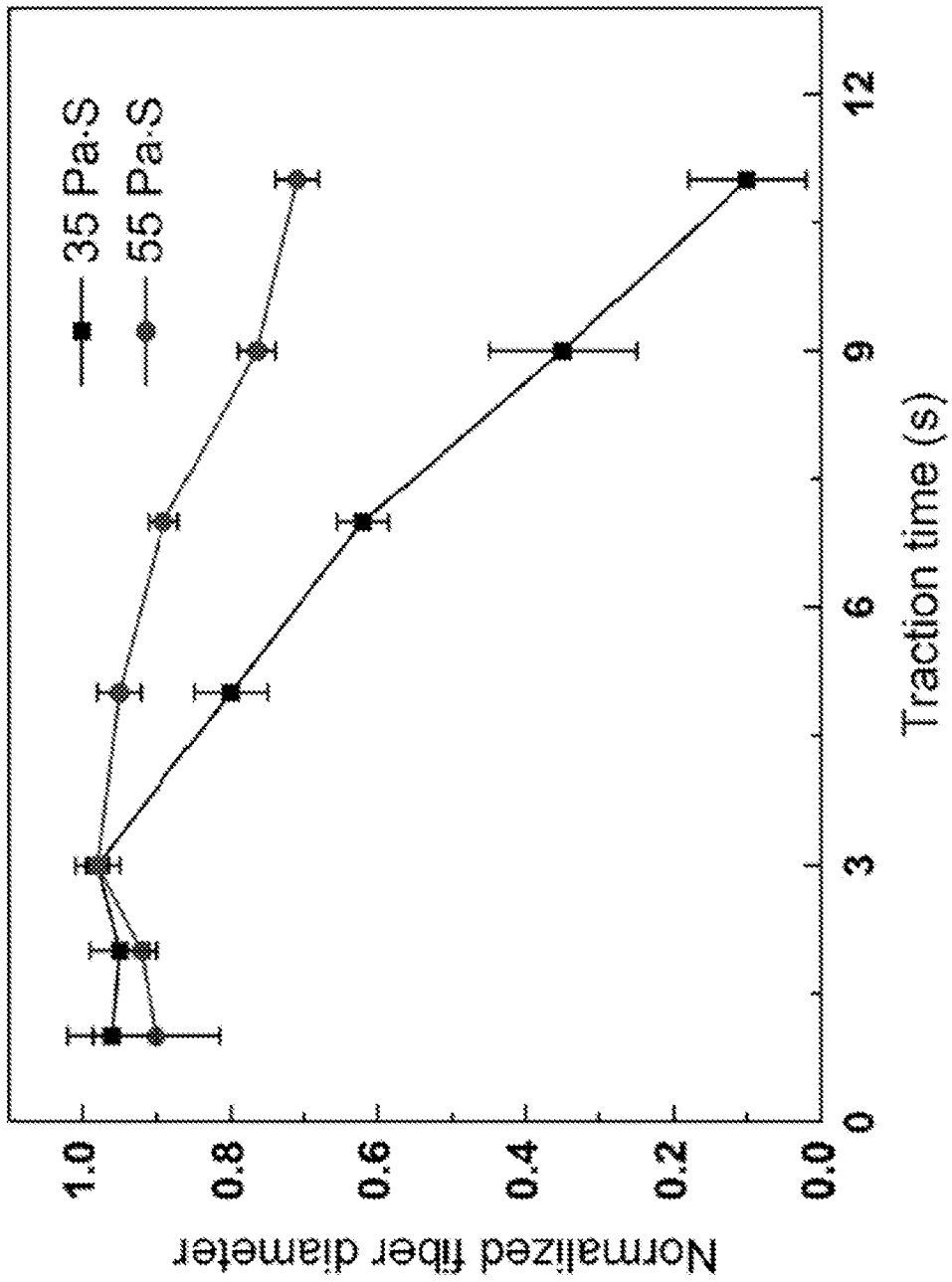
35 Pa·S
55 Pa·S
Normalized fiber diameter
1.0
0.8
0.6
0.4
0.2
0.0
0
3
6
9
12
Traction time (s)

FIG. 14A

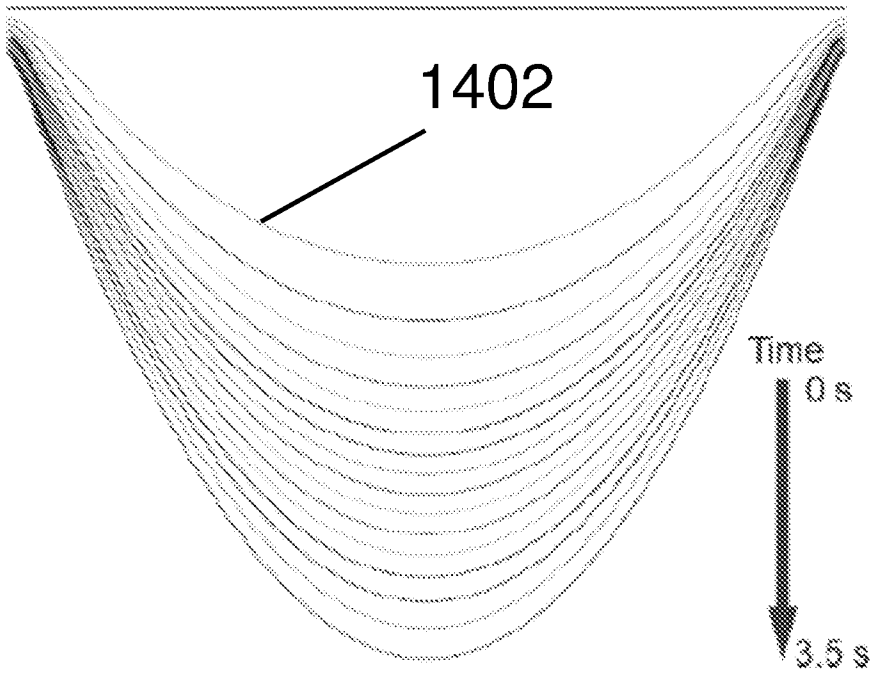

FIG. 14B

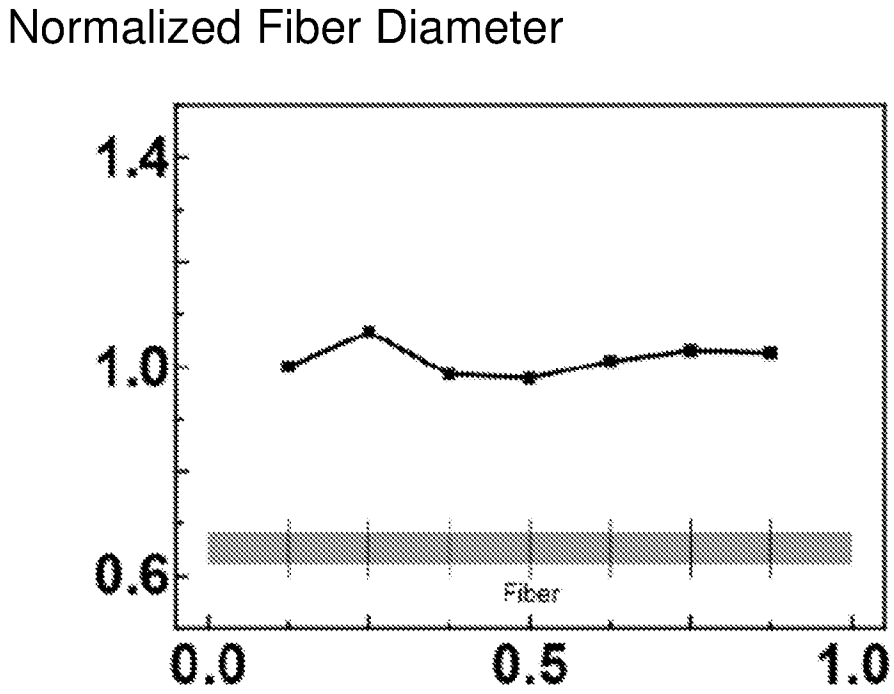

FIG. 15A

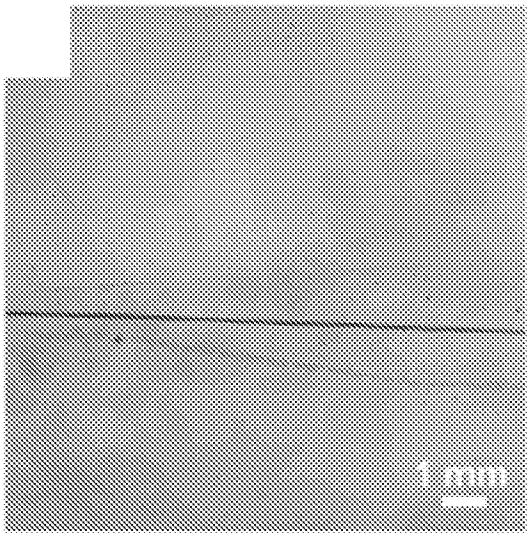

FIG. 15B

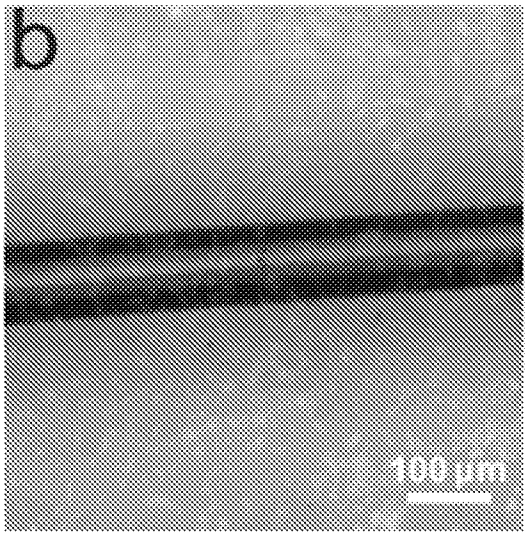

FIG. 15C

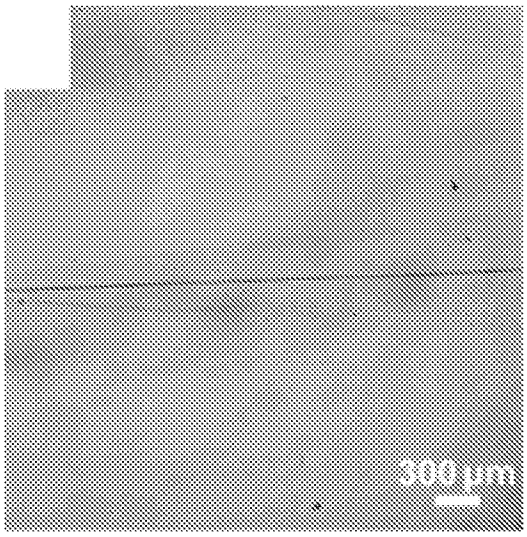

FIG. 15D

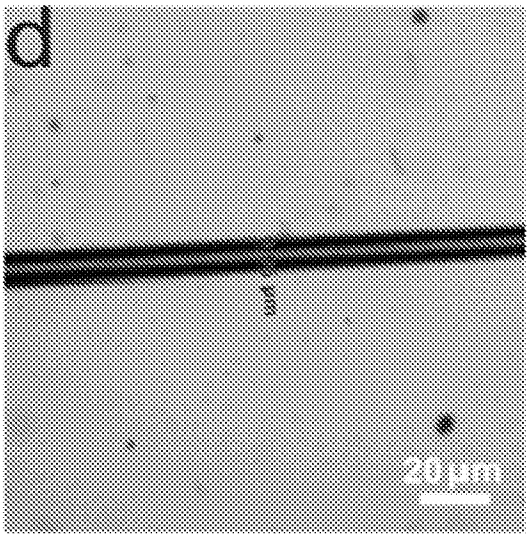

FIG. 15E

FIG. 16A

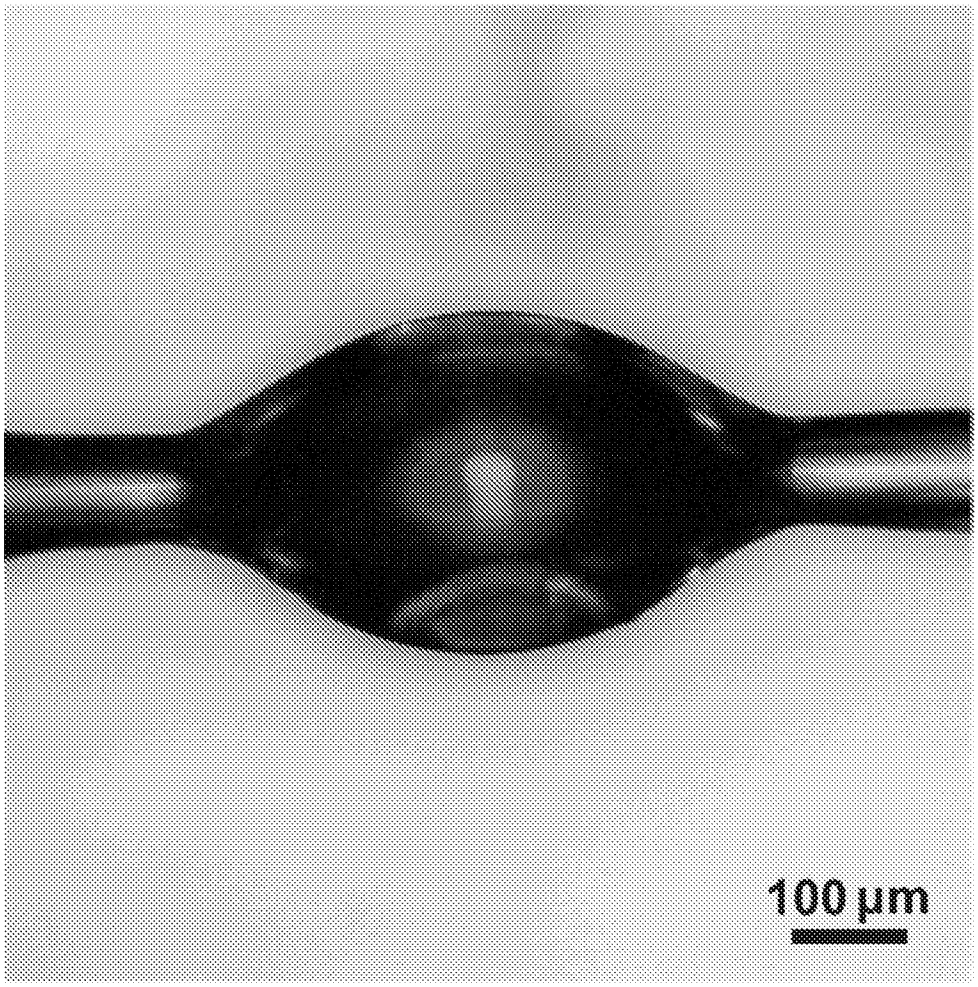

FIG. 16B

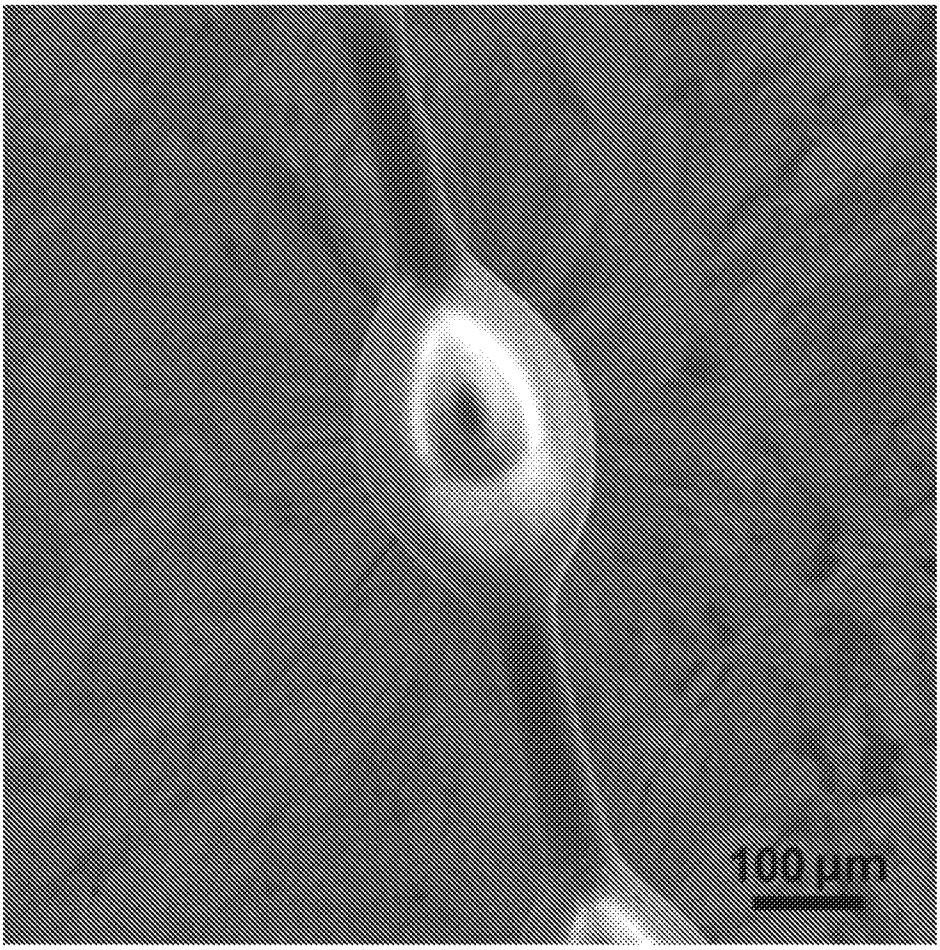

FIG. 16C

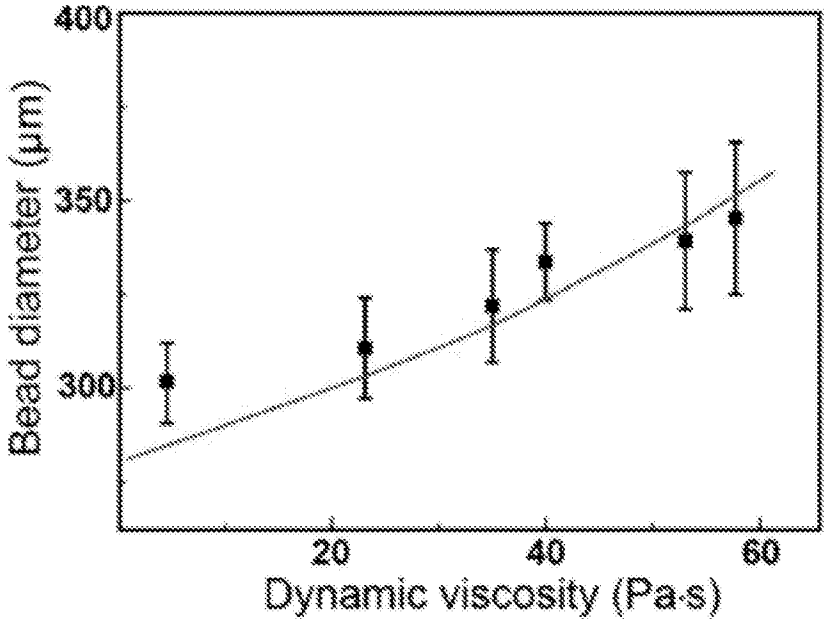

FIG. 16D

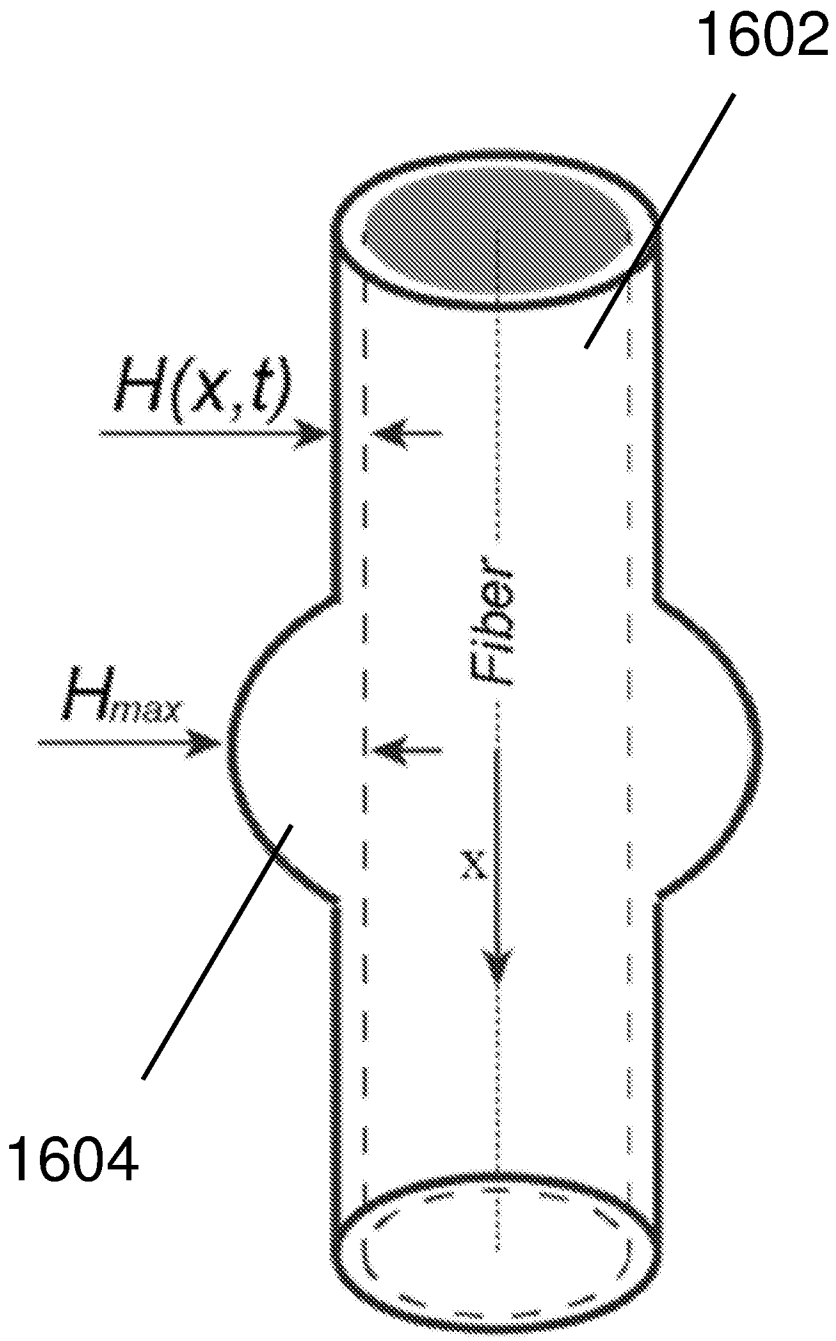

FIG. 16E

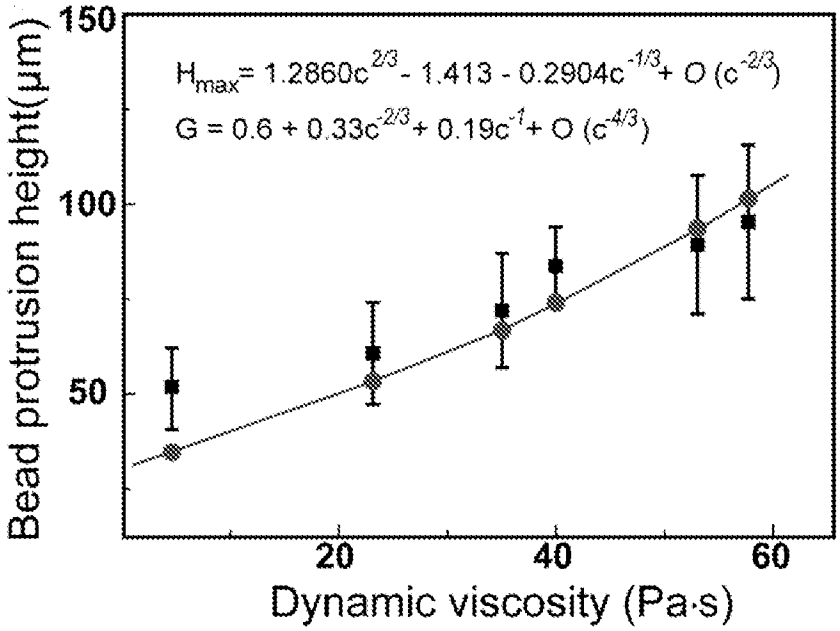
H_{max}= 1.2860c$^{2/3}$ - 1.413 - 0.2904c$^{-1/3}$+ O (c$^{-2/3}$)
G = 0.6 + 0.33c$^{-2/3}$+ 0.19c^{-1}+ O (c$^{-4/3}$)
Bead protrusion height(μm)
150
100
50
20
40
60
Dynamic viscosity (Pa·s)

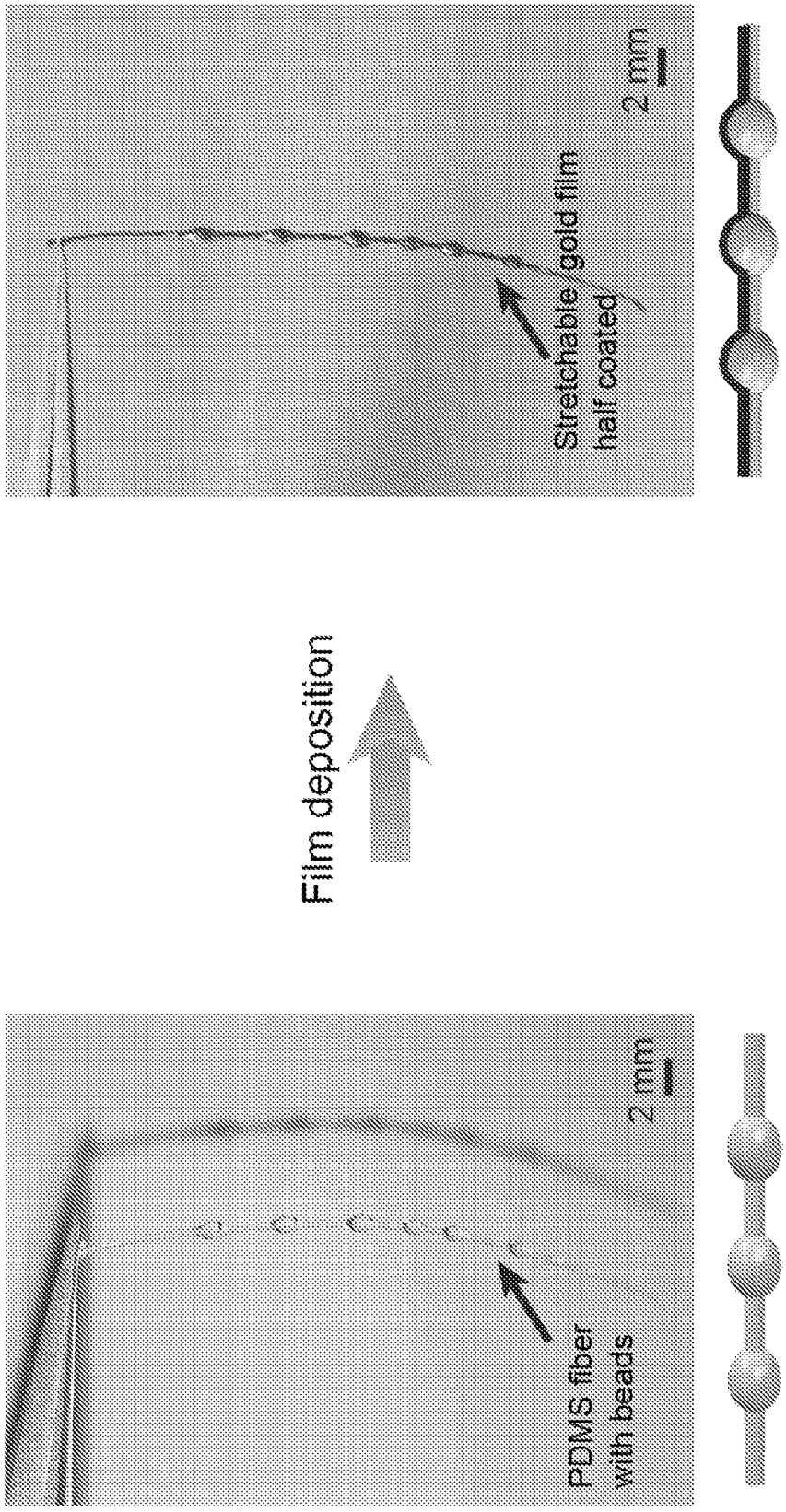
Stretchable gold film
half coated
2 mm
Film deposition
PDMS fiber
with beads
2 mm

FIG. 17A

FIG. 17B

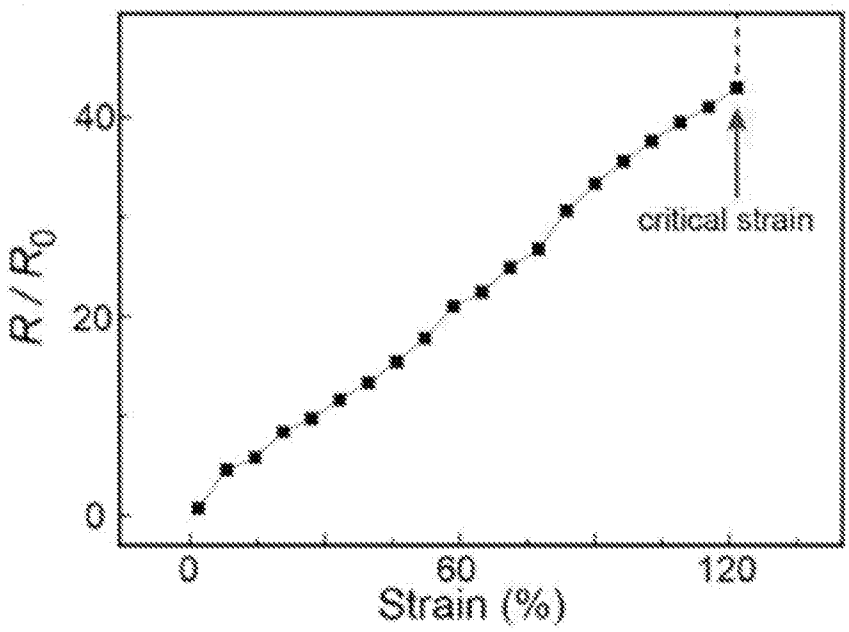

FIG. 17C

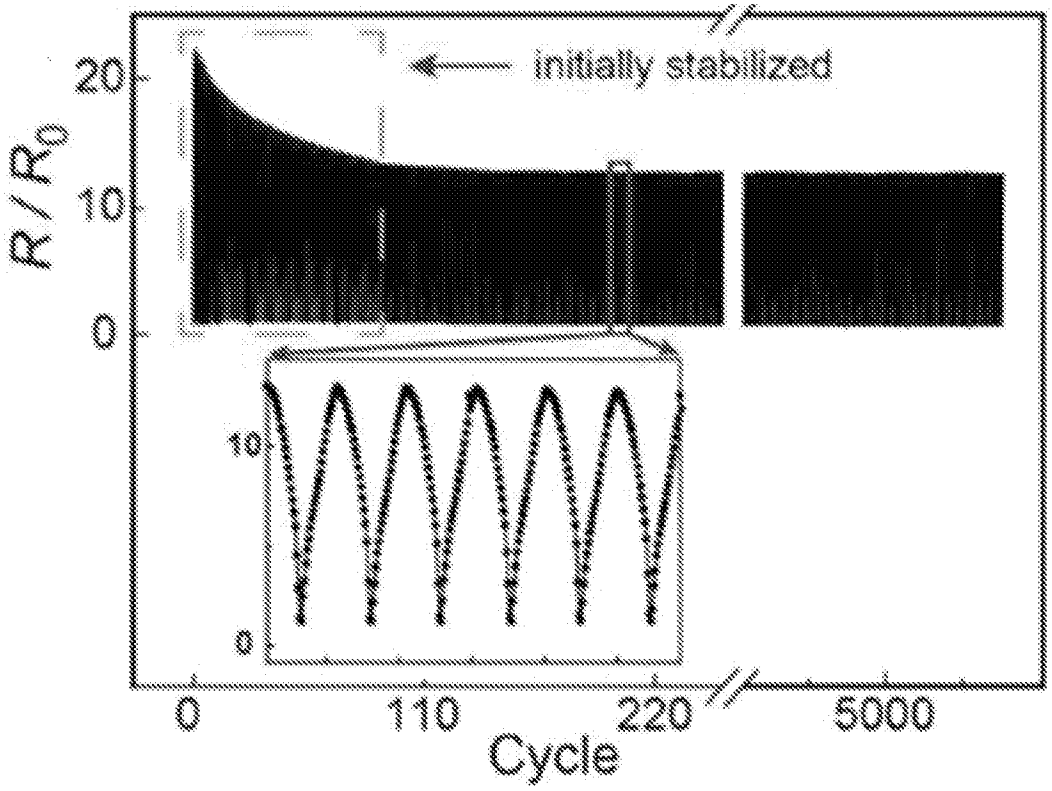

FIG. 18A

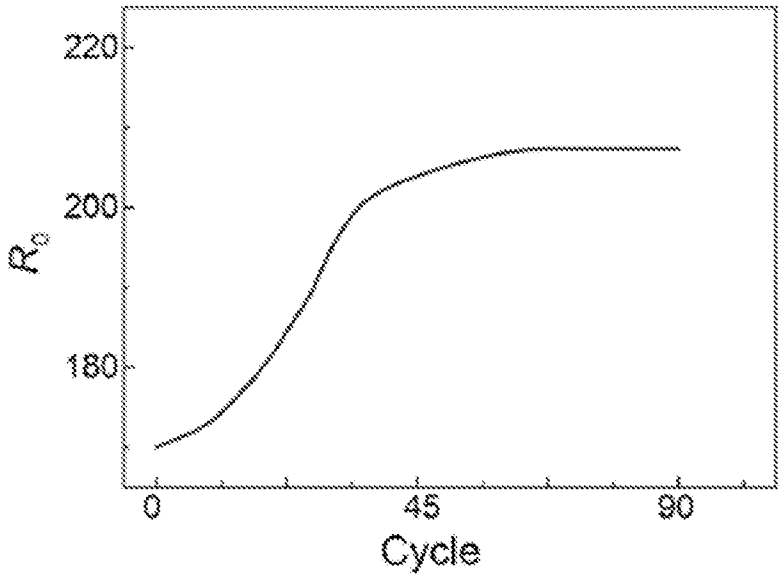

FIG. 18B

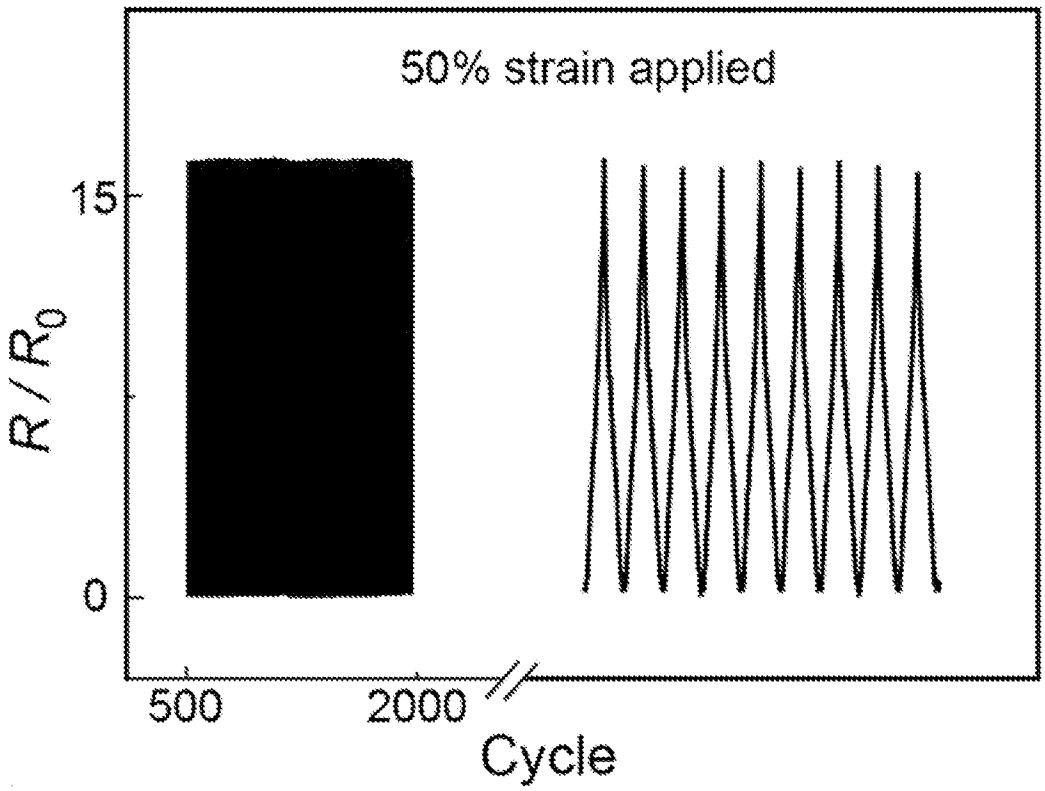

FIG. 18C

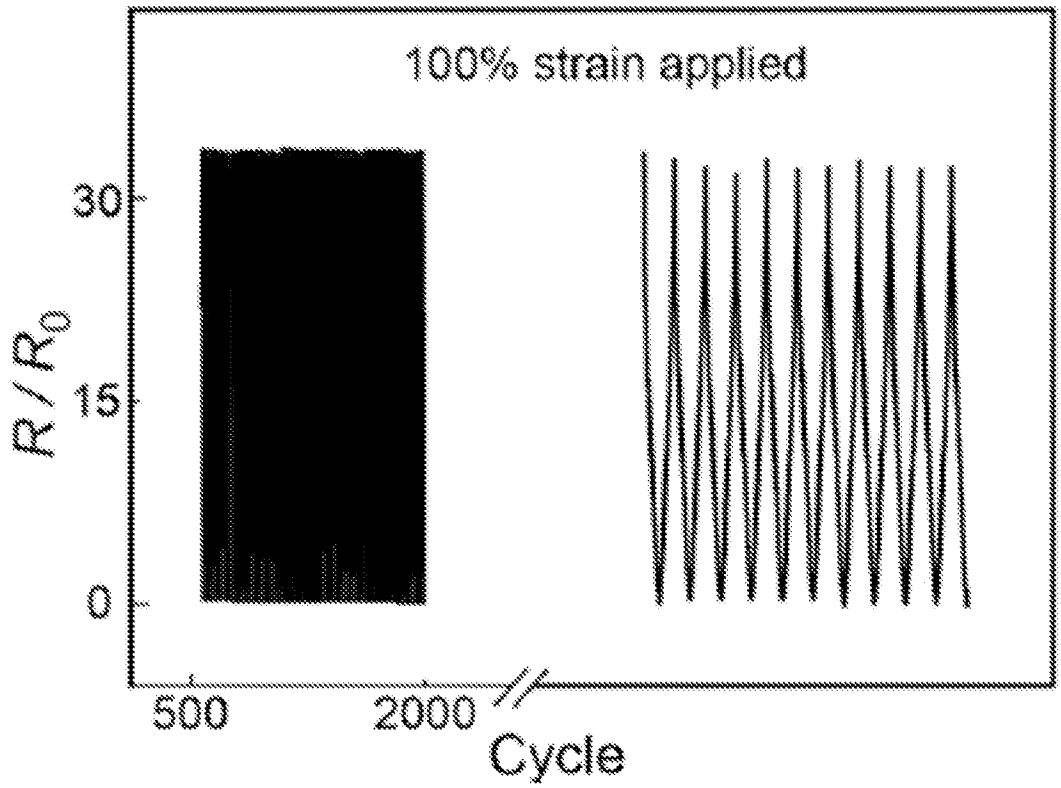

FIG. 18D

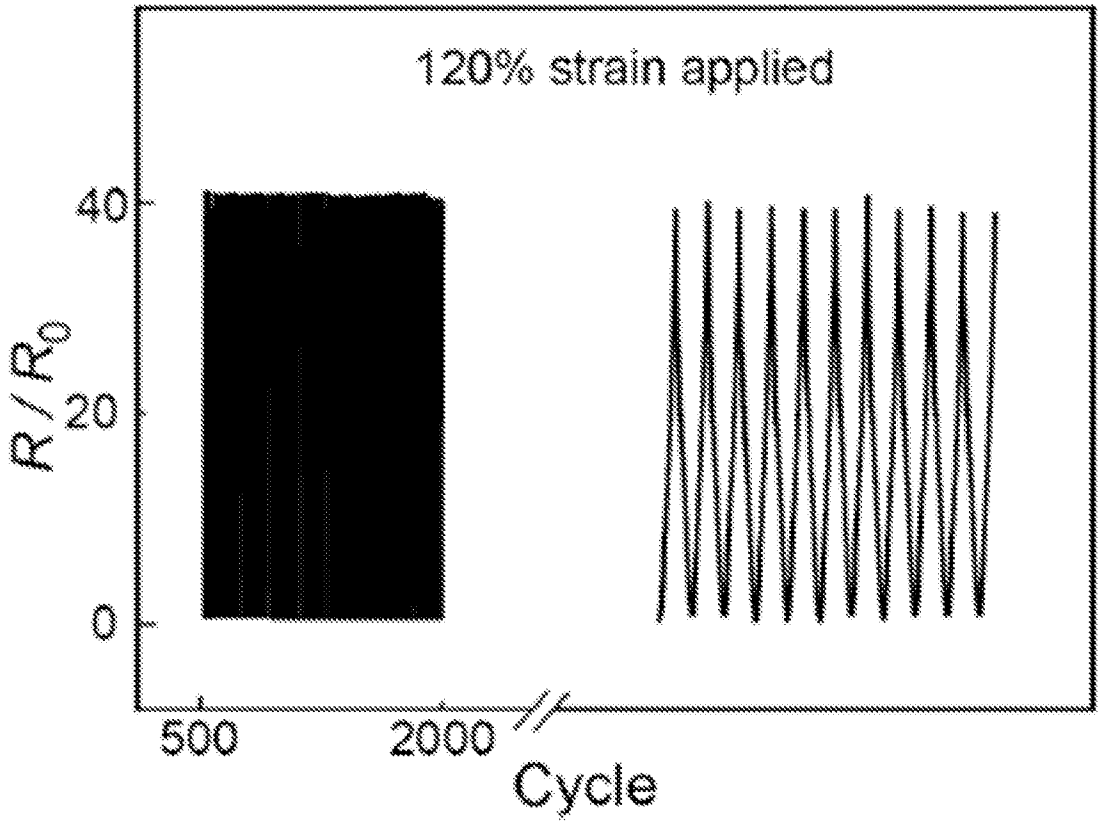

FIG. 19A

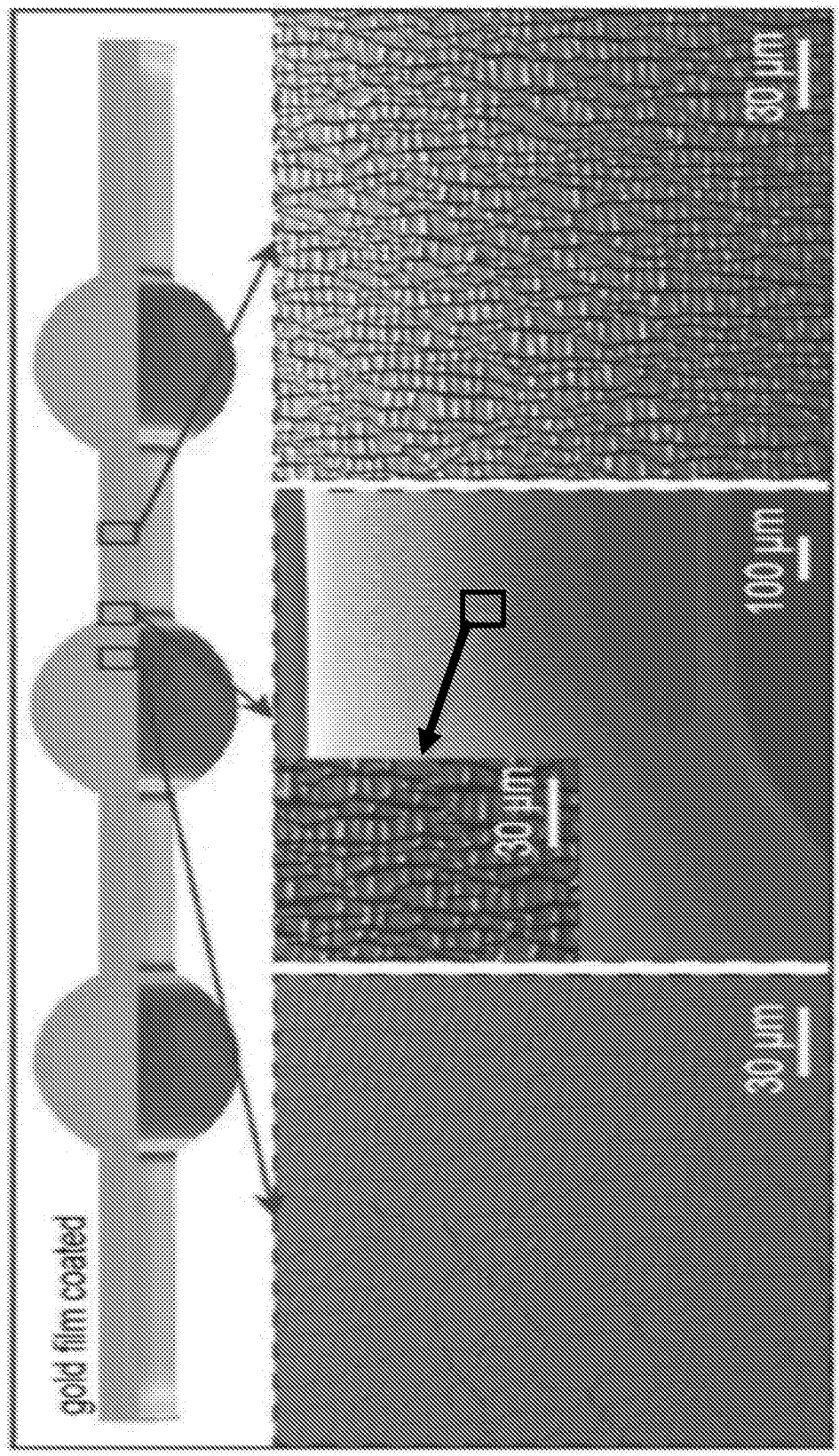

FIG. 19B

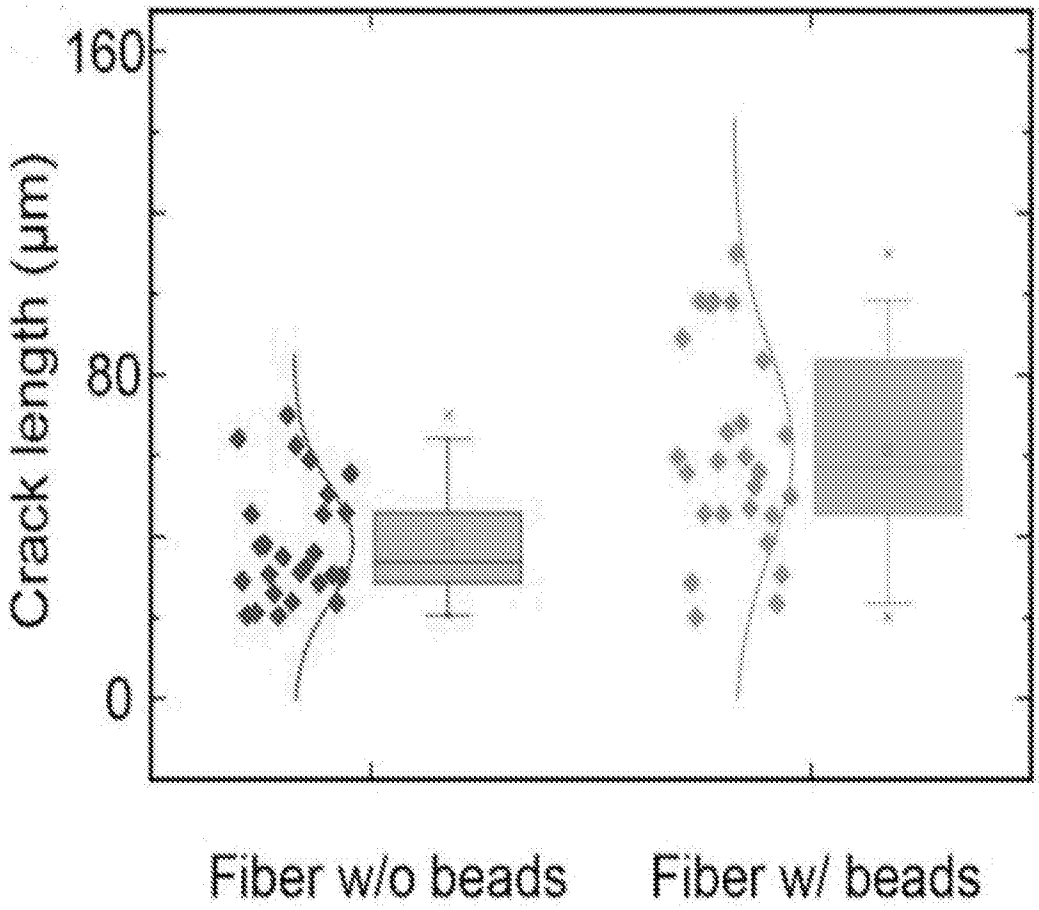

FIG. 20A

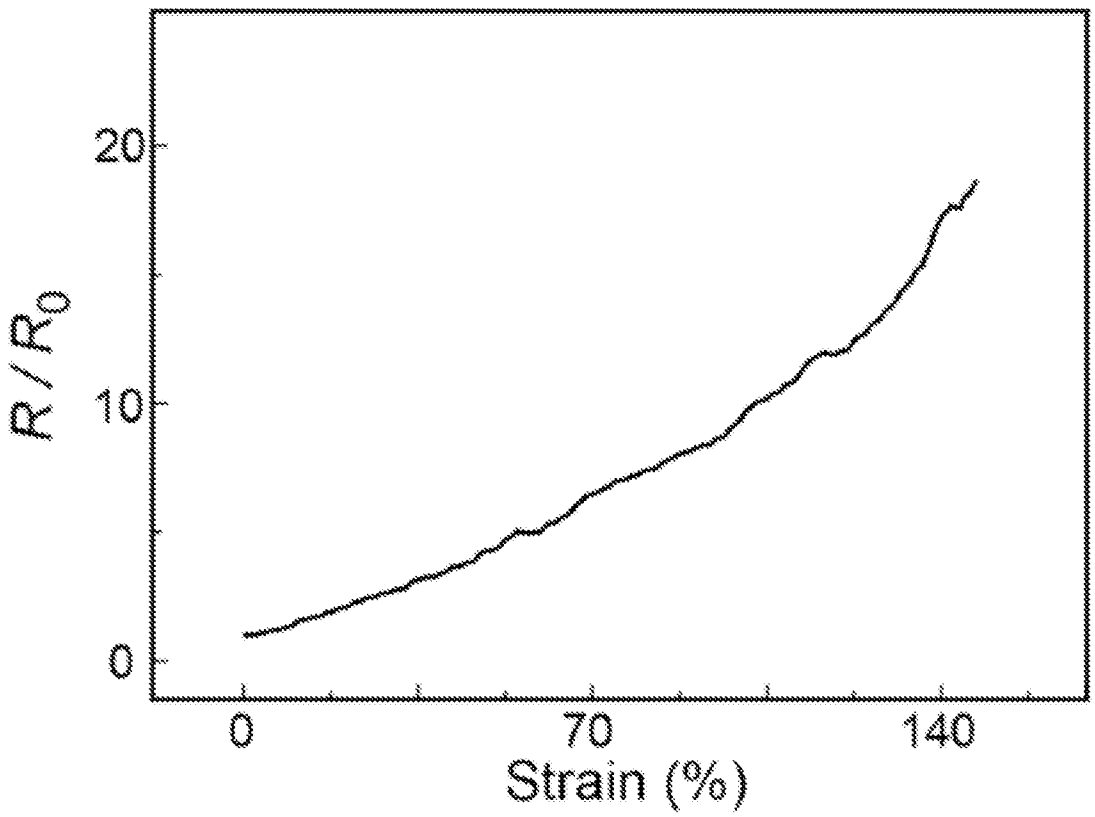

FIG. 20B

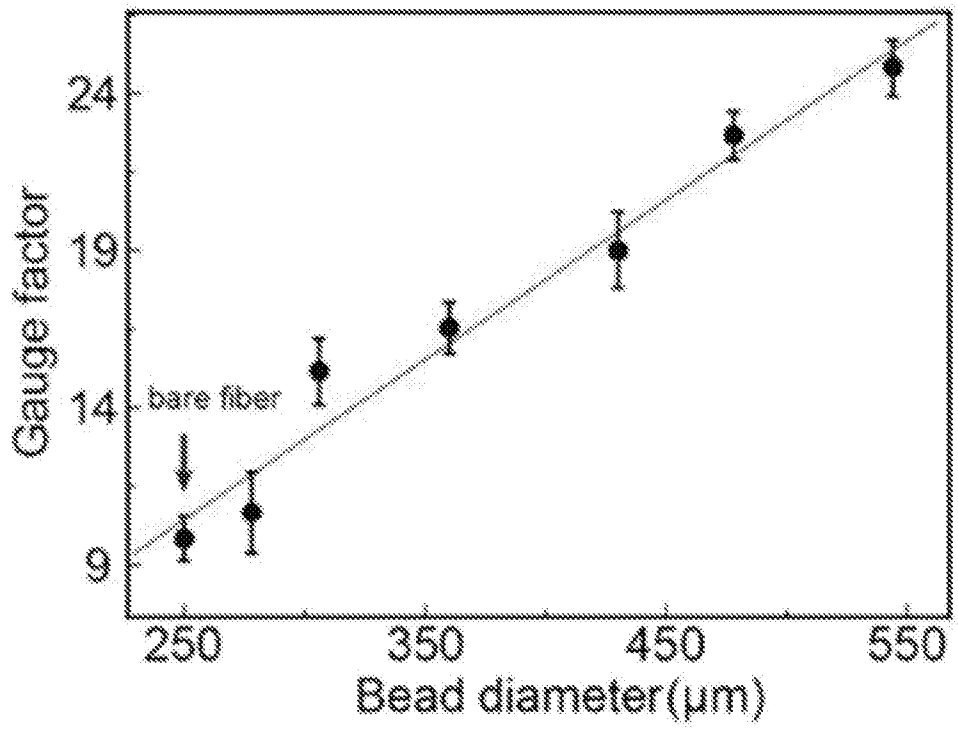
Gauge factor
24
19
14
9
bare fiber
250
350
450
550
Bead diameter(μm)

FIG. 20C

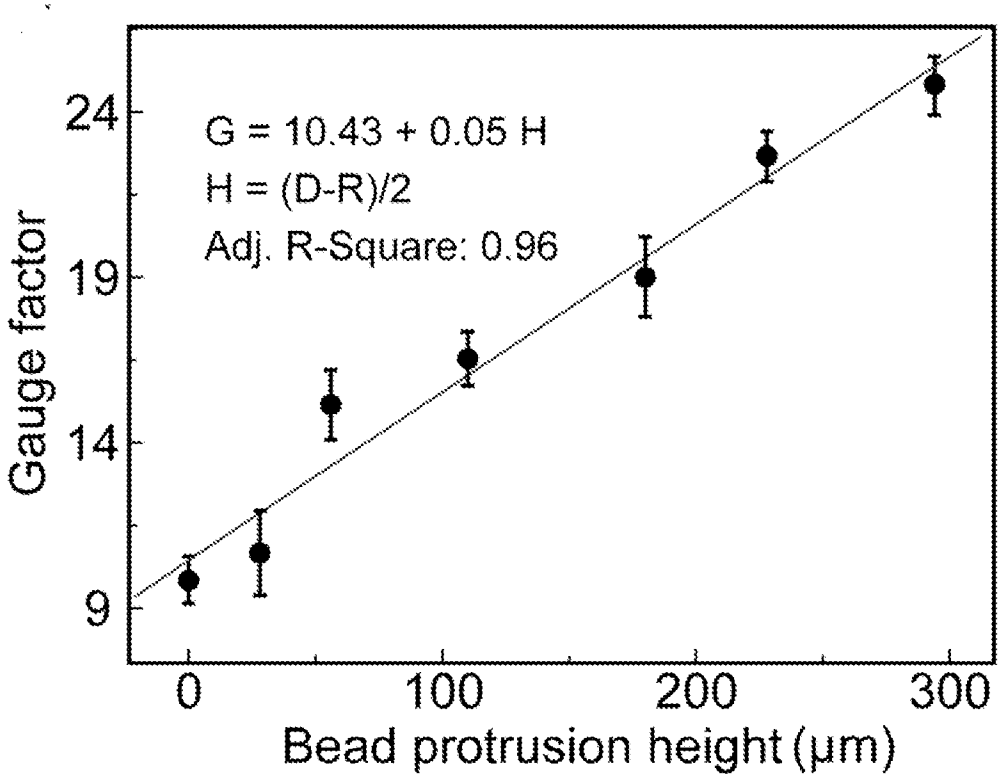
G = 10.43 + 0.05 H
H = (D-R)/2
Adj. R-Square: 0.96
Gauge factor
24
19
14
9
0
100
200
300
Bead protrusion height (μm)

FIG. 20D

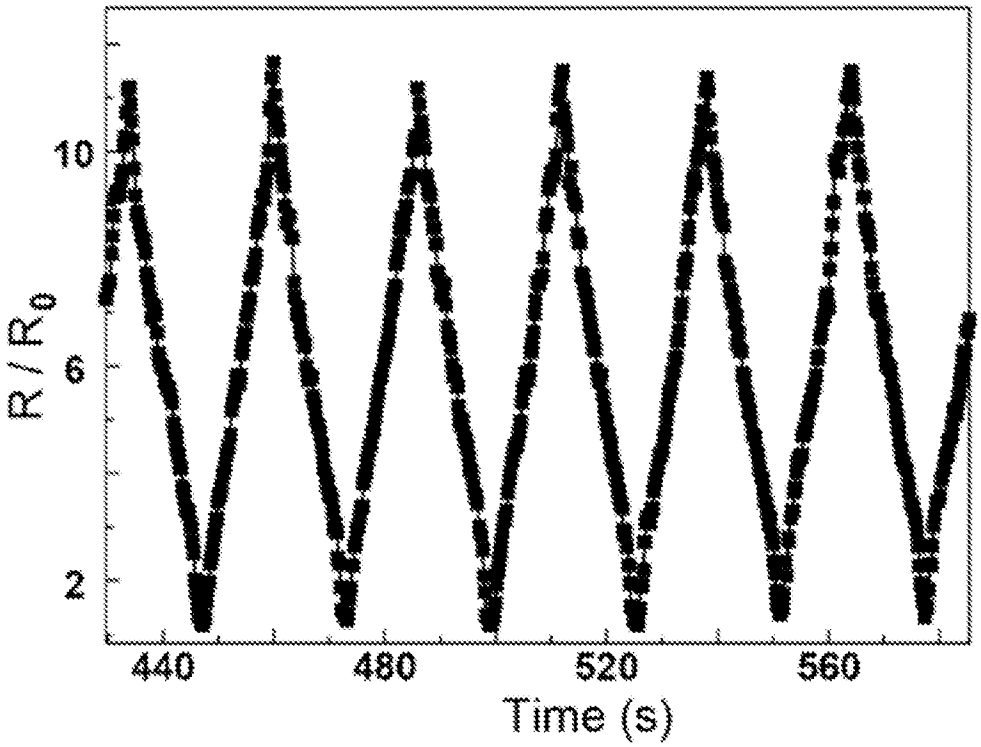

FIG. 20E

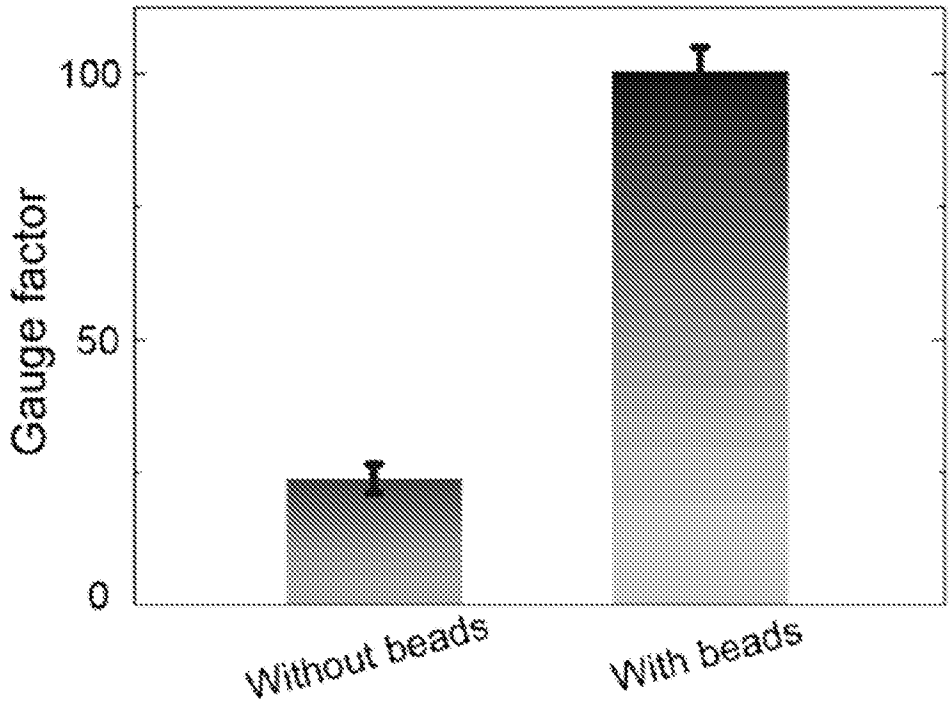

FIG. 21

Materials	Maximum Uniaxial strain	Gauge factor	Methods to enhance sensitivity
Gold**	120% (Decided by substrate)	42.3	Structured fibers
CNTs**	80%	100	Structured fibers
PEDOT:PSS	160%	-1	Not shown
AgNWs	100%	3	Not shown
CNTs	800%	0.3	Not shown
Ionic conductive ink	800%	0.348	Not shown
AgNWs	50%	5.326	Not shown
Liquid metal	8%	5.2	Not shown

** This work

FIG. 22

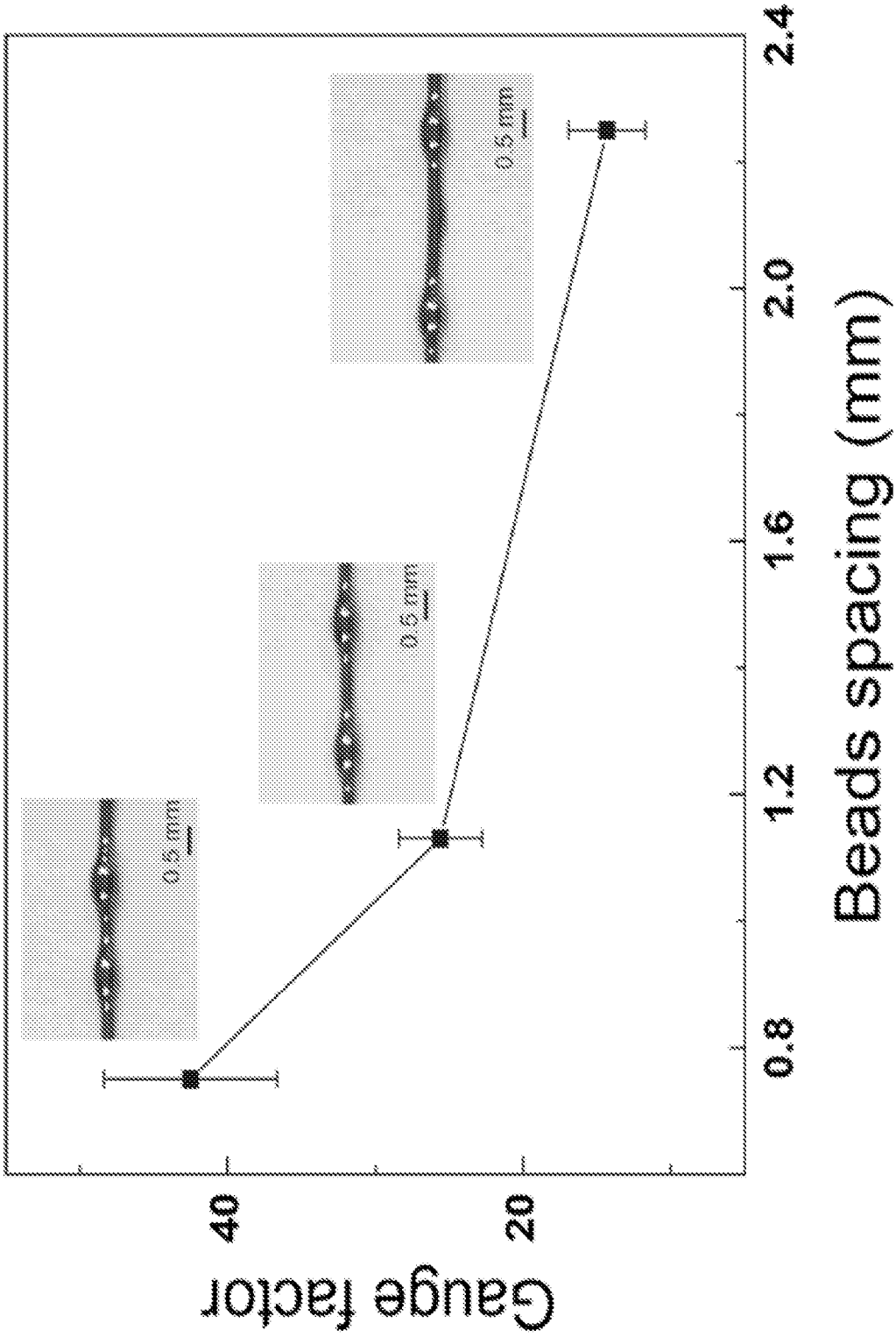
Gauge factor
40
20
Beads spacing (mm)
0.8
1.2
1.6
2.0
2.4
0.5 mm
0.5 mm
0.5 mm

FIG. 23A

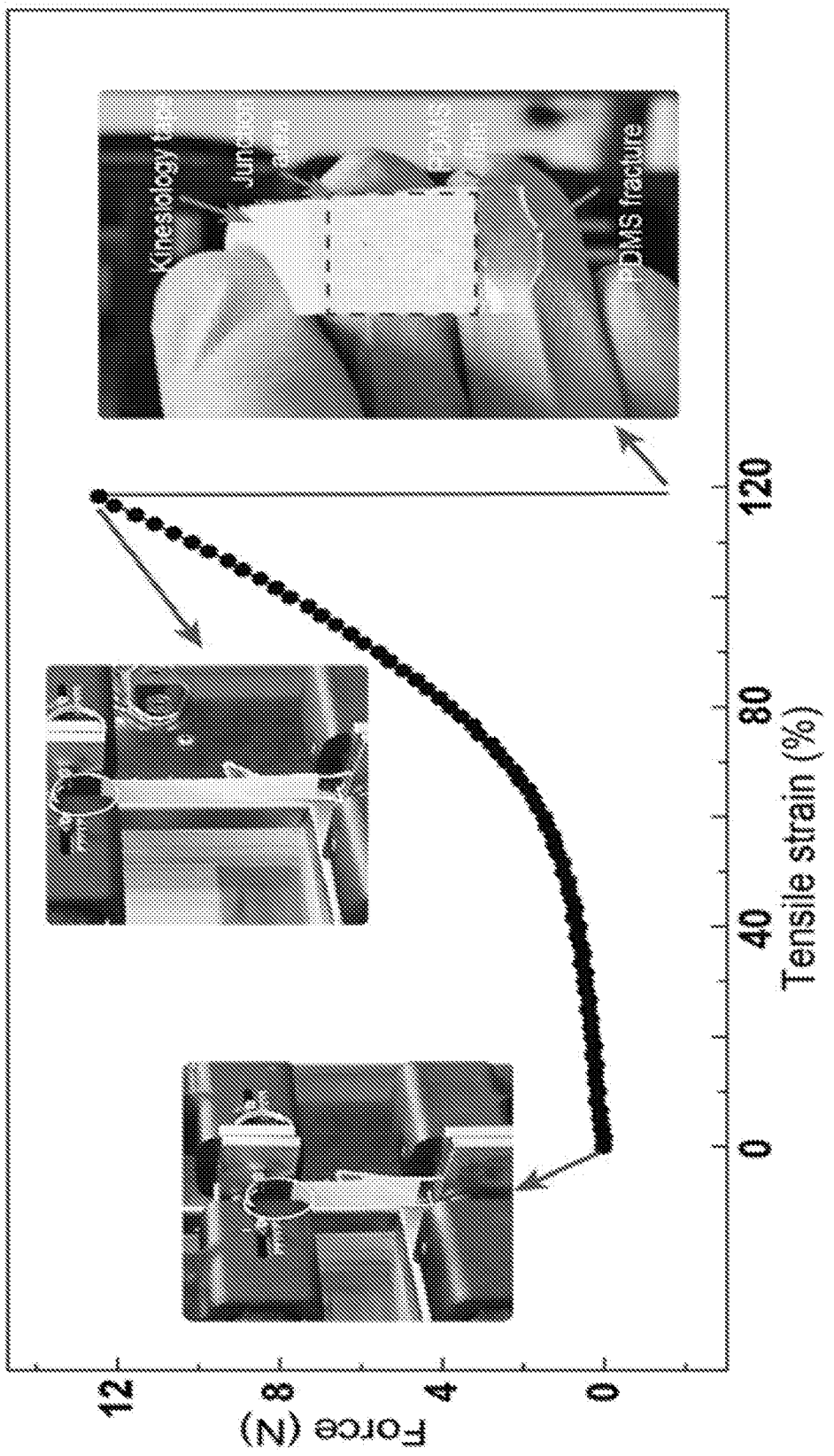
Force (N)
12
8
4
0
0
40
80
120
Tensile strain (%)
Knee bent
Jump
PDMS fracture

FIG. 23B

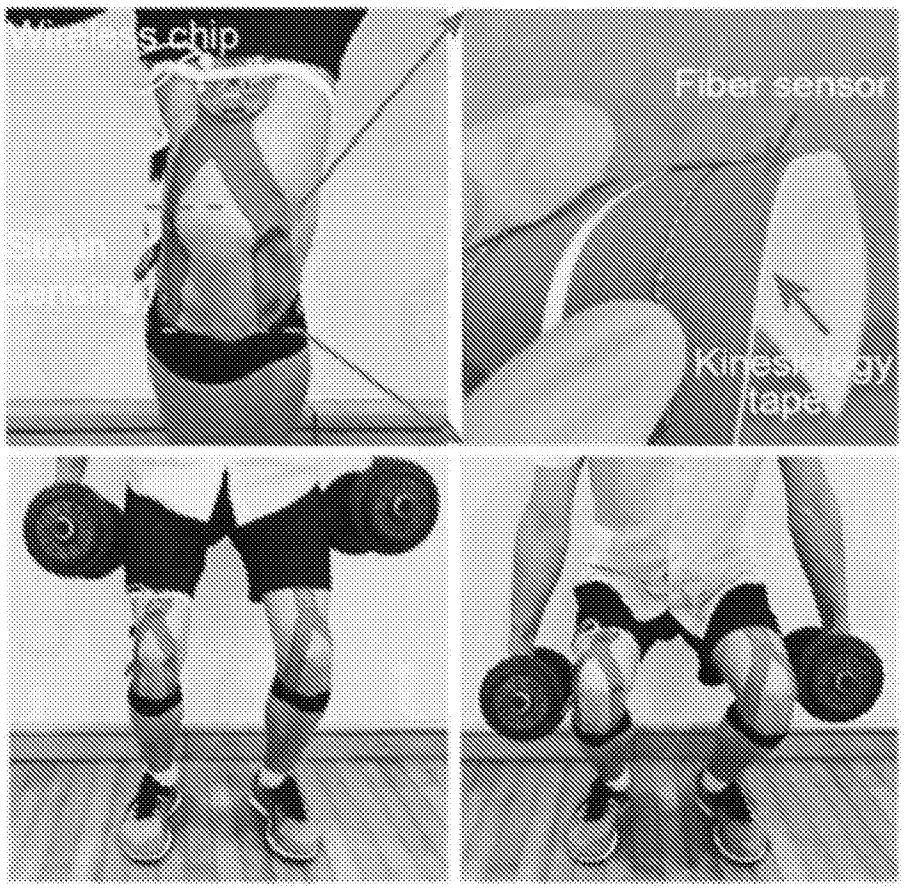

FIG. 23C

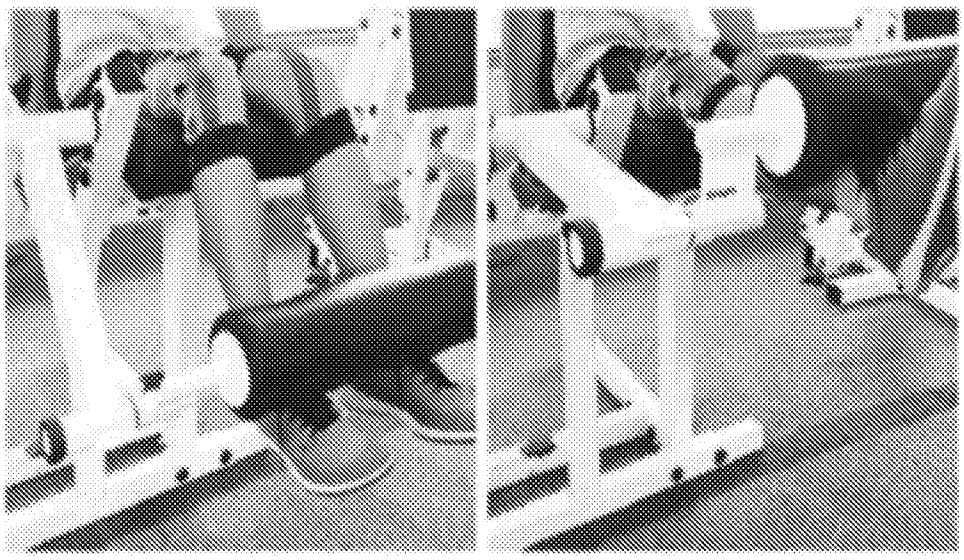

FIG. 23D

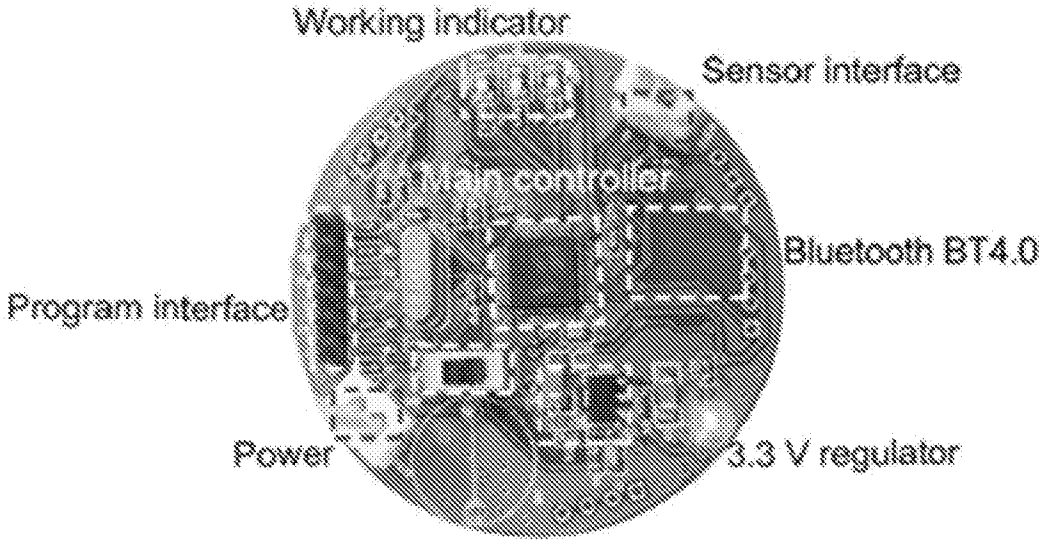

FIG. 23E

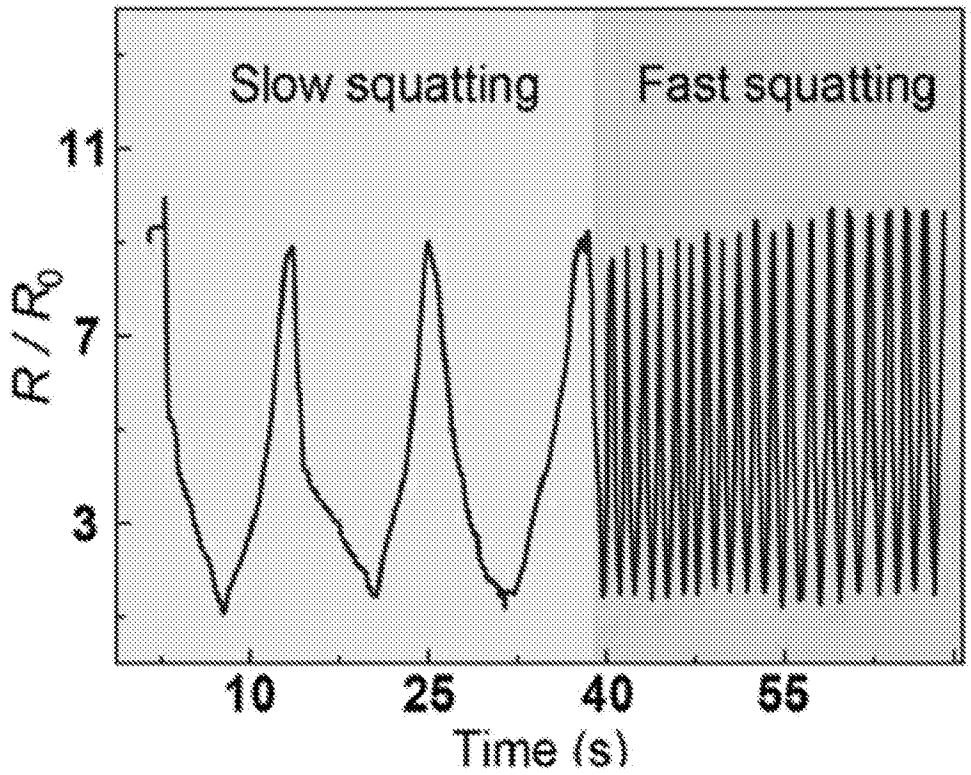

FIG. 23F

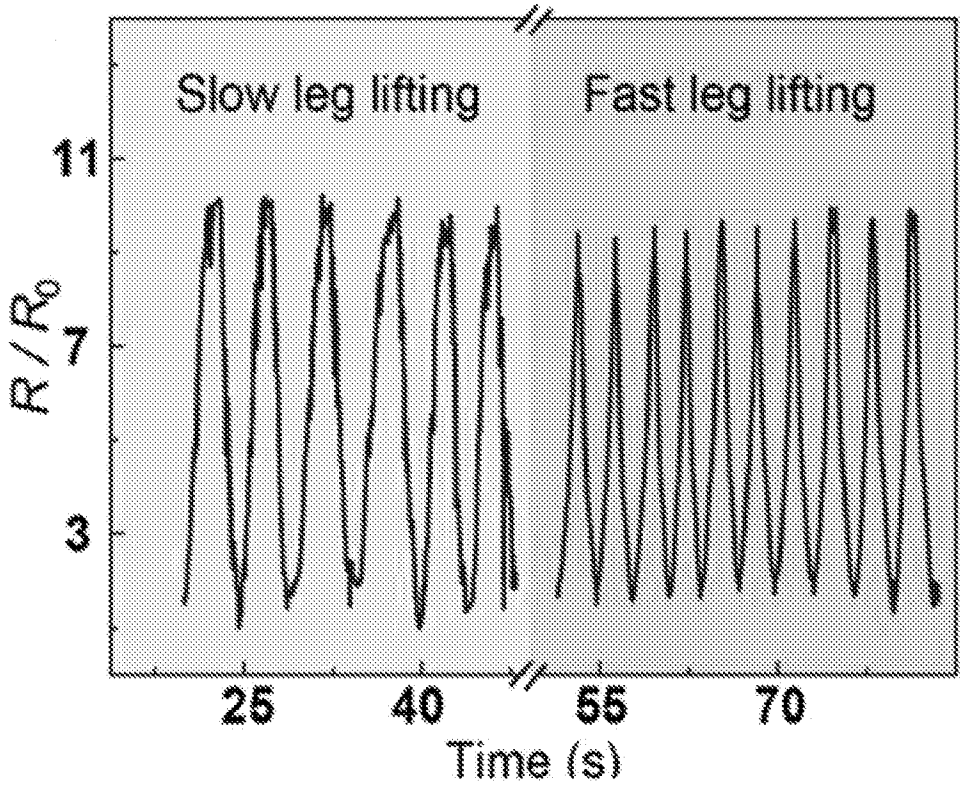

FIG. 24A

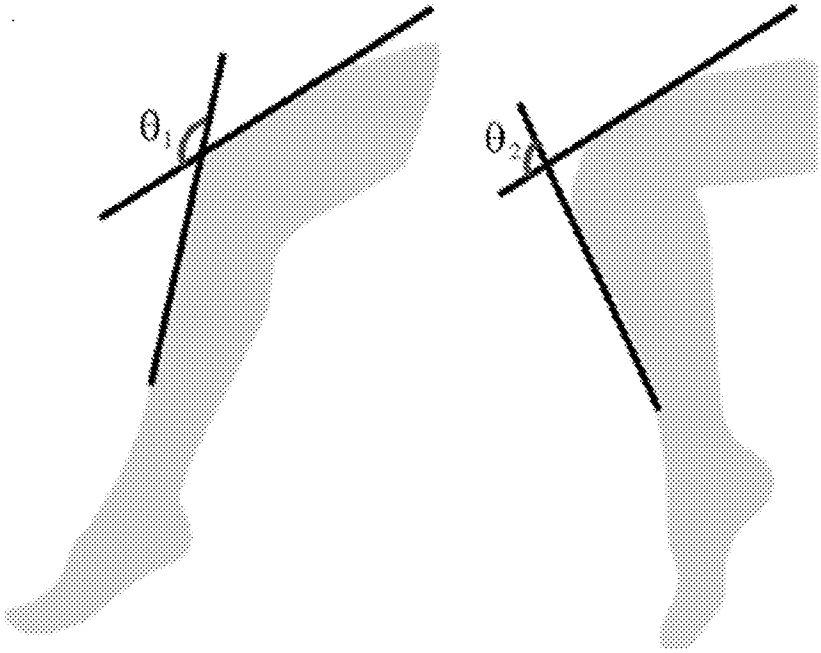

FIG. 24B

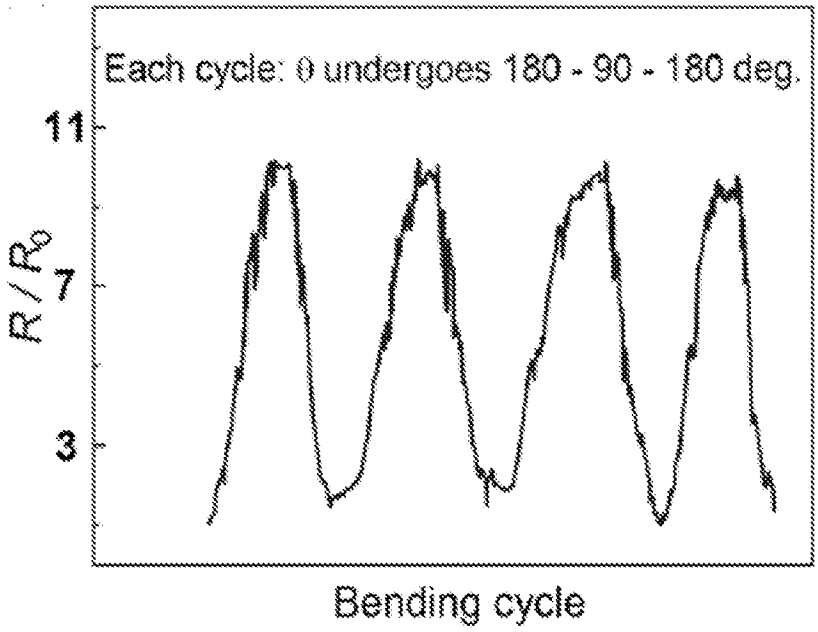

FIG. 25

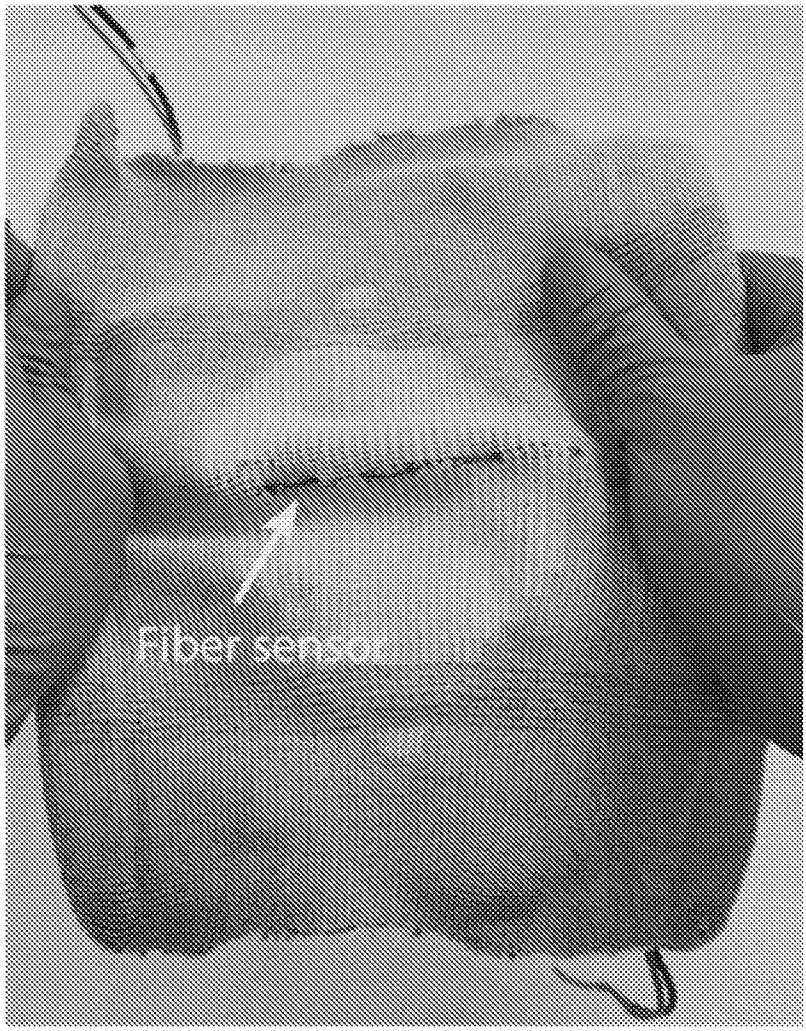

FIG. 26A

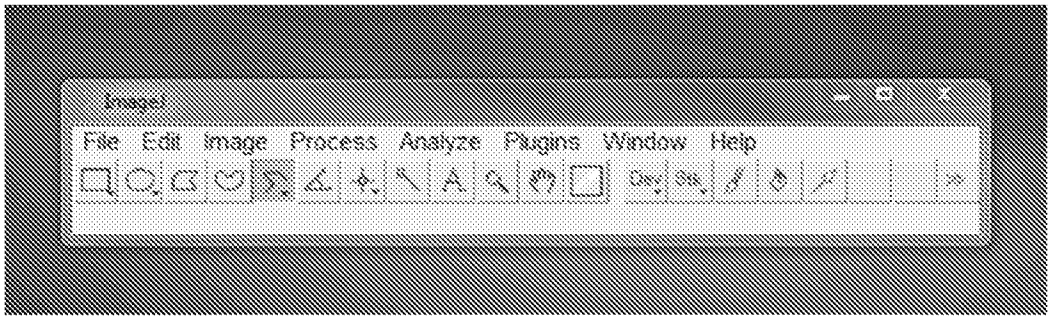

FIG. 26B

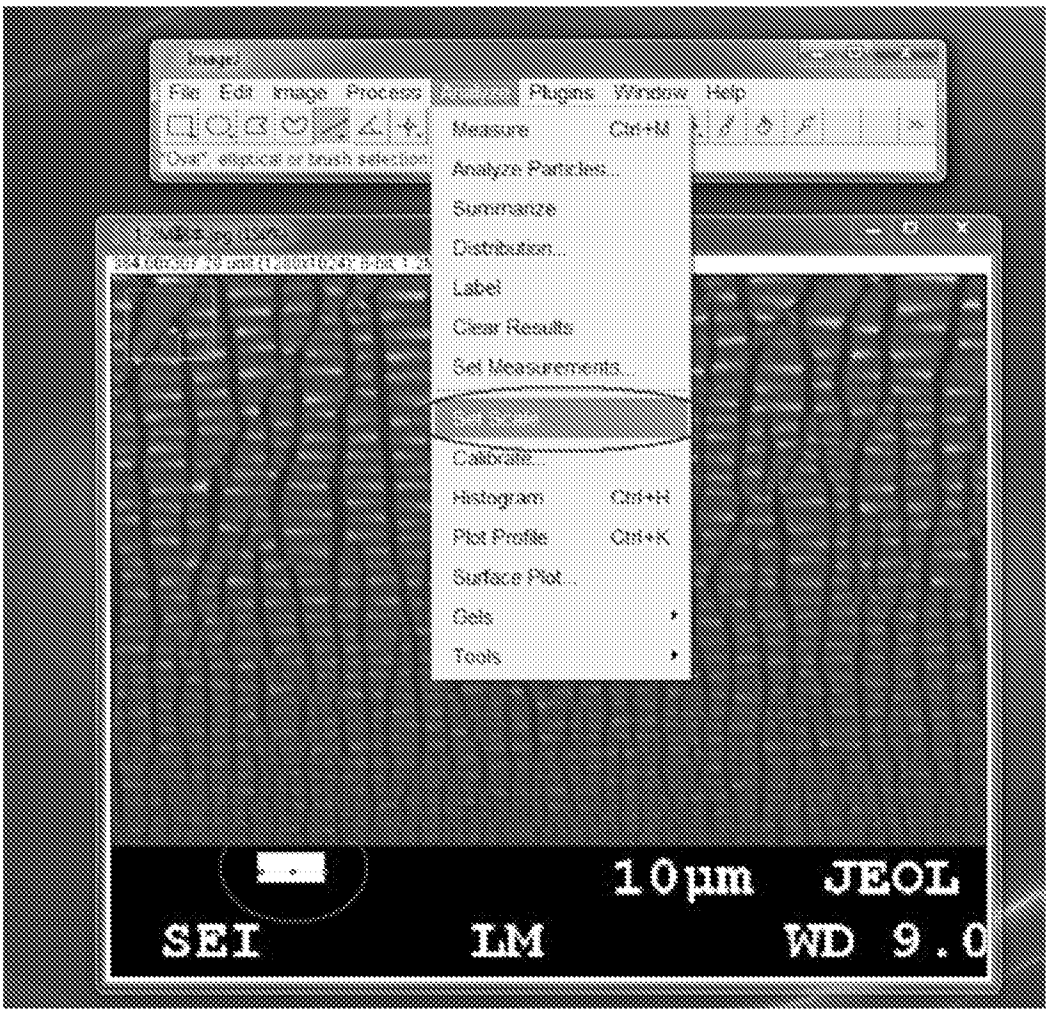

FIG. 26C

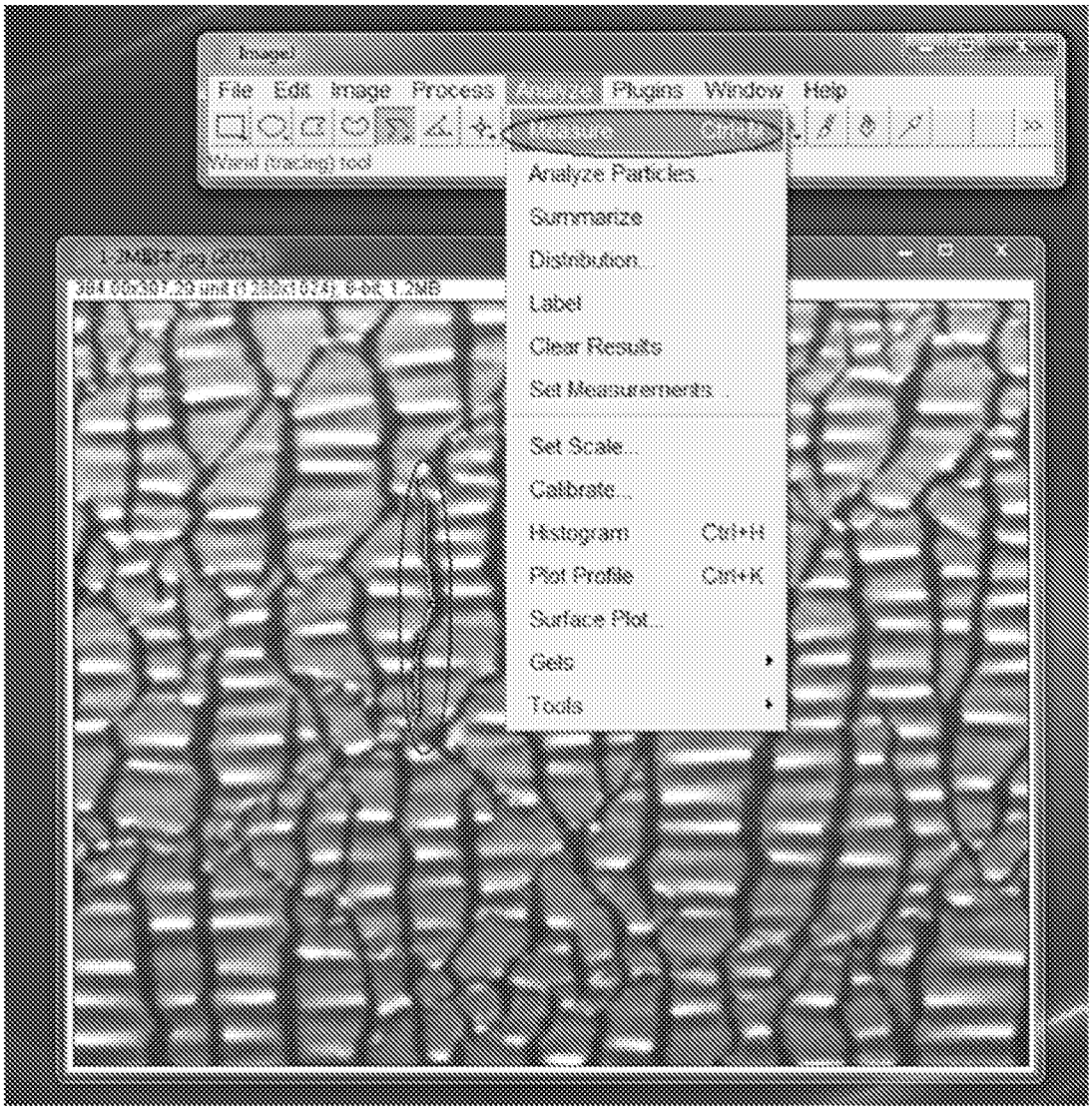
File Edit Image Process Plugins Window Help
Analyze Particles...
Summarize
Distribution...
Label
Clear Results
Set Measurements...
Set Scale...
Calibrate...
Histogram Ctrl+H
Plot Profile Ctrl+K
Surface Plot...
Gels
Tools

FIG. 27A

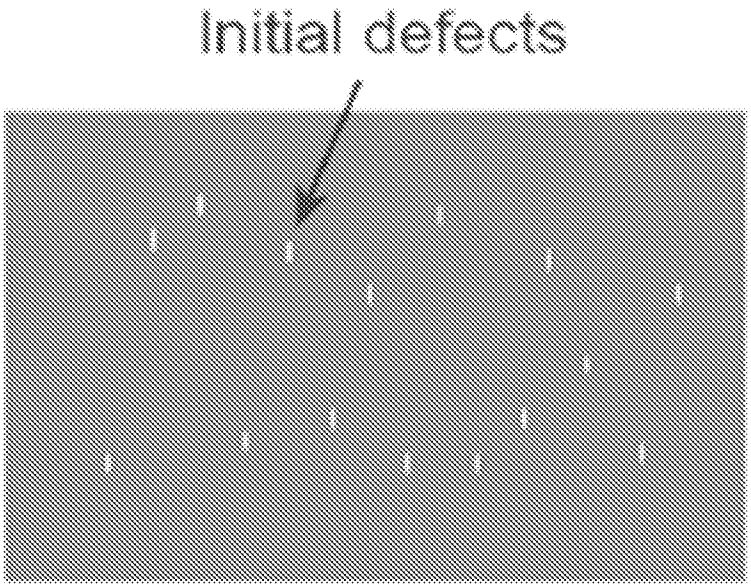

FIG. 27B

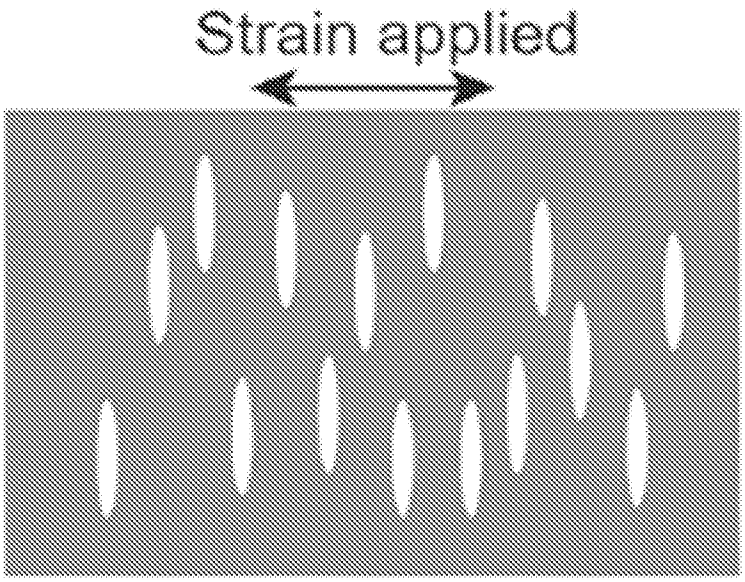

FIG. 27C

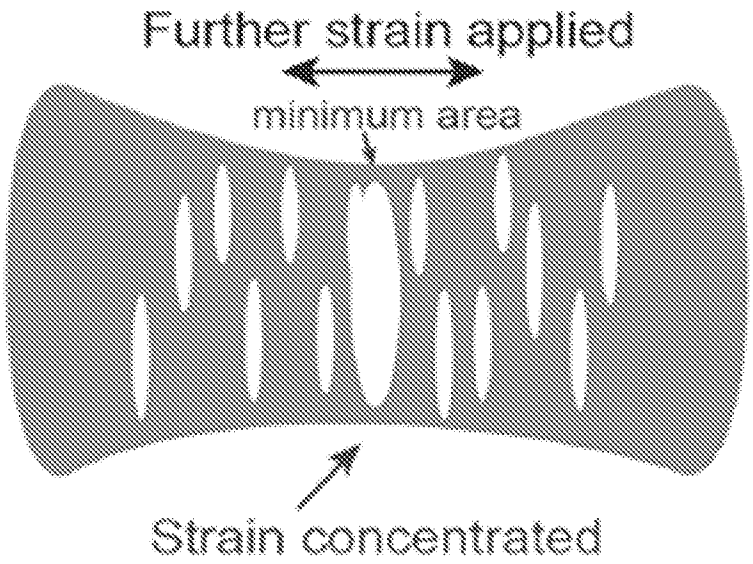

FIG. 28A

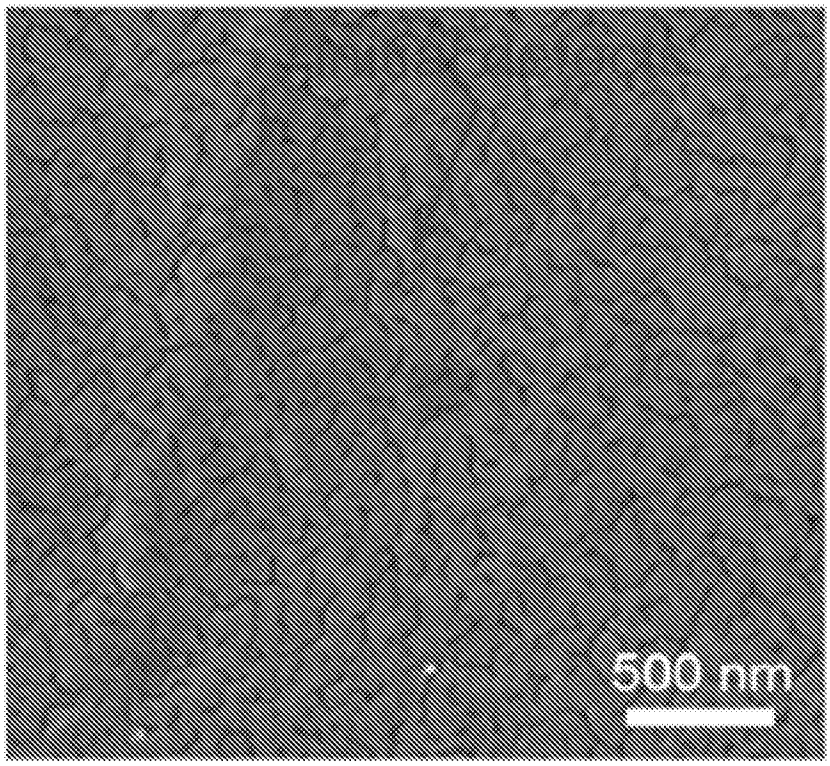

FIG. 28B

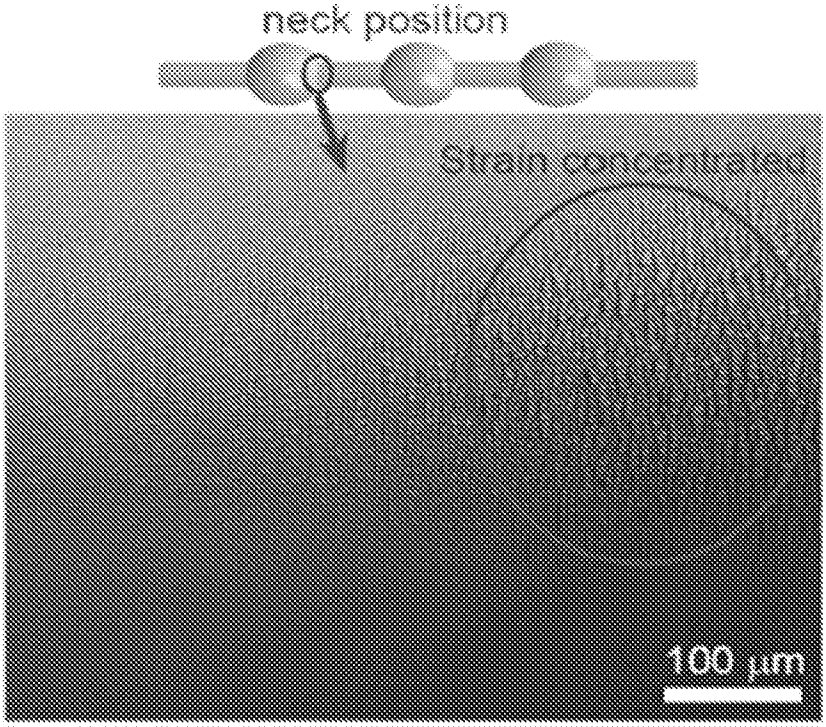

FIG. 28C

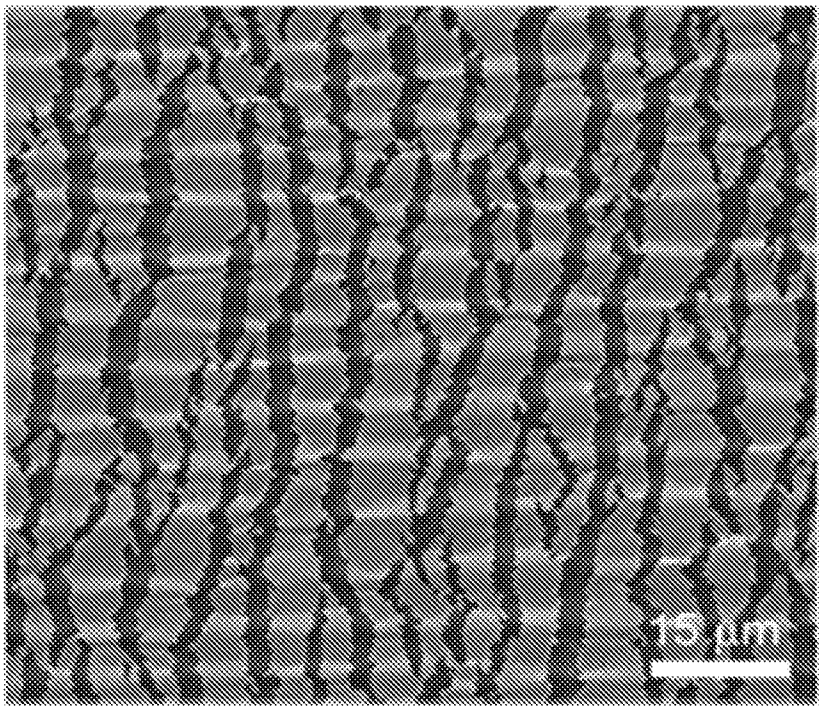

FIG. 29A

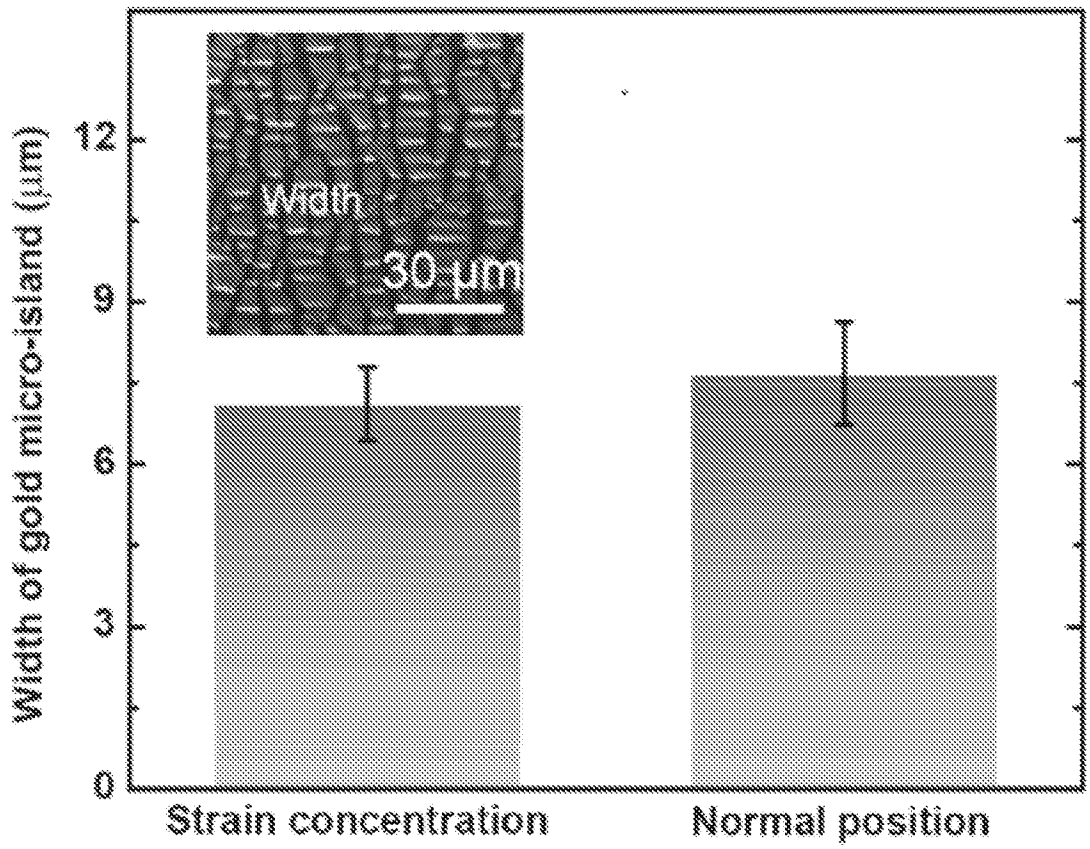
Width of gold micro-island (μm)
0
3
6
9
12
Width
30 μm
Strain concentration
Normal position

FIG. 29B

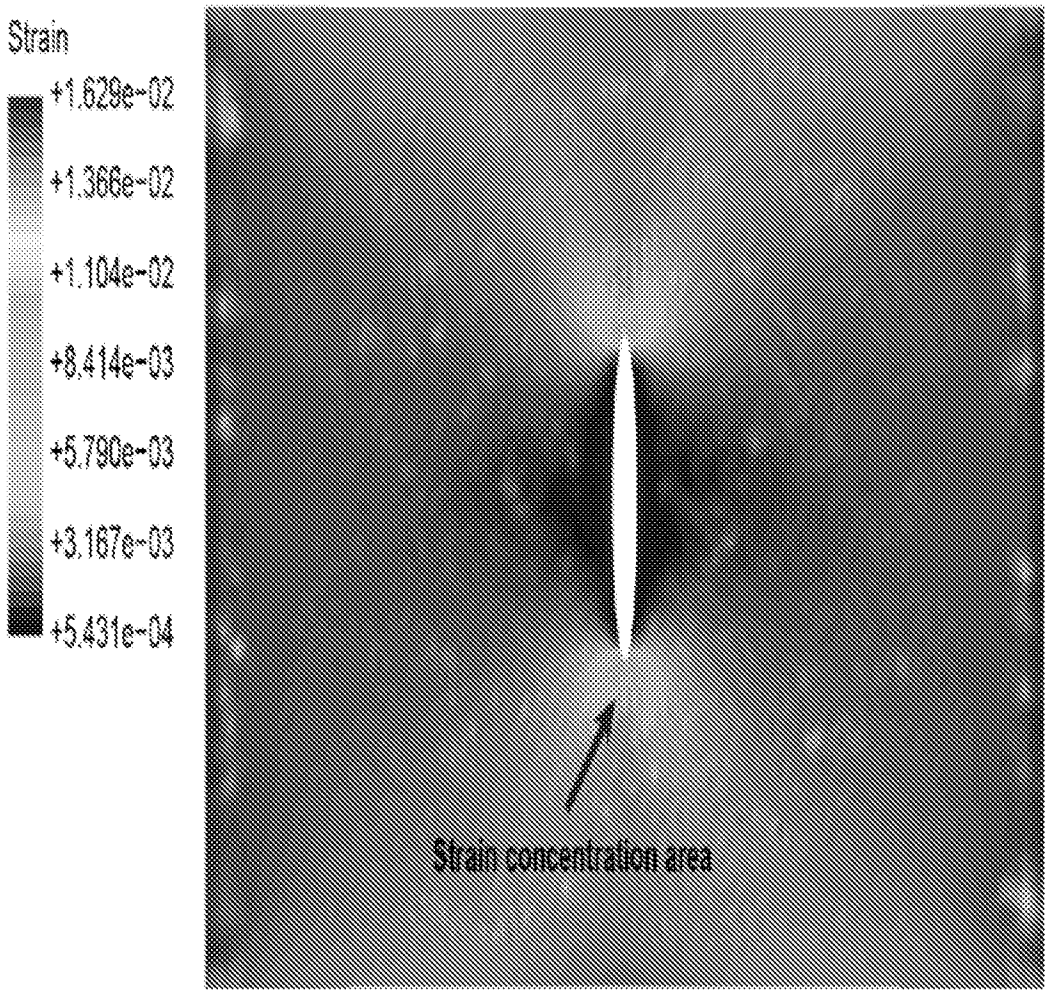
Strain
+1.629e-02
+1.366e-02
+1.104e-02
+8.414e-03
+5.790e-03
+3.167e-03
+5.431e-04
Strain concentration area

INTERNATIONAL SEARCH REPORT

International application No.
PCT/SG2018/050161

A. CLASSIFICATION OF SUBJECT MATTER

G01L 1/22 (2006.01) ***G01B 7/16 (2006.01)*** *A61B 5/11 (2006.01)*

According to International Patent Classification (IPC)

B. FIELDS SEARCHED

Minimum documentation searched (classification system followed by classification symbols)

G01L, G01B, A61B

Documentation searched other than minimum documentation to the extent that such documents are included in the fields searched

Electronic data base consulted during the international search (name of data base and, where practicable, search terms used)

FAMPAT, INCOPAT, COMPENDEX and INSPEC: strain, deformation, sensor, gauge, fiber, microstructure, bead, polymer, conductive layer, 应变, 变形, 位移, 传感, 器件, 元件, 球, 珠, 微结构, 纤维, 丝, 线, 条, 带, 涂层, 薄膜, 导电 and similar terms.

C. DOCUMENTS CONSIDERED TO BE RELEVANT

Category*	Citation of document, with indication, where appropriate, of the relevant passages	Relevant to claim No.
A	ZHANG M. ET AL., Sheath–Core Graphite/Silk Fiber Made by Dry-Meyer-Rod-Coating for Wearable Strain Sensors. *ACS Applied Materials & Interfaces*, 27 July 2016, Vol. 8, pages 20894-20899 [Retrieved on 2018-05-23] <DOI: 10.1021/ACSAMI.6B06984> entire document, in particular, figures 1 and 3	1-21
A	DE 102010022878 A1 (KISIELINSKI KAI STEFAN) 8 December 2011 entire document of the machine translation	
A	JP H09-005175 A (HITACHI LTD) 10 January 1997 entire document, in particular, figures 1 and 3 of the machine translation	
A	WO 2015/179320 A1 (THE REGENTS OF THE UNIVERSITY OF CALFORNIA) 26 November 2015 entire document	

☒ Further documents are listed in the continuation of Box C. ☒ See patent family annex.

*Special categories of cited documents:

"A" document defining the general state of the art which is not considered to be of particular relevance

"E" earlier application or patent but published on or after the international filing date

"L" document which may throw doubts on priority claim(s) or which is cited to establish the publication date of another citation or other special reason (as specified)

"O" document referring to an oral disclosure, use, exhibition or other means

"P" document published prior to the international filing date but later than the priority date claimed

"T" later document published after the international filing date or priority date and not in conflict with the application but cited to understand the principle or theory underlying the invention

"X" document of particular relevance; the claimed invention cannot be considered novel or cannot be considered to involve an inventive step when the document is taken alone

"Y" document of particular relevance; the claimed invention cannot be considered to involve an inventive step when the document is combined with one or more other such documents, such combination being obvious to a person skilled in the art

"&" document member of the same patent family

Date of the actual completion of the international search	Date of mailing of the international search report
23/05/2018 *(day/month/year)*	12/06/2018 *(day/month/year)*

Name and mailing address of the ISA/SG

IPOS INTELLECTUAL PROPERTY OFFICE OF SINGAPORE

Intellectual Property Office of Singapore
51 Bras Basah Road
#01-01 Manulife Centre
Singapore 189554

Email: pct@ipos.gov.sg

Authorized officer

Zhang Jixuan (Dr)

IPOS Customer Service Tel. No.: (+65) 6339 8616

INTERNATIONAL SEARCH REPORT

International application No.
PCT/SG2018/050161

C (Continuation). DOCUMENTS CONSIDERED TO BE RELEVANT

Category*	Citation of document, with indication, where appropriate, of the relevant passages	Relevant to claim No.
A	WO 2016/019087 A1 (PRESIDENT AND FELLOWS OF HARVARD COLLEGE) 4 February 2016 entire document	
P,X	LIU Z. ET AL., Surface Strain Redistribution on Structured Microfibers to Enhance Sensitivity of Fiber- Shaped Stretchable Strain Sensors. *Advanced Materials Communication*, 11 December 2017, Vol. 30, No. 5, pages 1704229 [Retrieved on 2018-05-23] <DOI: 10.1002/ADMA.201704229> entire document	1-21
P,A	CN 106943147 A (UNIV NANJING TECH) 14 July 2017 entire document, in particular, figure 2 of the original non-English language document (a machine translation is enclosed **only** for your reference)	1-21

INTERNATIONAL SEARCH REPORT

Information on patent family members

International application No.

PCT/SG2018/050161

Note: This Annex lists known patent family members relating to the patent documents cited in this International Search Report. This Authority is in no way liable for these particulars which are merely given for the purpose of information.

Patent document cited in search report	Publication date	Patent family member(s)	Publication date
DE 102010022878 A1	08/12/2011	NONE	
JP H09-005175 A	10/01/1997	NONE	
WO 2015/179320 A1	26/11/2015	US 2017/0219331 A1 EP 3146534 A1	03/08/2017 29/03/2017
WO 2016/019087 A1	04/02/2016	NONE	
CN 106943147 A	14/07/2017	NONE	